

CZECH TECHNICAL UNIVERSITY IN PRAGUE

FACULTY OF CIVIL ENGINEERING

DEPARTMENT OF STEEL AND TIMBER STRUCTURES



DOCTORAL THESIS

PROBABILISTIC ASSESSMENT OF EQUILIBRIUM OF STEEL RAILWAY
BRIDGES BASED ON WIND TUNNEL TESTING, TRAFFIC AND WIND
RECORDS

Author: Ing. Jan Žitný

Supervisor: Prof. Ing. Pavel Ryjáček, Ph.D.

Consultant: Doc. Ing. Miroslav Sýkora, Ph.D.

Prague, 2023

Declaration

Ph.D. student's name: Ing. Jan Žitný

Title of the doctoral thesis: Probabilistic Assessment of Equilibrium of Steel Railway Bridges Based on Wind Tunnel Testing, Traffic and Wind Records

I hereby declare that this doctoral thesis is my work and effort written under the guidance of the tutors Prof. Ing. Pavel Ryjáček, Ph.D. and Doc. Ing. Miroslav Sýkora, Ph.D.

All sources and other materials used have been quoted in the list of references.

The doctoral thesis was written in connection with research on the project: 8301604A085 Pokročilé metody posuzování existujících ocelových mostů (Advanced methods of assessment of existing steel bridges).

.....

Jan Žitný

Prague, February 28th 2023

Abstract

The European railway network includes many steel bridges, both plate girder and truss girder, often dated back to the end of the 19th century. The assessment by the partial factor method according to Eurocodes often reveals insufficient reliability of these bridges. In particular, they often fail to satisfy the equilibrium limit state (EQU) when strong wind occurs simultaneously with an unloaded train crossing the bridge or in the strength limit state (STR) when the strong wind is combined with extreme traffic live load. To avoid unnecessary structural interventions and expensive traffic restrictions, eight representative types of these bridges are tested in the wind tunnel to refine force coefficients of wind pressure for the specific bridge shape and selected types of light-weight vehicles. The values of force coefficients based on wind tunnel tests correspond on average to 70-80 % of those determined according to EN 1991-1-4. Traffic flow records for three representative railway lines are then utilized to obtain distributions of weights and heights of light-weight trains, for low to high traffic intensity. Wind records covering around last 50 years are utilized to establish wind speed distributions characteristic for wind zones in the Czech Republic, thus representative for the Central European inland mild climate. Detailed probabilistic analysis of all cases demonstrates that reliability of these bridges is close to the target level specified for EQU assessment when the wind tunnel force coefficients are considered along with site-specific free-field wind and railway traffic records. It is shown that case-specific information may help to reduce numerous “hidden safeties” in reliability assessments, often included in the models for permanent actions and geometry, wind pressure, traffic load, and the combination of the last two.

Keywords:

Wind load; traffic load; bridges; reliability; probabilistic assessment; existing structures; equilibrium.

Abstrakt

Ocelové železniční mosty tvoří významnou část evropské železniční sítě a některé z těchto mostů pocházejí z počátku 19. století. Tyto mosty často vykazují nedostatečnou spolehlivost při hodnocení metodou dílčích součinitelů dle Eurokódu, a to především v mezním stavu překlopení (EQU) při uvážení současného působení lehké dopravy a silného větru nebo v mezním stavu únosnosti (STR), kde se kombinují účinky větru s extrémním vlivem dopravního zatížení. To často vede k nákladným dopravním omezením, konstrukčním úpravám nebo výměně nosné konstrukce mostu. Aby bylo možno těmto konstrukčním zásahům předejít, bylo potřeba najít přílehavější řešení k nadhodnoceným postupům dle platných předpisů. Z tohoto důvodu bylo vytvořeno 8 modelů charakteristických ocelových železničních mostů a vybraných typů vlakových souprav a byla provedena série měření ve větrném tunelu pro aktualizaci aerodynamických součinitelů. Hodnoty součinitelů založené na zkouškách ve větrném tunelu odpovídají v průměru 70-80 % hodnot stanoveným dle EN 1991-1-4. Dále byly využity záznamy o dopravních intenzitách ve třech vybraných dopravních uzlech na jejichž základě byl vytvořen pravděpodobnostní model zatížení lehkou železniční dopravou. Data o rychlostech větru za posledních 50 let byla využita k tvorbě rozdělení zatížení větrem pro větrné oblasti České republiky reprezentativní pro středoevropské klima. Podrobná pravděpodobnostní analýza založená na aktualizovaných aerodynamických součinitelích, reálných rozdělení železniční dopravy a větru ukazuje, že přestože většina vybraných mostů nevychází dle platných předpisů Eurokódu, jejich spolehlivost je dostatečná. Při využití zpřesněných modelů zatížení lze snížit nadbytné rezervy při posouzení spolehlivosti, které jsou často zahrnuty v modelech pro stálá zatížení a geometrii, tlak větru, dopravní zatížení a v popisu kombinace těchto dvou proměnných zatížení.

Klíčová slova:

Zatížení větrem; zatížení dopravou; mosty; spolehlivost; pravděpodobnostní posouzení; existující konstrukce; rovnováha.

Acknowledgment

First of all I would like to thank my supervisor Prof. Pavel Ryjáček and consultant supervisor Doc. Miroslav Sýkora for their support and professional guidance in the development of my doctoral thesis and encouragement throughout my whole PhD study program. Their deep knowledge and experience in the field and ability to quickly reveal and solve what is essential was a great inspiration for me. Furthermore, I am very grateful for their patient and friendly approach.

I thank to Doc. Stanislav Pospíšil, Prof. Sergii Kuznetsov (†2019) and Ing. Michael Macháček from Institute of Theoretical and Applied Mechanics of the Czech Academy of Science for performing the wind tunnel experiments and professional guidance in the field of aerodynamics.

I would like to express my gratitude to all professors and my colleagues from the Department of steel and timber structures for many valuable comments and interesting insights, especially to Doc. Tomáš Rotter for inspiring discussions on the dissertation topic.

I thank to Správa Železnic for financial and technical support through project 8301604A085 Pokročilé metody posuzování existujících ocelových mostů. Especially I would like to thank to Ing. Miroslav Teichman and Ing. Jan Laifr for coordination and deliverance of crucial data regarding traffic distribution.

I thank to company TOPCON for sharing the model of the Hracholusky bridge.

I would like to express my special thanks to my friend and classmate Ing. Tomáš Vachutka for performing initial wind study of the Červená bridge as a part of his diploma thesis.

My deepest thanks belong to my family, who supported me during my studies. First of all, I would like to thank my amazing wife Lucie for her unlimited support and patience, my parents who supported me all those years and my sons Cyril and Filip.

Contents

Declaration	iii
Abstract	v
Abstrakt	vii
Acknowledgment	ix
Contents	xi
List of Figures	xv
List of Tables	xxi
1 Introduction	1
2 State of Art	3
2.1 Wind Load on Bridges	3
2.2 Wind Load According to Design Codes	5
2.3 Wind Tunnel Testing	8
2.4 Probabilistic Analysis and Reliability Verification	10
3 Dissertation Objectives and Methods	13
3.1 Objectives	13
3.2 Methods	14
4 Selected Bridges and Railway Vehicles	15
4.1 Summary of Bridges and Vehicles	15
4.2 Bridge B1 – Plate Girder Bridge with Rail Directly Fixed to Top Flange .	18
4.3 Bridge B2 – Plate Girder Bridge without Bridge Deck	21

4.4	Bridge B3 – Plate Girder Bridge with Intermediate Bridge Deck	24
4.5	Bridge B4 – Plate Girder Bridge with Lower Bridge Deck	27
4.6	Bridge B5 – Truss Girder Bridge with Upper Bridge Deck and Ballast Bed	30
4.7	Bridge B6 – Truss Girder Bridge with Upper Bridge Deck	33
4.8	Bridge B7 – Truss Girder Bridge with Intermediate Bridge Deck	35
4.9	Bridge B8 – Truss Girder Bridge with Lower Bridge Deck	38
5	Wind Tunnel Experiments	41
5.1	Wind Tunnel	41
5.2	Measuring Tools	42
5.3	Definitions	45
5.4	Experimental Determination of Aerodynamic Coefficients	48
5.4.1	Experiment Calibration	48
5.4.2	Bridge B1 – Plate Girder Bridge with Rail Directly Fixed to Top Flange	52
5.4.3	Bridge B2 – Plate Girder Bridge without Bridge Deck	53
5.4.4	Bridge B3 – Plate Girder Bridge with Intermediate Bridge Deck .	54
5.4.5	Bridge B4 – Plate Girder Bridge with Lower Bridge Deck	55
5.4.6	Bridge B5 – Truss Girder Bridge with Upper Bridge Deck and Ballast Bed	56
5.4.7	Bridge B6 – Truss Girder Bridge with Upper Bridge Deck	57
5.4.8	Bridge B7 – Truss Girder Bridge with Intermediate Bridge Deck .	59
5.4.9	Bridge B8 – Truss Girder Bridge with Lower Bridge Deck	60
5.5	Results of Specific Measurements	61
5.5.1	Effect of Turbulence on Aerodynamic Coefficients	61
5.5.2	Terrain Effect on Aerodynamic Coefficients	68
5.5.3	Effect of Truss Girder Spacing on Leeward Truss Girder Coeffi- cients	72
6	Evaluation of Experimental Results	77
6.1	Wind Load according to EN 1991-1-4	77
6.2	Comparison of Wind Tunnel Results to EN 1991-1-4	80
6.2.1	Horizontal Wind Load – Plate Girder Bridges	80
6.2.2	Horizontal Wind Load – Truss Girder Bridges	81
6.2.3	Vertical Wind Load	83
6.3	Force Coefficients in EQU	84

7	Wind Pressure Model	87
7.1	Wind on Bridges	87
7.2	Wind Speed	88
7.3	Windstorms	89
7.4	Wind Zone Models	91
7.5	Notes on Wind Load Model	94
8	Light-weight Traffic Model	97
8.1	Traffic Load Models based on Traffic Records	97
8.2	Available Data for Traffic Model Specification	98
8.3	Unloaded Train Distribution	101
9	Reliability Verification	105
9.1	Basic Assumptions	105
9.2	Partial Factor Method	107
9.3	Probabilistic Model	108
9.3.1	Limit State Function	108
9.3.2	Basic Variables	109
9.3.3	Evaluation of Failure Probability	110
9.4	Target Reliability	112
9.5	Probabilistic Assessment	113
9.6	Sensitivity Analysis	116
9.7	Probabilistic Analysis	119
10	Conclusions	127
	Bibliography	133
	Author's Publications	143

List of Figures

2.1	Collapse of Tay bridge (left) (Prebble, 1979) and Tacoma Narrows bridge (right) (Karman, 2005).	4
2.2	Wind induced train derailment of train passing a bridge, Huey P. Long Bridge Louisiana US (left), bridge over Canadian river New Mexico (right).	4
2.3	Wind tunnel test of truss girder bridge sectional model (NPL, 1954).	6
2.4	Values of drag coefficient based on B/H ratio (Hay, 1992).	7
2.5	Structural models in the wind tunnel, climatic section (left) (Kuznetsov et al., 2015), aerodynamic section (right) (Ryjacek et al., 2017).	8
2.6	Example of PIV visualization of one of the bridge under investigation.	10
4.1	Bridge B1 – plate girder bridge with rail directly fixed to the top flange.	18
4.2	Bridge B1 – 3D bridge model.	19
4.3	Bridge B2 – plate girder bridge without bridge deck.	21
4.4	Bridge B2 – 3D bridge model.	22
4.5	Bridge B3 – plate girder bridge with intermediate bridge deck.	24
4.6	Bridge B3 – 3D bridge model.	25
4.7	Bridge B4 – plate girder bridge with lower bridge deck.	27
4.8	Bridge B4 – 3D bridge model.	28
4.9	Bridge B5 – truss girder bridge with upper bridge deck and ballast bed.	30
4.10	Bridge B5 – 3D bridge model.	31
4.11	Bridge B6 – truss girder bridge with upper bridge deck.	33
4.12	Bridge B7 – truss girder bridge with intermediate bridge deck.	35
4.13	Bridge B7– 3D bridge model.	36
4.14	Bridge B8 – truss girder bridge with lower bridge deck.	38
4.15	Bridge B8– 3D bridge model.	39
5.1	Plan view of the climatic wind tunnel (Kuznetsov et al., 2015).	42

5.2	Experimental equipment for investigating the aerodynamic properties of bridge models in the working part of the wind tunnel section.	43
5.3	Vortex generating grid to create turbulent flow in the range of 5 to 30%.	44
5.4	Longitudinal turbulence spectra in the wind tunnel. Best fitting curve is given by the von Karman spectrum (Kuznetsov et al., 2015).	45
5.5	Definition of dimensions, aerodynamic forces and wind attack angle rotation.	46
5.6	Aerodynamic scales – kinematic diagram and wiring of strain gauges.	48
5.7	Graph of cylinder drag coefficient dependent on Reynolds number.	50
5.8	Graph of relationship between drag coefficient and Reynolds number – Bridge B3.	51
5.9	Graph of relationship between drag coefficient and Reynolds number – Bridge B3 and Cylinder for two turbulence intensities.	51
5.10	Bridge B1 – Aerodynamic model.	52
5.11	Bridge B1 – aerodynamic coefficients.	52
5.12	Bridge B2 – Aerodynamic model.	53
5.13	Bridge B2 – aerodynamic coefficients.	53
5.14	Bridge B3 – Aerodynamic model.	54
5.15	Bridge B3 – aerodynamic coefficients.	54
5.16	Bridge B4 – Aerodynamic model.	55
5.17	Bridge B4 – aerodynamic coefficients.	55
5.18	Bridge B5 – Aerodynamic model.	56
5.19	Bridge B5 – aerodynamic coefficients.	56
5.20	Diagram of the climatic section of the tunnel with bridge placement.	57
5.21	Diagram of the climatic section of the tunnel with bridge placement.	57
5.22	Bridge B6 – aerodynamic coefficients.	58
5.23	Bridge B7 – Aerodynamic model.	59
5.24	Bridge B7 – aerodynamic coefficients.	59
5.25	Bridge B8 – Aerodynamic model.	60
5.26	Bridge B8 – aerodynamic coefficients.	60
5.27	Experiment setup with turbulence generator in the aerodynamic section.	61
5.28	Experimental relationship between turbulence intensity and the distance to the test site.	62
5.29	Bridge B2 – Comparison of force and moment coefficient values for laminar (L) and turbulent (T) airflow.	63

5.30	Bridge B7 – Comparison of force and moment coefficient values for laminar (L) and turbulent (T) airflow.	64
5.31	Bridge B8 – Comparison of force and moment coefficient values for laminar (L) and turbulent (T) airflow.	65
5.32	PIV visualization of Bridge B8 without and with Class A train.	67
5.33	The experiment setup to investigate the effect of ground level distance from the bridge.	68
5.34	Bridge B2 – Effect of terrain on aerodynamic coefficients, (NT) = No terrain, (T) = terrain.	69
5.35	Bridge B7 – Bridge B2 – Effect of terrain on aerodynamic coefficients, (NT) = No terrain, (T) = terrain.	70
5.36	Bridge B8 – Bridge B2 – Effect of terrain on aerodynamic coefficients, (NT) = No terrain, (T) = terrain.	71
5.37	Experiment setup for determination of leeward truss girder aerodynamic coefficients.	72
5.38	Model of bridge B8 main truss girders separated to leeward and windward truss.	73
5.39	Bridge B8 – Ratio of leeward against windward aerodynamic drag coefficient.	74
5.40	Bridge B8 – Drag coefficient for all model setups based on variable (scaled) truss girder spacing.	75
6.1	Force coefficient Figure 8.3 per EN 1991-1-4 with plotted wind tunnel drag coefficients C_D for bridges B1 thru B4 without and with traffic. . . .	80
6.2	Box plot of the ratio of $F_{D,tunnel}$ and $F_{W,EN}$ for truss girder bridges B5 thru B8. $F_{W,EN}$ calculated for height of Class A thru E trains.	81
6.3	Box plot of the ratio of $F_{D,tunnel}$ and $F_{W,EN}$ for truss girder bridges B5 thru B8. $F_{W,EN}$ calculated for 4 m train height per EN 1991-2.	82
6.4	Lift force coefficient Figure 8.6 per EN 1991-1-4 with plotted wind tunnel lift force coefficients C_L for bridges B1 thru B8 without and with traffic. . .	83
6.5	Designation of variables in Eq. 6.9.	84
6.6	Box plot of the ratio of $c_{f,EQU,tunnel}$ and $c_{f,EQU,EN}$ for all bridge types. . .	85
7.1	Wind map of the Czech Republic (EN 1991-1-4).	89

7.2	Histogram of annual maxima of wind speed in m/s, probability density function of Gumbel distribution and characteristic value determined as 98% quantile of the annual maxima.	92
7.3	Q-Q diagnostic plot for wind speeds ≥ 10 m/s.	93
8.1	Operational load map.	101
8.2	Unloaded train distribution – high-intensity line (Class 2).	102
8.3	Unloaded train distribution – medium-intensity line (Class 4).	102
8.4	Unloaded train distribution – low-intensity line (Class 5).	103
9.1	Monte Carlo simulation of limit state function Eq. 9.3.	111
9.2	Annual reliability index β_1 for Classes A thru E as a function of limiting wind speed $v_{b,lim}$ (wind pressure based on wind tunnel tests).	114
9.3	Lower and upper bound on annual system reliability index $\beta_{bridge,1}$ as a function of limiting wind speed $v_{b,lim}$ for wind pressure based on wind tunnel tests and EN 1991-1-4.	116
9.4	Global Sensitivity Analysis – Pearson’s correlation coefficient related to reliability index β	117
9.5	Global Sensitivity Analysis – Pearson’s correlation coefficient related to reliability index β	118
9.6	Bridge B1: $v_{b,lim}$ – Utilization Level, Wind tunnel (left), EN 1991-1-4 (right).	120
9.7	Bridge B2: $v_{b,lim}$ – Utilization Level, Wind tunnel (left), EN 1991-1-4 (right).	120
9.8	Bridge B3: $v_{b,lim}$ – Utilization Level, Wind tunnel (left), EN 1991-1-4 (right).	121
9.9	Bridge B4: $v_{b,lim}$ – Utilization Level, Wind tunnel (left), EN 1991-1-4 (right).	121
9.10	Bridge B5: $v_{b,lim}$ – Utilization Level, Wind tunnel (left), EN 1991-1-4 (right).	122
9.11	Bridge B6: $v_{b,lim}$ – Utilization Level, Wind tunnel (left), EN 1991-1-4 (right).	122
9.12	Bridge B7: $v_{b,lim}$ – Utilization Level, Wind tunnel (left), EN 1991-1-4 (right).	123
9.13	Bridge B8: $v_{b,lim}$ – Utilization Level, Wind tunnel (left), EN 1991-1-4 (right).	123

9.14	Bridge in km 4.256 Hanušovice – Staré Město pod Sněžníkem.	124
9.15	Bridge in km 4.256 Hanušovice – Staré Město pod Sněžníkem (cross-section).	125

List of Tables

4.1	Summary of representative steel railway bridge types.	16
4.2	Summary of representative types of railway vehicles.	17
4.3	Bridge B1 – plate girder bridge with rail directly fixed to the top flange (additional parameters).	20
4.4	Bridge B2 – plate girder bridge without bridge deck (additional parameters).	23
4.5	Bridge B3 – plate girder bridge with intermediate bridge deck (additional parameters).	26
4.6	Bridge B4 – plate girder bridge with lower bridge deck (additional pa- rameters).	29
4.7	Bridge B5 – truss girder bridge with upper bridge deck and ballast bed (additional parameters).	32
4.8	Bridge B6 – truss girder bridge with upper bridge deck (additional param- eters).	34
4.9	Bridge B7 – truss girder bridge with intermediate bridge deck (additional parameters).	37
4.10	Bridge B8 – truss girder bridge with lower bridge deck (additional param- eters).	40
6.1	Ratio of $C_{D,tunnel}$ and $c_{f,x0,EN}$ for plate girder bridges.	81
6.2	Ratio of $F_{D,tunnel}$ and $F_{W,EN}$ for truss girder bridges.	82
6.3	Ratio of $C_{L,tunnel}$ and $c_{f,z,EN}$ for all bridge types.	83
6.4	Ratio of $c_{f,EQU,tunnel}$ and $c_{f,EQU,EN}$ for all bridge types.	85
7.1	Basic wind speed characteristics.	92
7.2	Results of the analysis of high wind speeds – upper tail fit.	93
8.1	Unloaded train distribution.	103
9.1	Probabilistic models of basic variables in Eq. 9.1.	108

9.2	Probabilistic models of factors affecting the time-invariant component of wind pressure.	108
9.3	Global sensitivity analysis input.	117
9.4	Bridge B1 – plate girder bridge with rail directly fixed to the top flange (additional parameters).	126

Chapter 1

Introduction

The vast majority of European railway bridges were built more than 50 years ago and 35% of the bridge stock is older than 100 years (Wisniewski et al., 2009). Many of these bridges inherently fail to comply with the requirements of modern codes of practice such as Eurocodes, even with the use of refined codes for existing structures. Permanently increasing railway traffic necessitates special considerations regarding reliability assessment of existing railway bridges (Bien et al., 2007).

Many existing railway bridges in the Czech Republic are made of structural steel or other historic metal materials; light-weight steel bridges are one of four main types of railway bridges (Bien et al., 2007). They were mostly designed according to historical design codes. The detailed surveys focusing on the important defects should be performed (Ryjacek, 2019; Macho et al., 2019b,a; Ryjacek et al., 2016) and based on the results, as these bridges have to be re-assessed to prove conformity with the requirements of modern railway traffic. The load capacity assessment of existing bridges based on modern structural codes is often too conservative and may lead to excessively costly and unnecessary upgrades. In particular, equilibrium (hereafter “EQU” for brevity) verification for the simultaneous effects of wind and traffic loads usually indicate insufficient reliability of light-weight steel bridges while no wind induced overturning steel railway bridge failure mode was ever recorded unlike the wind induced train overturning derailment (Fujii et al., 1999; Zhang et al., 2013). As the wind induced train derailment is commonly not followed by the train overturning (with a subsequent change of wind exposed area), this study focuses on the EQU verification of eight representative types of existing steel railway bridges commonly found within the European railway network. Only single-track railway bridges are considered as those tend to fail the EQU requirements.

In order to preserve these bridges, often under the cultural heritage protection, the

method for refining the wind load effects using wind tunnel tests is presented. The wind tunnel experiments are performed on a selection of eight typical steel railway bridges, indicating that the values of force coefficients based on wind tunnel tests correspond to 70-80% of those provided in EN 1991-1-4, (Ryjacek et al., 2017). These wind load reductions are also applicable in ultimate limit state STR when the bridge is assessed for combination of strong wind with extreme effect of traffic live load.

Significant uncertainties in the combined load effect of the wind pressure and crossing light-weight trains dominate reliability in the EQU verification of light-weight steel bridges. These uncertainties are described by the probabilistic approach, utilizing site-specific data. While a few studies focused on probabilistic assessment of existing railway bridges are available (O'Connor et al., 2009; Wisniewski et al., 2012), to the authors' best knowledge the presented study provides a novel application of the equilibrium assessment of an existing bridge based on local wind speed and railway traffic measurements, utilizing probabilistic methods. The adopted approach is in agreement with the findings of (Wisniewski et al., 2009) indicating that the explicit consideration of uncertainty in estimating the most important parameters can be significant and may lead to considerable economic benefits when assessing reliability of existing railway bridges.

In the previous studies (Ryjacek et al., 2016; Plachy et al., 2017; Zitny and Ryjacek, 2017; Zitny et al., 2019, 2023) focused on investigation of "hidden safety" of the models in EN 1991-1-4 and EN 1991-2, the application of the proposed method is illustrated by the case study of a steel railway bridge in Southern Bohemia that fails to satisfy the EQU limit state when verified by the partial factor method given in the Eurocodes.

Chapter 2

State of Art

2.1 Wind Load on Bridges

The first ever recorder failure of the bridge due to wind and railway traffic was the collapse of the Tay railway bridge in Scotland in 1879 during a wind storm when the train was crossing the bridge (Prebble, 1979; Burt, 2004). Another milestone in 20th century was the bridge collapse of the Tacoma Narrows bridge (Miyata, 2003; Karman, 2005), see Figure 2.1, or the excessive vibration of the Golden Gate Bridge due to the dynamic response of the structure to the wind load, even during low wind speeds (Katembo et al., 2020). These catastrophic events triggered extensive research and wind tunnel experiments mainly focusing on dynamic response of long span bridges to wind (Scruton, 1952; Steinman, 1956). The aerodynamic shape and the response of the superstructure bridge deck has the most significant impact on the response of the whole bridges, this fact led to development of bridge deck section models and greatly increased the use of wind tunnel experiments and numerical methods (Scanlan and Sabzevari, 1969; Scanlan and Tomko, 1971; Diana et al., 2013).

Ever since trains became commonly used mean of public and freight transport there was a need to understand their response to cross-wind loading, first wind tunnel experiments on trains date to the end of 19th century (Goss, 1898). As the speed of the trains increases and over the past couple decades High Speed Rail (HSR) public transit is on the rise across the globe, it brings new challenges to investigate the complex train-bridge interaction in regards to wind forces (He and Zou, 2021; Xu et al., 2023). Wind induced derailment of trains leads to implementation various safety measures to operate HSR trains under high wind speeds, most commonly limiting wind speed (Fujii et al., 1999; Proppe and Wetzel, 2007). Some studies even focus on the complex topic of the extreme dynamic

response analysis of train-track-bridge-wind interaction system which makes it due to the randomness or irregularity of all input variables an in-deterministic problem which needs to be solved by stochastic methods or by large number of probabilistic simulations (Xia et al., 2008; Xu et al., 2023).

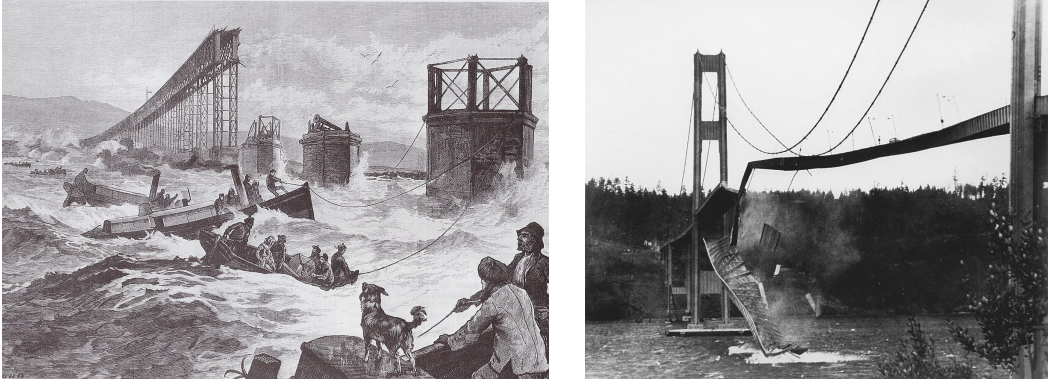


Figure 2.1: Collapse of Tay bridge (left) (Prebble, 1979) and Tacoma Narrows bridge (right) (Karman, 2005).

Wind induced derailments of trains passing a bridge during a wind storm are extremely rare but have been recorded several times, see Figure 2.2 for footage of these catastrophic events which happened in Louisiana or New Mexico US.



Figure 2.2: Wind induced train derailment of train passing a bridge, Huey P. Long Bridge Louisiana US (left), bridge over Canadian river New Mexico (right).

However, the train does not necessarily have to fall off the bridge, but may get stuck on the bridge deck. Such scenario might lead to unfavorable stability case for the whole system of the bridge and the train. Even though, according to available literature, the overturning

of the whole bridge with train has never been recorded (Zhang et al., 2022), such scenario is handled in the current design codes in the Equilibrium Limit State (EQU).

According to Eurocode, the EQU verification for railway bridges checks the stability of the bridge against overturning while it is loaded by unloaded train model and extreme wind force. The loading scenarios are specified in EN 1991-2 Traffic loads on bridges and EN 1991-1-4 Wind actions on structures. The verification of the load combination using the partial factor method is specified in EN 1990 Basis of structural design. The unloaded train model is specified as 10 kN/m uniformly distributed load acting on the whole length of the bridge, the dynamic factor Φ as well as load classification factor α shall not be considered in EQU. The value of wind load shall be determined assuming the bridge with railway traffic. The height of the train should be assumed as 4 m above the top of the rail along the whole length of the bridge.

AASHTO LRFD specifies that the structure and all its components shall be designed to resist sliding, overturning and uplift. However, no special provisions are given to evaluate overturning of the structure due to high wind and traffic effect. The only detailed verification procedure for structural overturning is specified for segmental bridges erected by balance cantilever method in Chapter 5.12.5.4.4. The required factor of safety against overturning shall be minimum 1.5 when comparing stabilizing and destabilizing moments.

2.2 Wind Load According to Design Codes

The determination of wind pressure is based on local characteristics, such as terrain orography, roughness or bridge exposure, and wind force coefficient. The evaluation of the wind pressure according to Eurocode are explained in detail in Section 6 as well as various approaches how to determine the wind force coefficient on bridges (in different standards also known as shape factor).

The values of the aerodynamic coefficients in BS 5400 were determined from extensive wind tunnel measurements by Cowdrey (Cowdrey, 1971, 1972). These measurements cover all types of girder and slab bridges except truss girder bridges. Models of plate girder and box bridge bridges were made in a scale of 1:50 and were placed in aerodynamic balances in the working section of the wind tunnel. The horizontal and vertical components of wind loads were measured. The wind speed in the tunnel was 25 m/s. The decks of the bridges were equipped with various types of parapets, railings, barriers or sound protection walls. The influence of traffic on the bridge was also taken into account

using models of trucks and buses. Measurements were taken for variation of wind attack angle $\alpha = \pm 10^\circ$. After evaluating the drag coefficients C_D , no systematic similarity was found in such a large set of bridge shapes. However, it was observed that for solid beam girder bridges with a vertical windward web, the drag coefficient decreases with increasing deck width, while for welded thin-wall I-shaped beam bridges, this tendency was opposite. Furthermore, it was found that the drag coefficient of box bridges decreases with the angle of the inclined windward web of the box girder. The bridges were therefore divided into three categories.



Figure 2.3: Wind tunnel test of truss girder bridge sectional model (NPL, 1954).

The coefficient for solid beam girder bridges with vertical windward web was related to the dimensionless ratio of the width to the height of the bridge B/H . The drag coefficient decreases with increasing ratio (branch m). It was not clear to what extent can the coefficient decrease, so a lower limit was introduced at $C_D = 1$ (branch n). For box girder bridges with inclined windward web of angle ϕ , a reduction factor was introduced to adjust the drag coefficient values evaluated for the vertical web box girder. This reduction factor is equal to $\phi/2$ and is limited to 30% reduction. For thin-walled welded plate girder bridges, a tendency of increasing drag coefficient with increasing B/H ratio was measured. However, this increase was insignificant and was therefore attributed to the flow around the flanges of the welded girders. The lower limit of the coefficient was

set to $C_D = 1.3$ (branch p), see Figure 2.4. Although the basis and measurements on which the EN 1991-1-4 force coefficients were determined are unknown, the similarity of the graphs with BS 5400 shows that they were determined on the basis of the same wind tunnel experiments or were based on them to some extent.

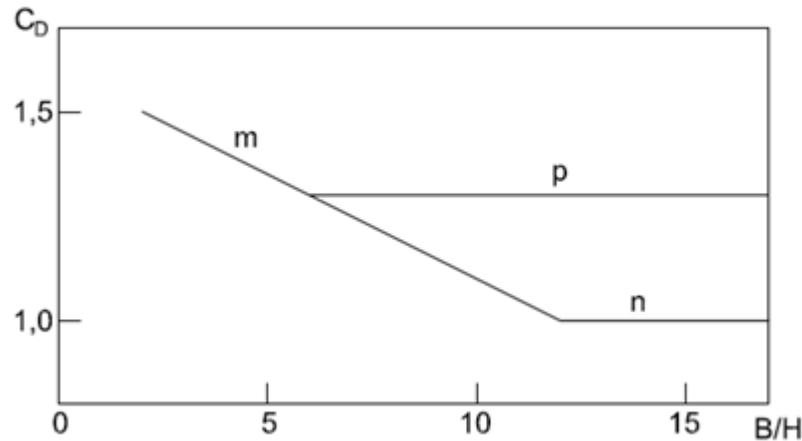


Figure 2.4: Values of drag coefficient based on B/H ratio (Hay, 1992).

Evaluation of the measurements with different inclination of the bridge to the wind direction showed no direct correlation between the drag coefficient C_D and the wind attack angle α . For some types of bridges, C_D increased with both positive and negative inclination, for some it decreased with positive inclination and increased with negative inclination, etc. In order to affect situations where the C_D increased, an increase of 15% was introduced for all branches of the graph.

Even though these measurements did not include the truss girder bridges, BS 5400 provides clear workflow how to determine the wind load on truss girder bridges. The wind load is evaluated separately for bridge deck with traffic, windward and leeward truss. The code provides the drag coefficient based on solidity ration of truss girder for windward truss and shielding factor for leeward truss based on spacing ratio. AASHTO LRFD provides similar approach, it specifies drag coefficient separately for windward and leeward truss.

Several studies have been conducted to determine the relationships of truss girder geometry to aerodynamic coefficients in the wind tunnel (Nakayama et al., 2010; He et al., 2016; Zhang et al., 2021). Similar to current design codes the relationship was established for drag coefficient based on aspect ratio of B/D , solidity ratio of the truss girder and wind attack angle α (Huan et al., 2021), this study was limited to Pratt and

Warren trusses which are common for modern truss girder bridge decks used on long-span cable stayed and suspension bridges. However, not so common for historical riveted structures with complex system of vertical and diagonal build-up members.

2.3 Wind Tunnel Testing

Wind tunnel testing is a commonly used method to study the aerodynamic behavior of bridges and to determine their aerodynamic coefficients. These coefficients are crucial for understanding the wind-induced forces and vibrations on bridges, which can have a significant impact on their structural integrity and serviceability. Wind tunnel testing typically involves the use of a small-scale model of the bridge, which is subjected to a controlled flow of wind in the tunnel. The forces and pressures exerted on the model by the wind are then measured, and these measurements are used to determine the aerodynamic coefficients of the bridge (Holmes and Bekele, 2020).

The most common type of wind tunnels used for engineering tasks are climatic wind tunnels, there are two major types of climatic wind tunnels; open circuit and closed circuit. Closed circuit climatic wind tunnel is usually divided into two sections; climatic section used for weather influence modeling including wind, temperature, rain, snow and heat radiation; and aerodynamic section suitable for measurement of wind load effects on scaled structural models (Kuznetsov et al., 2015), see Figure 2.5. For detailed description of used wind tunnel see Section 5.1.



Figure 2.5: Structural models in the wind tunnel, climatic section (left) (Kuznetsov et al., 2015), aerodynamic section (right) (Ryjacek et al., 2017).

There are several methods to determine the wind induced forces on scaled models. In recent years, significant advancements have been made in the field of wind tunnel testing

of bridges, particularly in terms of the accuracy and precision of the measurements. One important development has been the use of digital image correlation (DIC) techniques, which allow for the accurate measurement of deformations in the model during testing. This method is not only limited to wind tunnel testing but can be also used for in-situ measurements of bridges (AlSalih et al., 2021). Another non-intrusive measurement method is Particle Image Velocimetry (PIV), it is a technique used for measuring velocity fields in fluid flow. In PIV, a tracer particle is introduced into the fluid flow, and its motion is captured by a high-speed camera. By analyzing the motion of the tracer particle over time, the velocity field in the flow can be determined. This information can then be used to study the aerodynamic behavior of the bridge and to determine its aerodynamic coefficients (Seo et al., 2013). In the context of wind tunnel testing of bridges, PIV has been used in conjunction with other techniques, such as Computational Fluid Dynamics (CFD) simulations, to provide a more complete understanding of the flow field around the bridge. PIV has also been used in full-scale wind tunnel tests to validate the results of CFD simulations and to provide a more detailed understanding of the flow field (Zhang et al., 2019).

Despite these advancements, there are still challenges associated with wind tunnel testing of bridges. One of these challenges is the difficulty of accurately representing the complex geometry and material properties of the bridge in the model used for testing. Another challenge is the need for a significant amount of data to accurately determine the aerodynamic coefficients, which can be time-consuming and expensive to obtain. More simplified approach, suitable for large scale wind tunnel testing, can be used to determine the aerodynamic coefficients using aerodynamic scales. Aerodynamic scales, also known as balance systems or force balances, are instruments used to measure the forces acting on an object in a fluid flow (Truesdell and Rajagopal, 2000).

The aerodynamic scales have been used for aerodynamic coefficient measurement, PIV was used to better understand the air flow regime, see Figure 2.6. More detailed description of used measuring tools, measured and calculated properties are given in Section 5 and their comparison to Eurocode is shown in Section 5.4. All relationships are in accordance with valid laws of aerodynamic according to (Fisher et al., 1977; Pirner and Fischer, 2003; Jirsak, 2009).

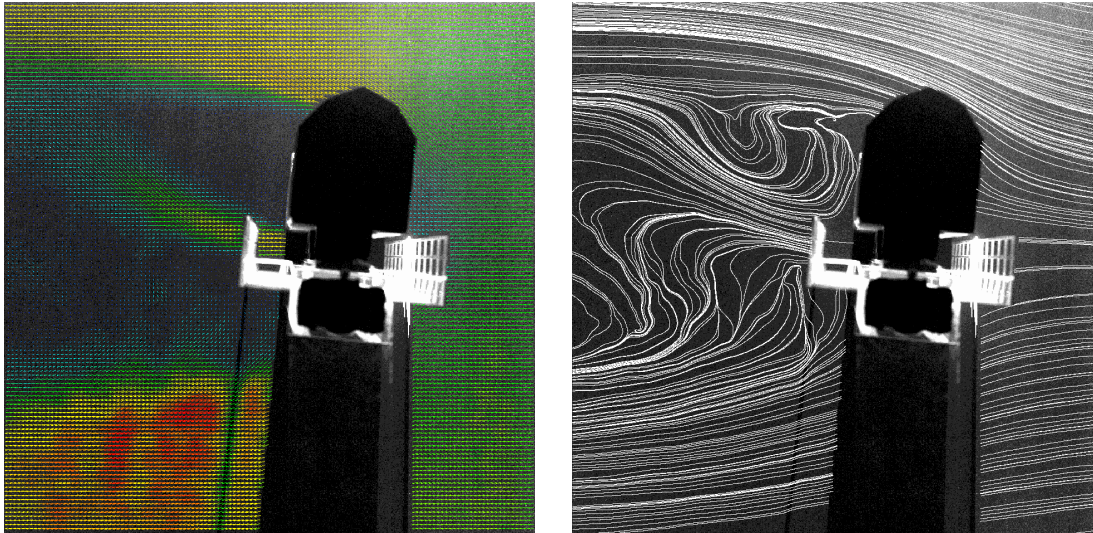


Figure 2.6: Example of PIV visualization of one of the bridge under investigation.

2.4 Probabilistic Analysis and Reliability Verification

Probabilistic methods are commonly used to evaluate the *structural reliability of bridges* under different loads and environmental conditions. These methods are based on the principle of evaluating the likelihood of failure of a structure and the uncertainty associated with the load and resistance parameters. Probabilistic methods can be used to determine the reliability index, which is a measure of the likelihood of the structure meeting its performance criteria. Reliability-based design and analysis are becoming increasingly important in the design of bridges. In this approach, the reliability index is used as the design criterion, and the structural design is optimized to ensure that the reliability index meets the required target level (Melchers, 2001; Holicky, 2009). Such methods are commonly applied to *verification of existing bridges* (Sifre and Lenner, 2021).

Probabilistic models are also used to estimate the residual life of bridges and to evaluate the effect of deterioration and aging on the structural reliability. This information is used to prioritize maintenance and rehabilitation activities, and to make informed decisions about the future use of the bridge. In recent years, there has been a growing interest in using advanced probabilistic models, such as Bayesian networks and Monte Carlo simulations, to perform uncertainty and sensitivity analyses. These methods can be used to quantify the effect of different sources of uncertainty, such as material properties, loading conditions, and environmental factors, on the reliability of bridges (Sykora, Holicky, Markova and Senberger, 2016).

Wind load probabilistic models based on wind speed records are widely used to evaluate the wind-induced loads on bridges. These models rely on the statistical analysis of wind speed records obtained from meteorological stations or other sources. The wind speed data is used to estimate the probability distribution of the wind speeds and the associated wind loads on the bridge. Section 7 provides detailed state of the art information on probabilistic modeling of wind load based on wind speed detailed wind speed records.

Probabilistic modeling of railway traffic load is a key aspect of railway bridge design and assessment. It involves using statistical methods to estimate the probability of different levels of traffic loads on a railway bridge and to evaluate the likelihood of the bridge failing under these loads. One common approach to probabilistic modeling of railway traffic loads is the use of loading models, which represent the different types of trains and the loads they generate. These loading models can be based on either historical data, such as train weight and axle load measurements, or on standard specifications for different types of trains. The loading models are then combined with statistical models of train traffic to estimate the probability of different traffic loads on the bridge. Another important aspect of probabilistic modeling of railway traffic loads is the consideration of dynamic effects, such as vibrations and oscillations caused by trains passing over the bridge. The dynamic behavior of a railway bridge can be modeled using finite element analysis or other numerical methods, and the results can be used to estimate the probability of excessive vibrations or resonances under different traffic loads. In addition, uncertainties in the traffic loads, such as changes in the train schedules and traffic patterns, can also be taken into account in probabilistic modeling. Monte Carlo simulation can be used to generate a large number of possible load scenarios, taking into account the uncertainties in the loading models and the traffic patterns. The results of the simulations can then be used to estimate the probability of failure of the bridge under different load scenarios (Reid, 2007; Adasooriya, 2016). Section 8 provides detailed state of the art information on probabilistic modeling of railway traffic based on traffic records.

Section 9 provides detailed state of the art information on **target reliability and reliability verification** of combined effect wind and traffic load in equilibrium limit state as well as usage of Monte Carlo simulations and sensitivity analysis of the probabilistic model.

Chapter 3

Dissertation Objectives and Methods

3.1 Objectives

In the bridge engineering practice, light-weight steel railway bridges tend to fail the code requirements when assessed for the combined effect of wind and traffic load. Objectives of the dissertation are specified to investigate and refine the wind induced forces on existing steel railway bridges and to determine possible hidden safeties in the current design and verification approaches:

1. Refine the method of wind force calculation on selected steel railway bridges while taking into account the wind-on-train effect for light-weight railway traffic.
2. Investigate the interaction of strong wind and light-weight railway traffic, considering the distribution of wind load and light-weight railway traffic based on available wind and traffic records.
3. Verify reliability of existing bridges in the EQU limit state applying the refined wind load and light-weight railway traffic effects in the probabilistic reliability assessment.
4. Investigate the effect of the operator's decision to disrupt traffic during strong wind events on reliability of bridges, such as imposing operational wind speed limit.
5. Summarize the wind load refinement and reliability assessment findings into the methodology applicable to load capacity assessment of existing bridges.

3.2 Methods

Following are the proposed methods to achieve the objectives of the dissertation.

1. Selection of representative types of steel railway bridges and representative types of light-weight railway vehicles based on analysis of common bridge types and railway vehicles. Fabrication of experimental models of selected bridges and vehicles.
2. Performance of wind tunnel experiments on selected bridges in order to refine wind force aerodynamic coefficients.
3. Experimental analyses of additional effects on aerodynamic coefficients. The effect of turbulence, effect of low distance to terrain and effect of truss girder spacing for truss girder bridges.
4. Evaluation of aerodynamic coefficient adjustment factors and guidance for their operational use in engineering practice.
5. Analysis of available railway traffic records in the SŽ railway network. Determination of distribution of light-weight traffic: frequency of trains, weight of trains and height of trains. Development of the probabilistic model for light-weight railway traffic.
6. Evaluation of wind speed records, frequency and length of windstorms from several meteorological stations in the Czech Republic. Development of a probabilistic model of strong wind distribution based on wind speed records.
7. Development of a probabilistic model for the combined effects of light-weight railway traffic and strong wind load.
8. Reliability analysis of measured data in wind tunnel using available light-weight railway traffic and wind records.
9. Determination of correlations between individual inputs into the reliability assessment using global sensitivity analysis and stochastic simulations.
10. Implementation of research findings into methodology S5/1 Diagnostics, load capacity and load rating of railway bridge structures.

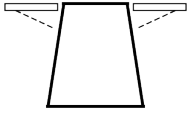
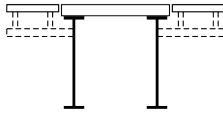
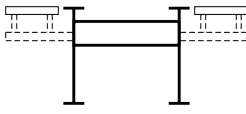
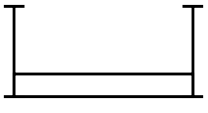
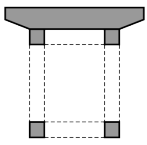

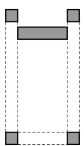

Chapter 4

Selected Bridges and Railway Vehicles

4.1 Summary of Bridges and Vehicles

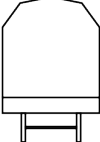
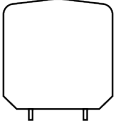
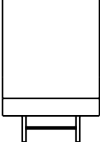
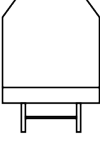
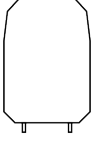
Detailed analysis of common steel railway bridge types in the Czech railway network was performed. A total of 8 representative types of steel railway bridges were selected for the dissertation. Plate girder and truss girder bridges with various types and location of bridge deck were assumed. Selected railway bridges exhibit to some extent issues with wind load when evaluated according to Eurocode, limiting their load capacity and load rating. Only single track bridges were selected as they tend to fail the equilibrium limit state (EQU) verification. Some of the bridges have been assumed to establish the lower boundary for EQU verification and to provide updated wind force coefficients. Table 4.1 shows the summary of selected bridge types. See Section 4.2 thru 4.9 for bridge details and basic information on wind loading and EQU verification.

Registry of available railway vehicles used by domestic or international railway operators REVOZ (Accessed 2016) (see Section 8.2) was analyzed and the selection of representative railway vehicles was discussed with SŽ representatives. A total of 5 types of railway vehicles commonly used in the Czech railway network were selected based on various height and aerodynamic shape. Table 4.2 shows the summary of selected railway vehicles.

No.	Bridge Type	b/d_{tot}^*	Cross-Section
B1	Plate girder bridge with rail directly fixed to the top flange	0.69	
B2	Plate girder bridge without bridge deck	0.89	
B3	Plate girder bridge with intermediate bridge deck	0.78	
B4	Plate girder bridge with lower bridge deck	1.25	
B5	Truss girder bridge with upper bridge deck and ballast bed	1.20	
B6	Truss girder bridge with upper bridge deck	0.79	
B7	Truss girder bridge with intermediate bridge deck	1.16	
B8	Truss girder bridge with lower bridge deck	1.18	

* b/d_{tot} is determined with 4 m train per EN 1991-1-4 Section 8.3.1.

Table 4.1: Summary of representative steel railway bridge types.

Class	Category	Weight* [t/m]	Height [m]	Cross-Section	Train Designation
A	Lightest and tallest cargo train used in CZ	1.07	4.29		Kils 12
B	Lowest train, public transport, local lines	1.39	3.51		Regionova
C	Cargo train with High Cube shipping container	1.53	4.15		SGS High Cube
D	Standard public transport train, same profile as Kils 12	1.70	4.29		Bdmpee
E	Double-decker suburban train, highest train used in CZ	1.96	4.64		City Elefant

* Unloaded train

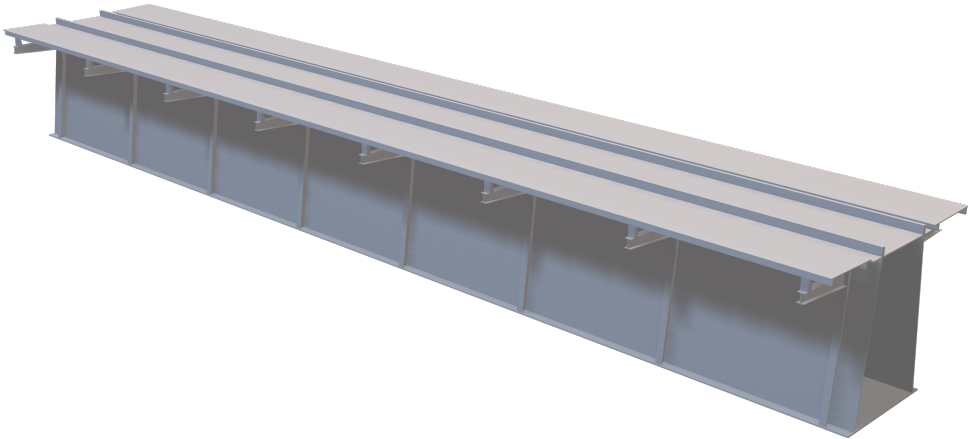
Table 4.2: Summary of representative types of railway vehicles.

4.2 Bridge B1 – Plate Girder Bridge with Rail Directly Fixed to Top Flange

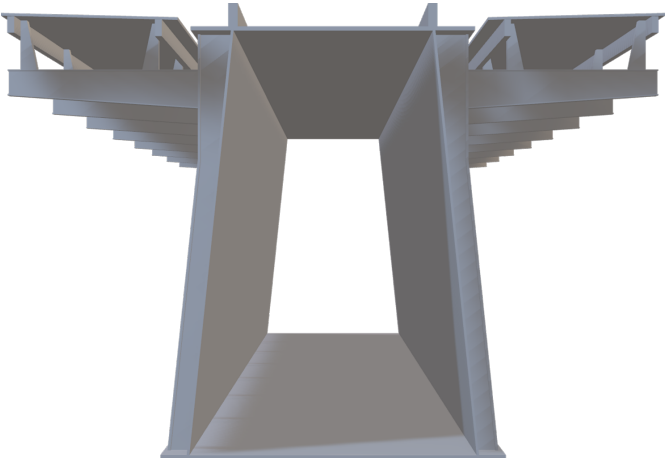
The aerodynamic section model of the plate girder bridge with rail directly fixed to the top flange is based on geometry of the Jizera bridge located in km 29.048 of the line Nymburk – Mladá Boleslav. The bridge has 4 simply supported spans. In span 1 and 4 there is riveted truss girder superstructure with intermediate bridge deck. In span 2 and 3 there is welded steel box girder superstructure (used for bridge type B1). The bridge is straight in plan with one track. The spans are $31.75 + 2 \times 39.40 + 31.75$ m long. The bridge has reinforced concrete substructure, perpendicular in all spans, see Figure 4.1 and 4.2. Additional parameters are defined in Table 4.3.



Figure 4.1: Bridge B1 – plate girder bridge with rail directly fixed to the top flange.



Isometric View



Section View



Elevation View

Figure 4.2: Bridge B1 – 3D bridge model.

Superstructure:	Span 1 & 4: steel riveted truss girders with intermediate bridge deck. Span 2 & 3: steel welded box girder with rail directly fixed to the top flange
Static layout of the superstructure:	4 simple spans
Total length of bridge:	155.0 m
Span length:	31.75 + 2x39.40 + 31.75 m
Number of tracks:	1
Transverse arrangement of the bridge:	VMP 2.5
Structural depth:	3.45 m (span 1 & 4) 3.50 m (span 2 & 3)
Clear depth (decisive):	5.00 m (above water level)
Structural width:	5.05 m
Wind load parameters	
Wind Zone:	II
Terrain category:	I
Reference height z_e :	8.75 m
Wind pressure $q_p(z_e)$:	1,046 Pa
Reference area A_{ref} :	7.34 m ² /m
Force coefficient $c_{f,x}$:	2.29
Wind load F_w :	17.6 kN/m
EQU verification per Eurocodes	
Bridge weight:	31.8 kN/m
Bearing spacing:	2.20 m
Center of wind reference area z_w :	3.67 m
Destabilizing moment M_w :	$17.6 \cdot 3.67 = 64.6$ kNm/m
Stabilizing moment M_G :	$(31.8 + 10) \cdot 2.20 / 2 = 46.0$ kNm/m
EQU verification:	$1.50 \cdot 64.6 / (0.95 \cdot 46.0) = 2.22$

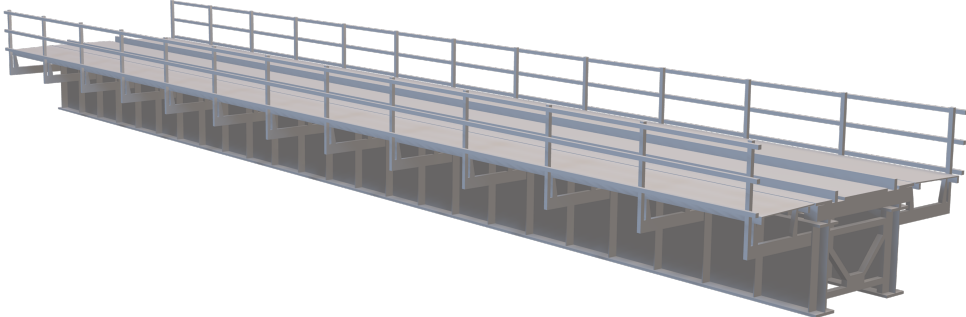
Table 4.3: Bridge B1 – plate girder bridge with rail directly fixed to the top flange (additional parameters).

4.3 Bridge B2 – Plate Girder Bridge without Bridge Deck

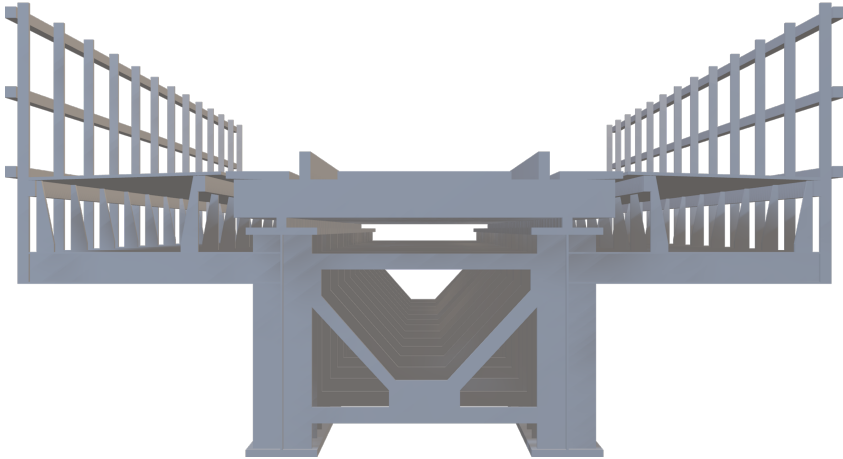
The aerodynamic section model of the plate girder bridge without bridge deck is based on geometry of the Brniště bridge located in km 108.493 of the line Česká Lípa – Liberec. The bridge has 2 simply supported spans with equal span length of 16.8 m and was built in 1989. The bridge is straight in plan with skewed stone substructure. The superstructure consists of two welded plate girders with total depth of 1.44 m. Girder webs are stiffened by vertical stiffeners on both sides. The transverse stability is provided by welded K shape cross-bracing. There is a lateral bracing at the top flange level. There is no bridge deck and the wooden sleepers are directly fixed to the main edge girders. The service walkways are cantilevered from the web vertical stiffeners and are covered by steel sheet metal, see Figure 4.3 and 4.4. Additional parameters are defined in Table 4.4.



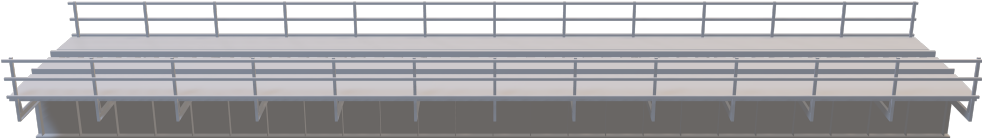
Figure 4.3: Bridge B2 – plate girder bridge without bridge deck.



Isometric View



Section View



Elevation View

Figure 4.4: Bridge B2 – 3D bridge model.

Superstructure:	Welded plate girder superstructure without bridge deck.
Static layout of the superstructure:	2 simple spans
Total length of bridge:	42.6 m
Span length:	2x16.80 m
Number of tracks:	1
Transverse arrangement of the bridge:	VMP 3.0
Structural depth:	1.97 m
Clear depth (decisive):	2.90 m
Structural width:	5.18 m
Wind load parameters	
Wind Zone:	II
Terrain category:	III
Reference height z_e :	5.9 m
Wind pressure $q_p(z_e)$:	537 Pa
Reference area A_{ref} :	5.81 m ² /m
Force coefficient $c_{f,x}$:	2.23
Wind load F_w :	6.96 kN/m
EQU verification per Eurocodes	
Bridge weight:	15.4 kN/m
Bearing spacing:	1.80 m
Center of wind reference area z_w :	2.91 m
Destabilizing moment M_w :	$6.96 \cdot 2.91 = 20.3$ kNm/m
Stabilizing moment M_G :	$(15.4+10) \cdot 1.80/2 = 22.9$ kNm/m
EQU verification:	$1.50 \cdot 20.3 / (0.95 \cdot 22.9) = 1.40$

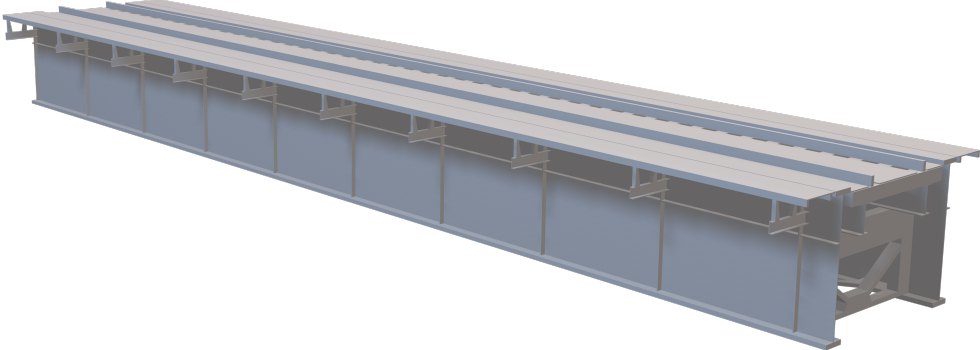
Table 4.4: Bridge B2 – plate girder bridge without bridge deck (additional parameters).

4.4 Bridge B3 – Plate Girder Bridge with Intermediate Bridge Deck

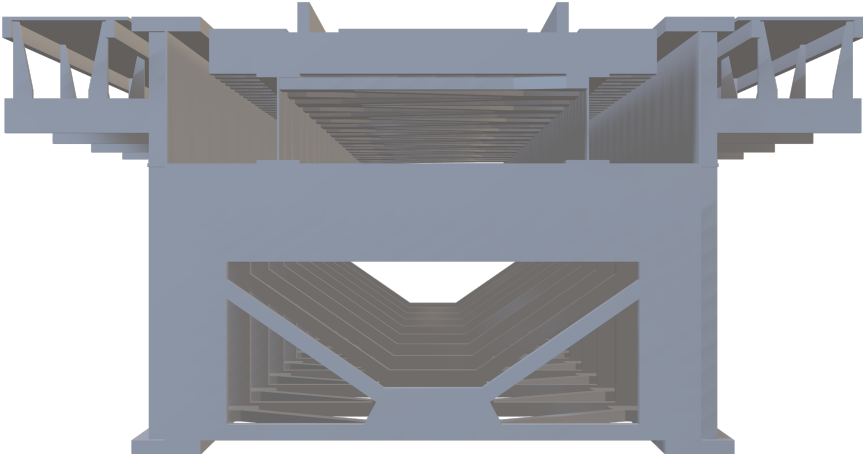
The aerodynamic section model of the plate girder bridge with intermediate bridge deck is based on geometry of the Prostřední Žleb end span bridge located in km 458.756 of the line Všetaty – Děčín. The bridge has 4 simply supported spans. In span 1 and 4 there is a plate girder superstructure with intermediate bridge deck (used for bridge type B3) built in 1972. In span 2 and 3 there is a riveted truss girder superstructure with lower bridge deck built in 1916. The bridge is curved in plan and supported on skewed stone substructure. The spans are $25.0 + 2 \times 99.4 + 25.7$ m long. The superstructure in span 1 and 4 consists of two riveted plate girders spaced at 3.15 m with total depth of 2.40 m. The I shape cross beams stiffened by K shape bracing support pair of longitudinal beams which carry the wooden sleepers. All members are riveted from plates and angles. The whole bridge deck is intermediate with top of rail at the same level as edge girder top flange. There are two layers of lateral bracing, one at the cross-beam level, and one at the edge girder bottom flange level. The edge girder webs are stiffened by both vertical and horizontal stiffeners. The service walkways are cantilevered from edge girder vertical stiffeners and are covered by steel sheet metal, see Figure 4.5 and 4.6. Additional parameters are defined in Table 4.5.



Figure 4.5: Bridge B3 – plate girder bridge with intermediate bridge deck.



Isometric View



Section View



Elevation View

Figure 4.6: Bridge B3 – 3D bridge model.

Superstructure:	Span 1 & 4: steel riveted plate girder superstructure with intermediate bridge deck. Span 2 & 3: steel riveted truss girder superstructure with lower bridge deck.
Static layout of the superstructure:	4 simple spans
Total length of bridge:	265.5 m
Span length:	25.0 + 2x99.4 + 25.7 m
Number of tracks:	1
Transverse arrangement of the bridge:	VMP 2.2
Structural depth:	2.46 m (span 1) 1.24 m (span 2 and 3) 2.65 m (span 4)
Clear depth (decisive):	6.50 m (span 1 and 4) 13.70 m (span 2 and 3)
Structural width:	5.13 m
Wind load parameters	
Wind Zone:	II
Terrain category:	I
Reference height z_e :	9.7 m
Wind pressure $q_p(z_e)$:	1,075 Pa
Reference area A_{ref} :	6.55 m ² /m
Force coefficient $c_{f,x}$:	2.27
Wind load F_w :	16.0 kN/m
EQU verification per Eurocodes	
Bridge weight:	26.9 kN/m
Bearing spacing:	3.15 m
Center of wind reference area z_w :	3.28 m
Destabilizing moment M_w :	$16.0 \cdot 3.28 = 52.5$ kNm/m
Stabilizing moment M_G :	$(26.9 + 10) \cdot 3.15 / 2 = 58.1$ kNm/m
EQU verification:	$1.50 \cdot 52.5 / (0.95 \cdot 58.1) = 1.45$

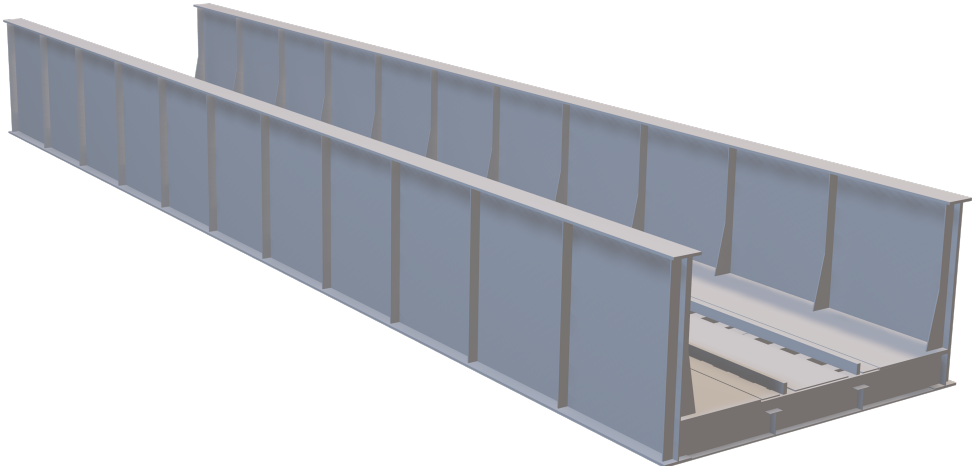
Table 4.5: Bridge B3 – plate girder bridge with intermediate bridge deck (additional parameters).

4.5 Bridge B4 – Plate Girder Bridge with Lower Bridge Deck

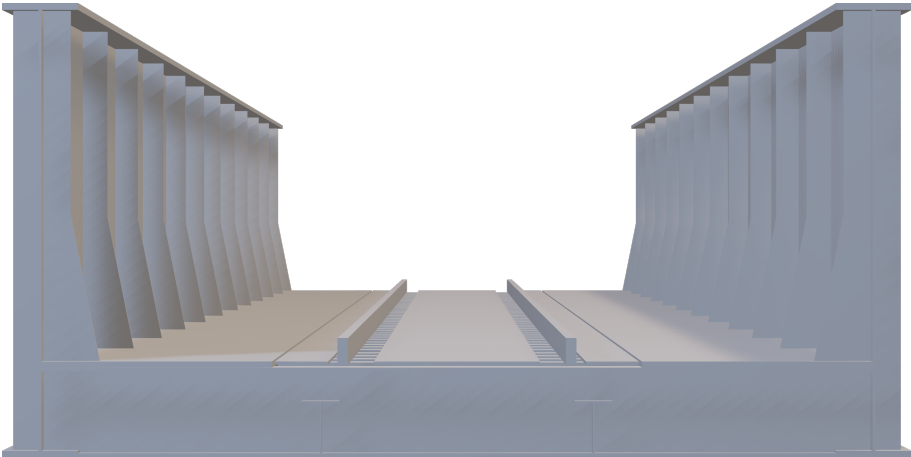
The aerodynamic section model of the plate girder bridge with lower bridge deck is based on geometry of the Babín bridge located in km 0.596 of the line Babín – Nymburk. Single span bridge was built in 2003. The bridge is straight with skewed substructure. The main span is 34.50 m long. The superstructure consists of pair of welded plate girders with parabolic top flange. Girder webs are stiffened by vertical stiffeners on both sides. The bridge has a lower bridge deck consisting of welded plate girder cross-beams with aligned bottom flange with the main girders. Hot rolled I-shape longitudinal girders are inserted between the cross-beams and support wooden sleepers. The lateral bracing of the bridge is at the bottom flange level of the main girders and cross-beams. The whole bridge deck is covered by steel sheet metal, see Figure 4.7 and 4.8. Additional parameters are defined in Table 4.6. The model was fabricated with constant depth. The end depth was used for the model purposes.



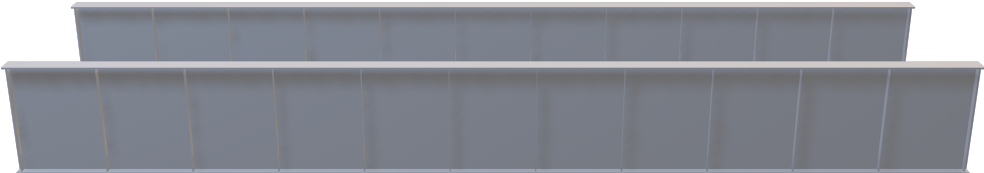
Figure 4.7: Bridge B4 – plate girder bridge with lower bridge deck.



Isometric View



Section View



Elevation View

Figure 4.8: Bridge B4 – 3D bridge model.

Superstructure:	Welded plate girder superstructure with parabolic top flange.
Static layout of the superstructure:	1 simple span
Total length of bridge:	44.7 m
Span length:	34.50 m
Number of tracks:	1
Transverse arrangement of the bridge:	VMP 2.5
Structural depth:	2.12 m (end – used for wind tunnel model) 2.92 m (middle)
Clear depth:	6.20 m
Structural width:	6.00 m
Wind load parameters	
Wind Zone:	I
Terrain category:	II
Reference height z_e :	8.6 m
Wind pressure $q_p(z_e)$:	714 Pa
Reference area A_{ref} :	4.79 m ² /m
Force coefficient $c_{f,x}$:	2.12
Wind load F_w :	7.3 kN/m
EQU verification per Eurocodes	
Bridge weight:	27.0 kN/m
Bearing spacing:	5.80 m
Center of wind reference area z_w :	2.39 m
Destabilizing moment M_w :	$7.3 \cdot 2.39 = 17.4$ kNm/m
Stabilizing moment M_G :	$(27.0 + 10) \cdot 5.80 / 2 = 107.3$ kNm/m
EQU verification:	$1.50 \cdot 17.4 / (0.95 \cdot 107.3) = 0.26$

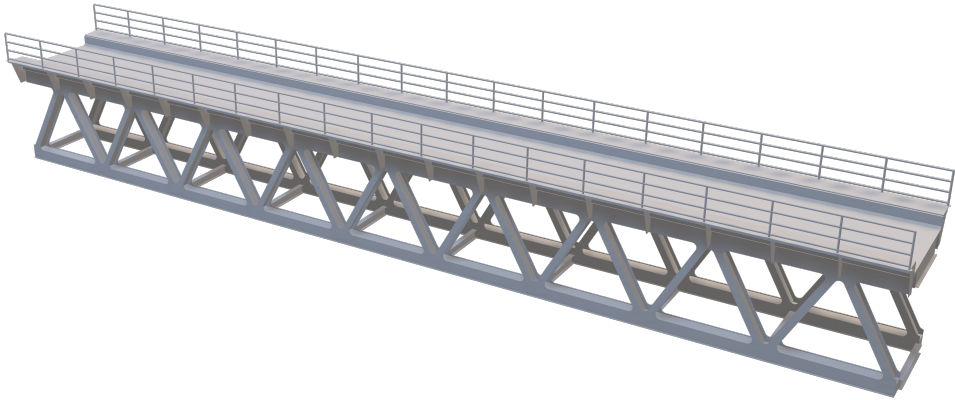
Table 4.6: Bridge B4 – plate girder bridge with lower bridge deck (additional parameters).

4.6 Bridge B5 – Truss Girder Bridge with Upper Bridge Deck and Ballast Bed

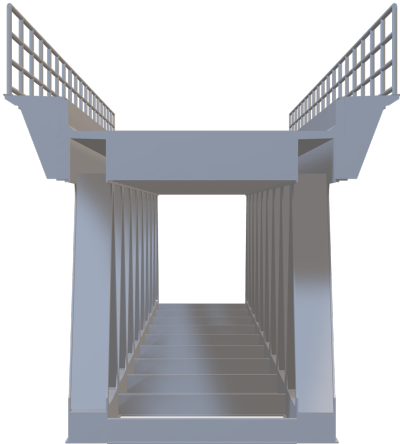
The aerodynamic section model of the truss girder bridge with upper bridge deck and ballast bed is based on geometry of the Znojemský viadukt bridge located in km 99.297 of the line Šatov – Znojmo. The bridge has 4 spans and in 2010 replaced historical truss girder bridge built in 1871. The bridge is straight in plan and supported by original stone substructure. The spans are $49.95 + 2 \times 59.94 + 49.95$ m long. The superstructure consists of pair of welded truss girders. The top and bottom chord of the truss have box cross-section and the diagonals are I-shape members. The truss superstructure has no vertical members, only diagonals. The bridge has upper orthotropic bridge deck with ballast bed, see Figure 4.9 and 4.10. Additional parameters are defined in Table 4.7.



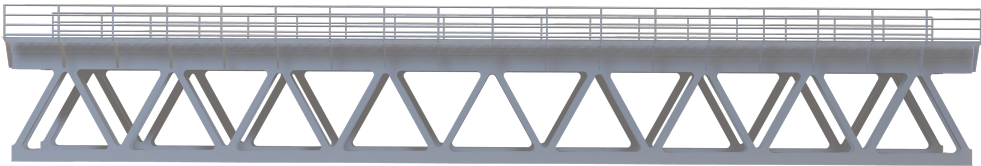
Figure 4.9: Bridge B5 – truss girder bridge with upper bridge deck and ballast bed.



Isometric View



Section View



Elevation View

Figure 4.10: Bridge B5 – 3D bridge model.

Superstructure:	Welded truss girder superstructure with upper orthotropic bridge deck and ballast bed.
Static layout of the superstructure:	4 continuous spans.
Total length of bridge:	220.97 m
Span length:	49.49 + 2x59.94 + 49.95 m
Number of tracks:	1
Transverse arrangement of the bridge:	VMP 3.0
Structural depth:	5.78 m
Clear depth (decisive):	43.4 m
Structural width:	6.06 m
Wind load parameters	
Wind Zone:	III
Terrain category:	II
Reference height z_e :	48.3 m
Wind pressure $q_p(z_e)$:	1.627 Pa
Reference area A_{ref} :	
Bridge deck:	4.66 m ² /m
Truss girders:	3.61 m ² /m
Force coefficient $c_{f,x}$:	
Bridge deck:	2.14
Truss girders:	1.55
Wind load F_w :	25.3 kN/m
EQU verification per Eurocodes	
Bridge weight:	85.5 kN/m
Bearing spacing:	3.75 m
Center of wind reference area z_w :	5.32 m
Destabilizing moment M_w :	$25.3 \cdot 5.32 = 134.6$ kNm/m
Stabilizing moment M_G :	$(85.5 + 10) \cdot 3.75 / 2 = 179.1$ kNm/m
EQU verification:	$1.50 \cdot 134.6 / (0.95 \cdot 179.1) = 1.20$

Table 4.7: Bridge B5 – truss girder bridge with upper bridge deck and ballast bed (additional parameters).

4.7 Bridge B6 – Truss Girder Bridge with Upper Bridge Deck

The aerodynamic section model of the truss girder bridge with upper bridge deck and ballast bed is based on geometry of the Hracholusky bridge located in km 1.429 of the line Pňovany – Bezručice. The bridge has 5 spans and was built in 1900. In span 1 and 5, there are stone masonry arches. In span 2 thru 4 there is a riveted steel truss girder superstructure with upper bridge deck and parabolic bottom chord. The bridge is straight in span 1 thru 4 and in transition curve in span 5. The main steel superstructure consists of pair of truss girders with one directional diagonal members and vertical members. The bridge deck consists of riveted I-shape cross-beams connected to the main girder vertical members and which supports the riveted longitudinal members with wooden sleepers. The main lateral bracing is at the parabolic bottom chord level. Vertical truss girder members are braced with X bracing. Vertical members with bracing and cross-beams function as enclosed diaphragms. The service walkways are located on the truss girder top chords and at the bottom chord lateral bracing, see Figure 4.11. The model was supplied by company TOPCON. Additional parameters are defined in Table 4.8.



Figure 4.11: Bridge B6 – truss girder bridge with upper bridge deck.

Superstructure:	Span 1 & 5: stone masonry arch. Span 2-4: riveted steel truss girder superstructure with upper bridge deck and parabolic bottom chords.
Static layout of the superstructure:	2 stone masonry arches + 3 simple spans.
Total length of bridge:	208.5 m
Span length:	7.50 + 3x57.00 + 10.50 m
Number of tracks:	1
Transverse arrangement of the bridge:	VMP 2.2
Structural depth:	2.20 m (span 1 & 5) 9.50 m (span 1-4)
Clear depth (decisive):	27.4 m
Structural width:	4.70 m
Wind load parameters	
Wind Zone:	II
Terrain category:	I
Reference height z_e :	34.1 m
Wind pressure $q_p(z_e)$:	1.386 Pa
Reference area A_{ref} :	
Bridge deck:	4.14 m ² /m
Truss girders:	3.30 m ² /m
Force coefficient $c_{f,x}$:	
Bridge deck:	2.26
Truss girders:	1.55
Wind load F_w :	20.1 kN/m
EQU verification per Eurocodes	
Bridge weight:	76.4 kN/m
Bearing spacing:	3.60 m
Center of wind reference area z_w :	2.94 m
Destabilizing moment M_w :	$20.1 \cdot 2.94 = 59.1$ kNm/m
Stabilizing moment M_G :	$(76.4 + 10) \cdot 3.60 / 2 = 155.5$ kNm/m
EQU verification:	$1.50 \cdot 59.1 / (0.95 \cdot 155.5) = 0.61$

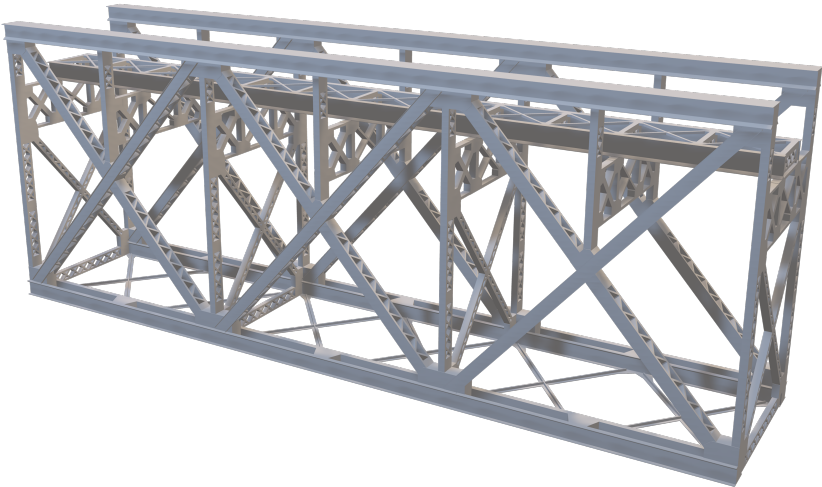
Table 4.8: Bridge B6 – truss girder bridge with upper bridge deck (additional parameters).

4.8 Bridge B7 – Truss Girder Bridge with Intermediate Bridge Deck

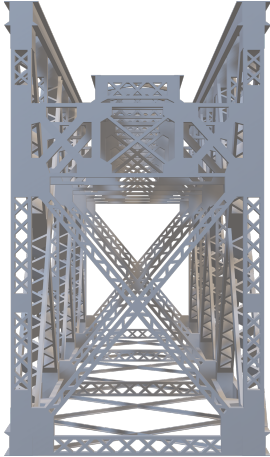
The aerodynamic section model of the truss girder bridge with intermediate bridge deck and ballast bed is based on geometry of the Červená bridge located in km 41.791 of the line Tábor – Písek. The bridge has 3 spans over Orlík dam and was built in 1889. The main superstructure consists of pair of riveted steel truss girders 9.88 m high with both-directional diagonal members and vertical members. The bridge has intermediate bridge deck consisting of truss girder cross-beams supporting riveted longitudinal girders with wooden sleepers. The cross beams are located between full-depth truss girder vertical members and at the intersection point of main truss girder diagonals, there they form only partial vertical member. The bottom chord bracing is located in each member intersection point. Vertical truss girder members are braced with X bracing. Vertical members with X bracing, bottom chord bracing and cross-beams function as enclosed diaphragms. The main lateral bracing is at the bottom chord level. The longitudinal bridge deck members are braced with transverse and lateral bracing as well. The span 1 and 3 are continuous over the pier and cantilevered into the main span. The middle of the main span is connected by hinges. The whole bridge deck is covered by steel sheet metal which work as service walkway., see Figure 4.12 and 4.13. Additional parameters are defined in Table 4.9.



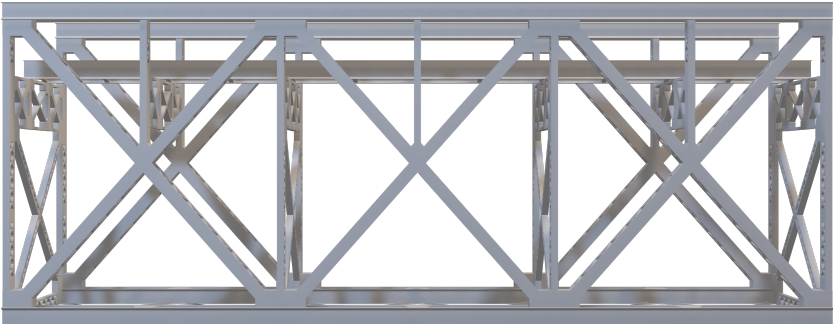
Figure 4.12: Bridge B7 – truss girder bridge with intermediate bridge deck.



Isometric View



Section View



Elevation View

Figure 4.13: Bridge B7– 3D bridge model.

Superstructure:	Riveted steel truss girder superstructure with intermediate bridge deck.
Static layout of the superstructure:	2 continuous spans cantilevered into the main span with hinge connected main span.
Total length of bridge:	254.2 m
Span length:	3x84.4 m (109.72 + 33.76 + 109.72 m)
Number of tracks:	1
Transverse arrangement of the bridge:	VMP 2.2
Structural depth:	9.88 m
Clear depth (decisive):	30.5 m
Structural width:	5.80 m
Wind load parameters	
Wind Zone:	II
Terrain category:	I
Reference height z_e :	35,2 m
Wind pressure $q_p(z_e)$:	1.394 Pa
Reference area A_{ref} :	
Bridge deck:	5.01 m ² /m
Truss girders:	3.36 m ² /m
Force coefficient $c_{f,x}$:	
Bridge deck:	2.15
Truss girders:	1.55
Wind load F_w :	22.3 kN/m
EQU verification per Eurocodes	
Bridge weight:	37.8 kN/m
Bearing spacing:	3.80 m
Center of wind reference area z_w :	7.25 m
Destabilizing moment M_w :	$22.3 \cdot 7.25 = 161.7$ kNm/m
Stabilizing moment M_G :	$(37.8 + 10) \cdot 5.80 / 2 = 138.6$ kNm/m
EQU verification:	$1.50 \cdot 161.7 / (0.95 \cdot 138.6) = 1.87$

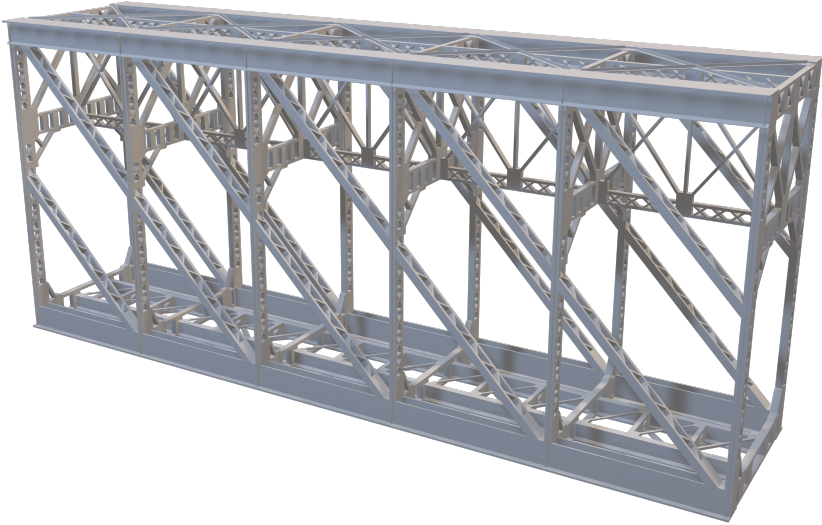
Table 4.9: Bridge B7 – truss girder bridge with intermediate bridge deck (additional parameters).

4.9 Bridge B8 – Truss Girder Bridge with Lower Bridge Deck

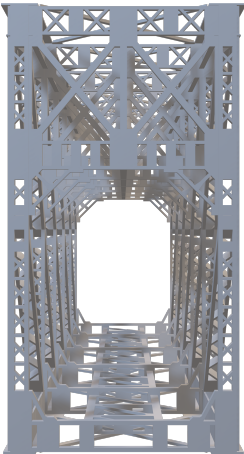
The aerodynamic section model of the truss girder bridge with lower bridge deck and ballast bed is based on geometry of the Prostřední Žleb main span bridge located in km 458.756 of the line Všetaty – Děčín. The bridge has 4 spans. In span 1 and 4 there is a plate girder superstructure with intermediate bridge deck built in 1972. In span 2 and 3 there is a riveted truss girder superstructure with lower bridge deck built in 1916 (used for bridge type B8). The bridge is curved in plan and supported on skewed stone masonry substructure. The spans are $25.0 + 2 \times 99.4 + 25.7$ m long. The superstructure in span 2 and 3 consists of pair of riveted steel truss girders with single directional diagonal members and vertical members. The lower bridge deck consists of cross-beams and longitudinal girders supporting wooden sleepers. The riveted cross-beams are located at each truss girder vertical member. The riveted longitudinal members are inserted between cross-beams. The longitudinal bridge deck members are laterally braced. The main lateral bracing is at the bottom chord level, under the bridge deck. The vertical members are at the upper part braced with the main transverse X bracing and together with transverse top chord bracing from a diaphragm. At the bridge centerline between the main cross bracing there is a longitudinal truss girder bracing, see Figure 4.14 and 4.15. Additional parameters are defined in Table 4.10.



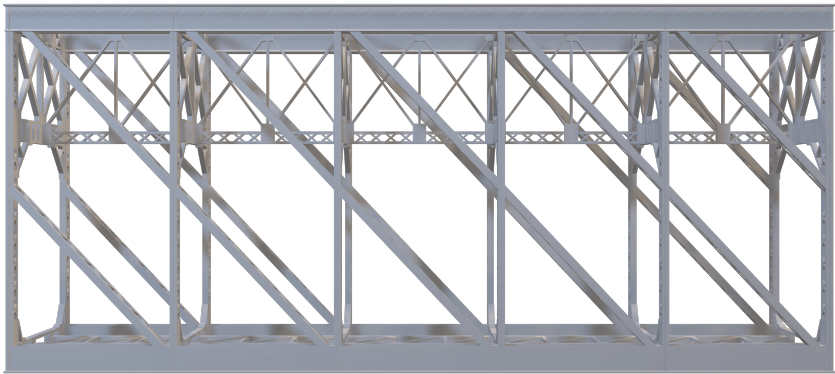
Figure 4.14: Bridge B8 – truss girder bridge with lower bridge deck.



Isometric View



Section View



Elevation View

Figure 4.15: Bridge B8– 3D bridge model.

Superstructure:	Span 1 & 4: steel riveted plate girder superstructure with intermediate bridge deck. Span 2 & 3: steel riveted truss girder superstructure with lower bridge deck.
Static layout of the superstructure:	4 simple spans
Total length of bridge:	265.5 m
Span length:	25.0 + 2x99.4 + 25.7 m
Number of tracks:	1
Transverse arrangement of the bridge:	VMP 2.2
Structural depth:	2.46 m (span 1) 1.24 m (span 2 and 3) 2.65 m (span 4)
Clear depth (decisive):	6.50 m (span 1 and 4) 13.70 m (span 2 and 3)
Structural width:	6.08 m
Wind load parameters	
Wind Zone:	II
Terrain category:	I
Reference height z_e :	19.3 m
Wind pressure $q_p(z_e)$:	1,240 Pa
Reference area A_{ref} :	
Bridge deck:	5.07 m ² /m
Truss girders:	3.69 m ² /m
Force coefficient $c_{f,x}$:	
Bridge deck:	2.15
Truss girders:	1.61
Wind load F_w :	20.7 kN/m
EQU verification per Eurocodes	
Bridge weight:	84.7 kN/m
Bearing spacing:	5.10 m
Center of wind reference area z_w :	4.99 m
Destabilizing moment M_w :	$20.7 \cdot 4.99 = 103.3$ kNm/m
Stabilizing moment M_G :	$(84.7 + 10) \cdot 5.10 / 2 = 236.3$ kNm/m
EQU verification:	$1.50 \cdot 103.3 / (0.95 \cdot 236.3) = 0.70$

Table 4.10: Bridge B8 – truss girder bridge with lower bridge deck (additional parameters).

Chapter 5

Wind Tunnel Experiments

5.1 Wind Tunnel

The wind tunnel measurements were carried out in a climatic wind tunnel located in the Center of Excellence in Telč (CET), which is part of the Institute of Theoretical and Applied Mechanics (UTAM) of the Czech Academy of Science. The wind tunnel is a closed-circuit aerodynamic wind tunnel of the Göttingen type, divided into a climatic and aerodynamic section (Zitny and Ryjacek, 2017), see Figure 5.1. The tunnel consists of two working sections: aerodynamic and climatic. In the aerodynamic section experiments are carried out in the field of wind effects on structures, wind characteristics, local wind flow conditions, pedestrian comfort, aeroelastic response of the structure, diffusion, dispersion of pollutants, effect of flow on heat loss of buildings and ventilation, effect of wind on transport systems and wind energy. The climatic section is used to synergistically model climatic factors such as temperature, rain, frost, and radiant heat. For the majority of bridge samples, the tests were performed in the aerodynamic section which is 1.9 m wide, 1.8 m high and 11 m long, one of the bridge models was too big to fit into the aerodynamic section and therefore it had to be measured in the climatic section of the wind tunnel. In the aerodynamic section, different types of the Atmospheric Boundary Layer can be simulated. The wind speed in empty section ranges between 0.5-33 m/s (Kuznetsov et al., 2015).

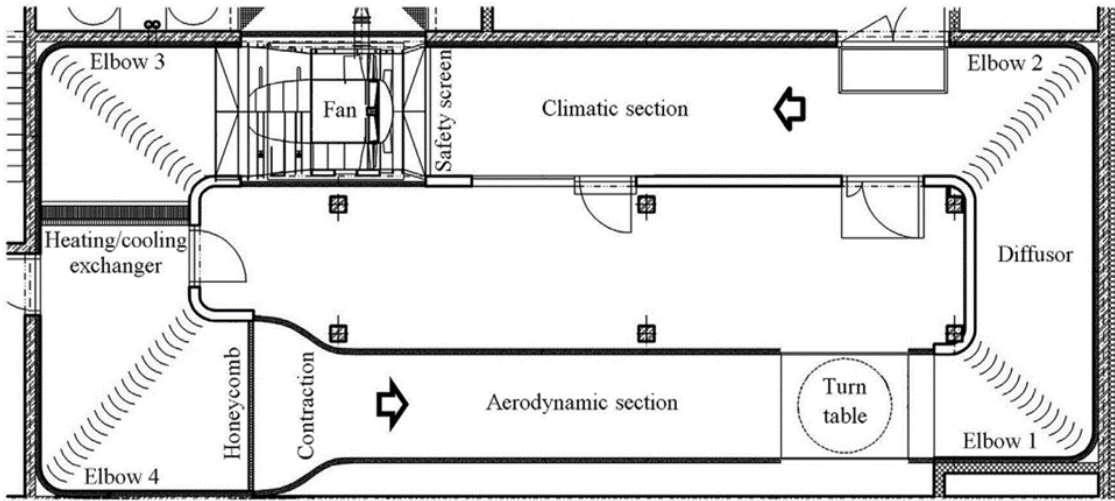


Figure 5.1: Plan view of the climatic wind tunnel (Kuznetsov et al., 2015).

5.2 Measuring Tools

The determination of the air velocity in the working part of the aerodynamic section can be evaluated according to Bernoulli's equation for incompressible liquids:

$$p_c - p_s = \frac{\rho V^2}{2} \quad (5.1)$$

where p_c is the total and p_s is the static airflow pressure; ρ is the density; and V is the air velocity. The **Prandtl-Pitot tube** is used to measure the total and static airflow pressures. The tube allows to measure the dynamic pressure p_d as the pressure difference between the total pressure p_c and the static pressure p_s .

$$p_d = p_c - p_s \quad (5.2)$$

Dynamic pressure can be represented as part of the flow velocity value:

$$p_d = \frac{\rho V^2}{2} \xi \quad (5.3)$$

The air flow velocity is determined from the formula:

$$V = \sqrt{\frac{2p_d}{\rho} \xi} \quad (5.4)$$

where ξ is the Prandtl-Pitot tube coefficient, which is determined during calibration.

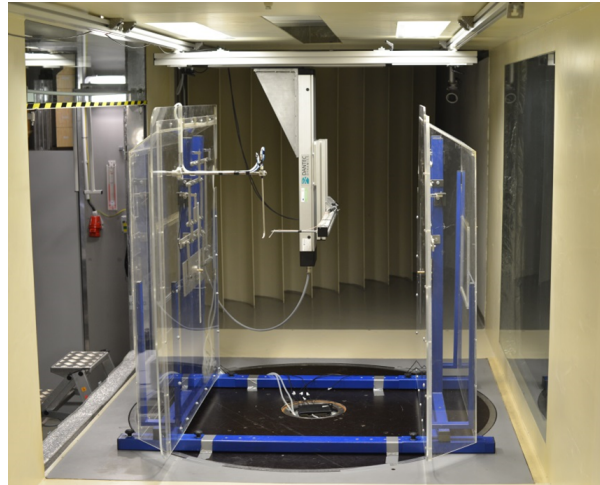


Figure 5.2: Experimental equipment for investigating the aerodynamic properties of bridge models in the working part of the wind tunnel section.

Constant Temperature Anemometry (CTA) is a method for measuring both air velocity and turbulence based on the observation that heat is dissipated from an electrically heated sensor (hot wire) due to circulation. The type of sensor used to measure the flow velocity was Dantec Dynamics 55R01, which is approximately 1 mm long, 2-10 μm in diameter and made of platinum, wolfram or tungsten, i.e. platinum coated wolfram. The advantages of this wind speed measurement system include a very small "measuring point", high sensitivity, high accuracy, high frequency and, above all, a large range of measured speeds (from 0.01 m/s for air). The disadvantages of this method include the fragility of the wire and the sensitivity of the probe to contamination. For this reason, wind speeds were determined with a Prandtl-Pitot probe that was calibrated according to the accurate CTA method.

The **Scanivalve Pressure Scanner** is used to measure air pressures. In this case, to measure the pressure on a Prandtl-Pitot tube and/or to measure the local pressure distribution on the surface of a structure. The pressures are recorded on a DEWETRON industrial and data computer, which is a multi-channel system designed for high sampling data records. The device is applicable for both analogue and digital signals with advanced processing methods. It can be used for single pressure measurements using pressure sensors, in combination with other types of dynamic sensors.

Turbulence generator – one of the measurements investigated the influence of turbulent on aerodynamic properties of the bridge models (turbulence intensity was 0.73 to 9.05 %) and near isotropic turbulence. Turbulent flow was generated using a wooden grating. The grating is composed of wooden prisms with a width of 55 mm and a thickness

of 25 mm, and the clear distance between the prisms is 180 mm. Experimental data from CTA were used to obtain the turbulence intensity and integral scale. The measurements were divided into blocks of one second time length and the spectrum was calculated for each block. The nonlinear least squares method was used to determine the maximum spectral frequency, this was obtained from the normalized average power spectrum and the von Karman velocity spectrum.

$$\frac{nS_U(n)}{\sigma_U^2} = 4 \frac{4n^x L_U / V}{\left[1 + 70.8 (n^x L_U / V)^2\right]^{5/6}} \quad (5.5)$$

where n is the gust frequency, $S_U(n)$ is the power spectral density, L_U is the length of the turbulence in the wind direction, σ_U is the standard deviation of the variable wind speed component in the direction of the mean wind speed U (the average velocity component in the longitudinal direction of the working part of the tunnel, along the X-axis).



Figure 5.3: Vortex generating grid to create turbulent flow in the range of 5 to 30%.

Airflow turbulence is usually expressed in terms of intensity:

$$I_U = \frac{\sigma_U}{U} \quad (5.6)$$

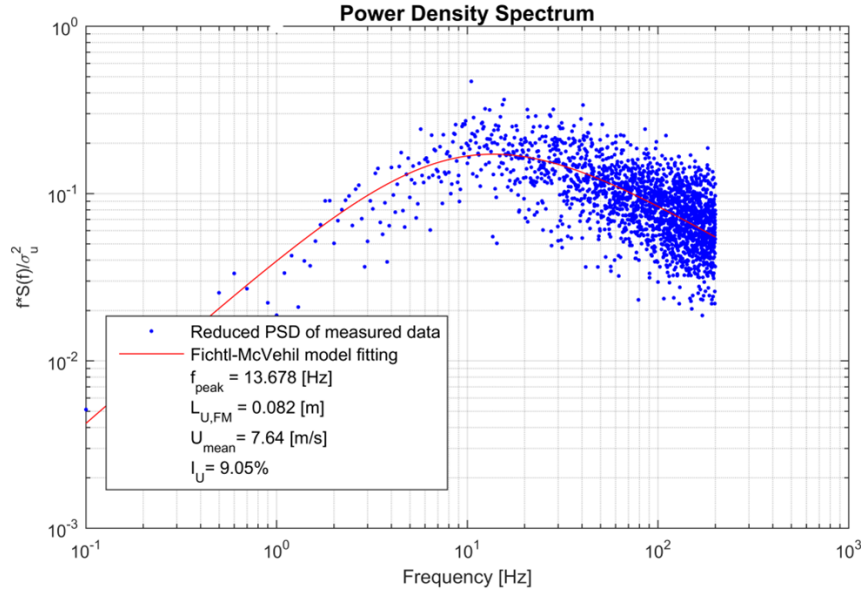


Figure 5.4: Longitudinal turbulence spectra in the wind tunnel. Best fitting curve is given by the von Karman spectrum (Kuznetsov et al., 2015).

5.3 Definitions

Air specific gravity – at air flow velocities corresponding to wind speeds, air can be considered an incompressible medium. Its specific gravity is $\rho_0 = 1.276 \text{ kg} \cdot \text{m}^{-3}$ at a temperature of 0°C and pressure $p_0 = 100,000 \text{ Pa}$. The specific gravity of air can also be determined at other temperatures and pressures. Whereby the thermal expansion of air is $\gamma = 0.000367 \text{ K}^{-1}$, p is the atmospheric pressure and t is the temperature in $^\circ\text{C}$.

$$\rho = \frac{\rho_0}{1 + \gamma \cdot (273 + t)} \cdot \frac{p}{p_0} \quad (5.7)$$

The internal friction coefficient is equal to $\eta = 17.177 \cdot 10^{-6} \text{ N} \cdot \text{s} \cdot \text{m}^{-2}$ at 0°C . It increases slightly with increasing temperature. Since the internal friction coefficient is very small, the internal friction is applied only in a very small area around the obstacle.

Reynolds number Re – The mode of air flow around a body is determined by the Reynolds number, the intensity of turbulence in the direction of the air flow and the surface roughness of the body being flown around. The Reynolds number is calculated as:

$$Re = \frac{V \cdot H}{\nu} \quad (5.8)$$

where H is the characteristic cross-sectional height of the model, ν is the kinematic viscosity of air (at temperature of 15°C and pressure of 980 hPa it is equal to $1.455 \cdot 10^{-6} \text{ m}^2 \cdot \text{s}^{-1}$). When making experimental measurements in a wind tunnel, it is important to achieve the same or similar Re number as for the real structure in order to achieve the same wrap-around mode for the model. When these conditions are met, the aerodynamic coefficients of drag, lift and moment of the model are identical to reality. It is sometimes very difficult to achieve this similarity of Re numbers, but it is possible to define an interval in which the character of the body wrapping is almost unchanged.

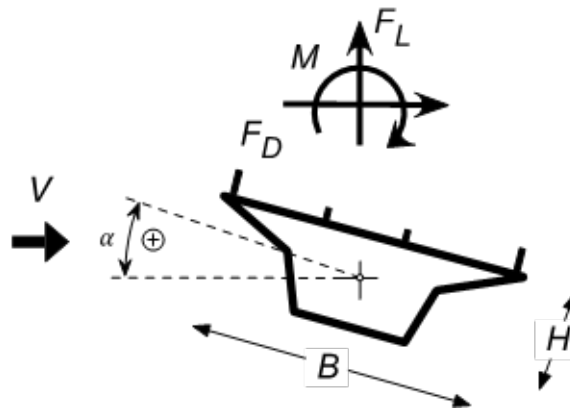


Figure 5.5: Definition of dimensions, aerodynamic forces and wind attack angle rotation.

The determination of the quasi-static wind load action on bridge structures is a typical problem of aerodynamics. It involves either finding the dynamic pressure p_d at a sufficient number of points on the surface of the structure to determine the dynamic pressure isolines and related compressive forces and moments acting on the entire structure. The second method involves determining the position and magnitude of the resultant of all elementary dynamic pressures and its component relative to the model coordinate system.

Drag force coefficient – The effects of static wind action are generally most pronounced in the direction of the wind. The total force on the structure in the direction of the wind can be expressed by:

$$F_D = \frac{1}{2} \rho v^2 C_D A_{ref} \quad (5.9)$$

$$C_D = \frac{2F_D}{\rho v^2 A_{ref}} \quad (5.10)$$

where C_D is the aerodynamic drag coefficient, A_{ref} is the projected area of the model into the plane perpendicular to the wind direction at the wind attack angle $\alpha = 0^\circ$. A_{ref}

can be calculated from H height and L length of the model for solid bodies (plate girder bridges), Eq. 5.11. However, for truss bridges with voids it should be assumed as the area of the bridge deck plus the unobstructed area of all trusses. The reference area is defined in different ways by many authors, therefore when taking and comparing aerodynamic coefficients from other sources, it is necessary to consistently check which reference area has been used to determine the aerodynamic coefficients. For truss girder bridges the reference area is considered according to Eq. 5.12.

$$A_{ref} = H \cdot L \quad (5.11)$$

$$A_{ref} = A_{deck} + n_{truss} \cdot A_{truss} \quad (5.12)$$

Lift coefficient – the second important static component of wind effects is the force acting perpendicular to the wind direction. The force acting in this direction can be expressed by:

$$F_L = \frac{1}{2} \rho v^2 C_L A_{ref} \quad (5.13)$$

$$C_L = \frac{2F_L}{\rho v^2 A_{ref}} \quad (5.14)$$

where C_L is the lift aerodynamic coefficient, A_{ref} is the area of projection of the structure into a plane parallel to the wind direction at the wind attack angle $\alpha = 0^\circ$.

$$A_{ref} = B \cdot L \quad (5.15)$$

where B is the dimension of the structure parallel to the airflow, at the wind angle $\alpha = 0^\circ$.

Moment coefficient – the component of the static wind action is the torque expressed by the relation:

$$F_M = \frac{1}{2} \rho v^2 C_D B^2 L \quad (5.16)$$

$$C_M = \frac{2F_M}{\rho v^2 B^2 L} \quad (5.17)$$

where C_L is the aerodynamic moment coefficient.

Aerostatic instability – as the air velocity increases, the moment acting on the bridge deck increases. At a certain speed of the airflow and a loss of static stability or divergence

may occur. Due to the aerodynamic moment, the bridge deck twists about the center of torsion by an angle denoted α , and this increases due to the increasing moment, thus increasing the torque again, until the loss of stability, provided that the derivative of the aerodynamic moment coefficient C'_M is positive.

$$M_\alpha = \frac{1}{2}\rho \cdot v^2 \cdot \left(C_M + \frac{dC_M}{d\alpha} \alpha \right) \quad (5.18)$$

from which a relationship can be derived for the critical wind speed causing the bridge deck to buckle:

$$V_{crit} = \sqrt{\frac{2K_\alpha}{\rho \cdot B^2 \cdot C'_M}} \quad (5.19)$$

where K_α is the torsional stiffness of the bridge deck, C'_M is the derivative of the aerodynamic moment coefficient with respect to rotation, and B is the width of the bridge deck.

5.4 Experimental Determination of Aerodynamic Coefficients

5.4.1 Experiment Calibration

Aerodynamic scales are an experimental equipment used to measure the aerodynamic response of a model. In this project, the verified scales produced at the UTAM CET were used, see Figure 5.6.

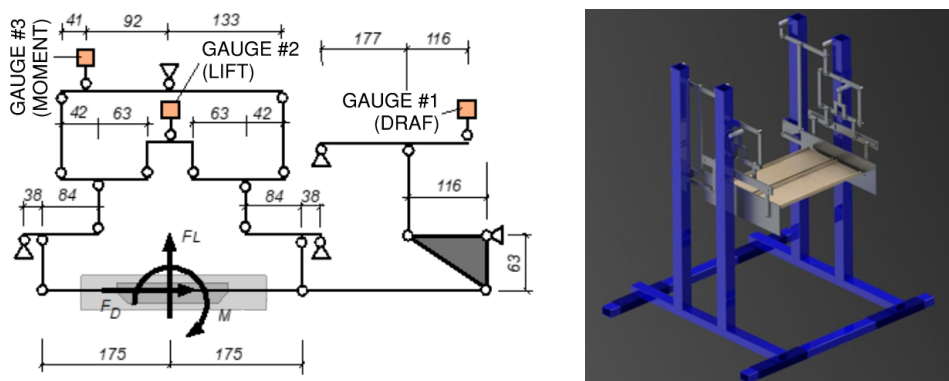


Figure 5.6: Aerodynamic scales – kinematic diagram and wiring of strain gauges.

The drag, lift and moment forces are measured by set of three strain gauges. The kinematic mechanism of scales is covered to prevent wind effects on the scale arms or to

prevent oscillation and other undesirable effects. The calculation of the ratio of drag force, moment and lift force is based on the kinematic system of aerodynamic scales. Strain gauge 1 measures the drag force, strain gauge 2 the lift force and strain gauge 3 the moment. The fixing mechanism allows rotation of the model around its centerline axis. This feature was used during the test to change the wind attack angle. From the moment equilibrium, the forces on the individual gauges can be derived. Knowing the kinematic relations of the aerodynamic scales, it is possible to calculate the individual aerodynamic forces:

$$F_{D,L,M} = \Delta U \frac{\alpha}{k_{D,L,M}} \quad (5.20)$$

where ΔU is the voltage change across the sensor, α is the calibration relation of each sensor, and $k_{M,L,D}$ are the kinematic coefficients for moment, lift and drag.

Aerodynamic model – models tested in a wind tunnel can be generally divided into two basic groups, aerodynamic and aeroelastic. For aerodynamic models, only geometric similarity to the real structure is required. Such models are mainly used to solve the problem of determining aerodynamic coefficients. In addition to geometric similarity, aeroelastic models must also satisfy certain modeling laws and it is necessary to model stiffness, mass and damping of the structure. For determination of aerodynamic coefficients of bridges full models as well as sectional model can be used. However, geometric similarity of the cross-section must be guaranteed. The bridge models tested in the wind tunnel were aerodynamic models stiff enough to prevent any aeroelastic behavior during the wind tunnel experiment, majority of the models were sectional (Jirsak, 2009; Fisher et al., 1977; Fisher and Pirner, 2003).

Model blocking – placing a model in a wind tunnel always results in a "blocking" effect. This effect must therefore be evaluated with each measurement. The aerodynamic model wrapping can affect the air flow velocity measured by the Prandtl-Pitot tube placed in front of the object. This effect is undesirable for the determination of the aerodynamic coefficients. For the determination of the aerodynamic coefficients, it is necessary to consider a wind speed flowing towards the model that is unaffected by the model, i.e. at a sufficient distance in front of the model. For these reasons, the wind velocity profile in the scales was investigated in detail using the CTA method. Using detailed velocity profiles and the known fan motor power input, a relationship could be established that determines the relationship between the model unaffected air velocity in the scales and the fan power input. Further, the fan power input was used to determine the wind speed in scales. This

method was verified and calibrated on a model of a cylinder placed in the aerodynamic scales. This measurement serves as a benchmark in aerodynamic tests since cylinder has a well-known aerodynamic coefficient of drag as a function of speed Figure 5.7.

The graph in Figure 5.7 shows that the calibration of the scales and the wind speed calculation is correct, since the aerodynamic coefficient of the cylinder is $C_D = 1.2$. The determination of the aerodynamic coefficient was based on three measurements. It can be observed that with larger Reynolds numbers there is a larger scatter in the measured values. This dispersion is caused by the proximity of the critical Re number where there is a large decrease in the drag coefficient.

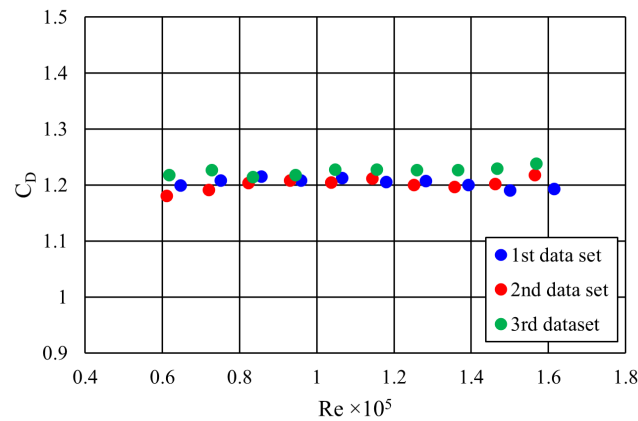


Figure 5.7: Graph of cylinder drag coefficient dependent on Reynolds number.

Determination of optimal wind flow velocity during measurements – the aerodynamic coefficients for all bridges were measured using the same airflow velocity. To maintain the model similarity, it would be optimal to achieve the same Re number as in reality. This would lead to high wind speeds with the assumed bridge model scale, which is uneconomical and even impossible in terms of the model strength. The nature of wrapping of the sharp-edge bodies such as models of bridges does not change from relatively low Re values as turbulent flow already occurs at low wind speeds. Therefore, it is unnecessary to keep the Re number of the model the same as in reality. In order to determine the optimal airflow velocity, one of the bridge models was tested with different Re values. For this experiment, the B3 bridge model was chosen. Figure 5.8 shows the relationship between the aerodynamic drag coefficient and the Re number. It was determined that the ideal speed for all wind tunnel experiments should be $Re = 9 \cdot 10^4$ which corresponds to approximately $v = 15 m/s$.

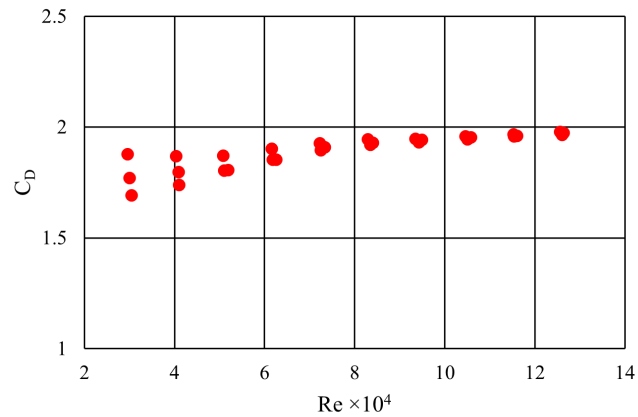


Figure 5.8: Graph of relationship between drag coefficient and Reynolds number – Bridge B3.

Turbulence effect. The turbulence intensity has a significant effect on the values of the aerodynamic coefficients. The intensity of airflow turbulence between the scales was measured by CTA. It was found that without the grid, which generates turbulent flow, the airflow turbulence is equal to $I_u = 0.73\%$ and with the grid it is equal to $I_u = 9.05\%$. The graph in Figure 5.9 shows the aerodynamic drag coefficients of both the cylinder and the bridge B3 in relationship with Re for two different turbulence intensities. All main experiments have been measured with turbulence intensity $I_u = 0.73\%$.

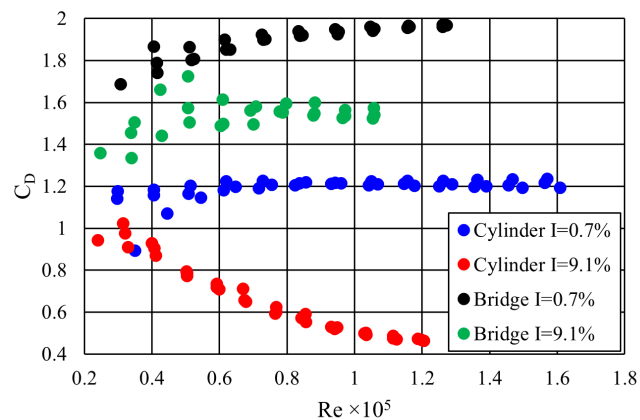


Figure 5.9: Graph of relationship between drag coefficient and Reynolds number – Bridge B3 and Cylinder for two turbulence intensities.

5.4.2 Bridge B1 – Plate Girder Bridge with Rail Directly Fixed to Top Flange

The aerodynamic model of the plate girder bridge with rail directly fixed to the top flange was fabricated from plastic board in a scale of 1:25. See Figure 5.10 for model mounted in the aerodynamic scales. See Figure 5.11 for measured aerodynamic coefficients.

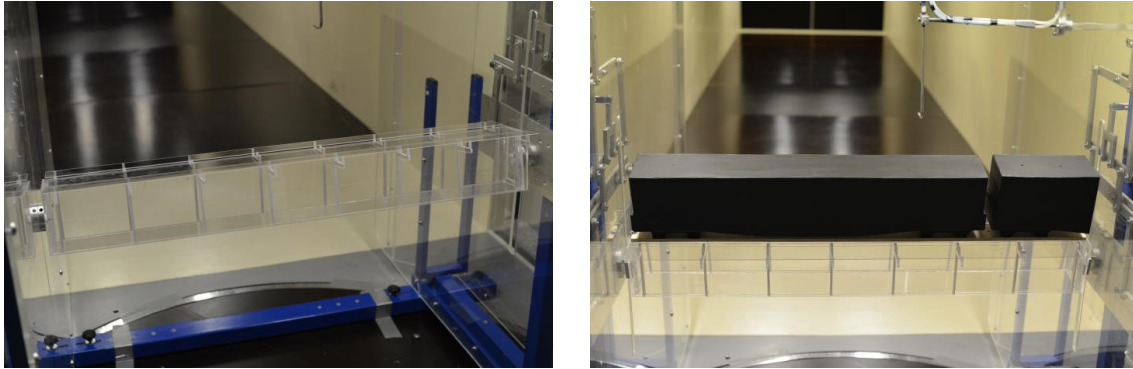


Figure 5.10: Bridge B1 – Aerodynamic model.

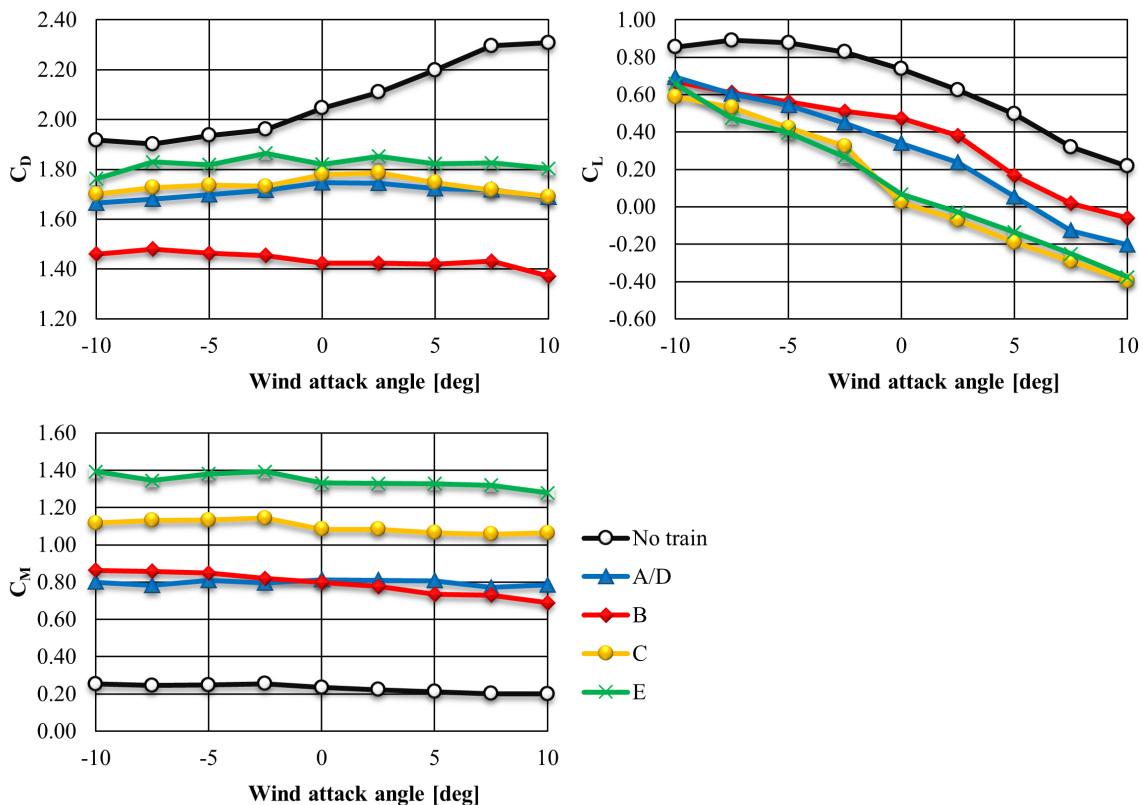


Figure 5.11: Bridge B1 – aerodynamic coefficients.

5.4.3 Bridge B2 – Plate Girder Bridge without Bridge Deck

The aerodynamic model of the plate girder bridge without bridge deck was fabricated from plastic board in a scale of 1:25. See Figure 5.12 for model mounted in the aerodynamic scales. See Figure 5.13 for measured aerodynamic coefficients.

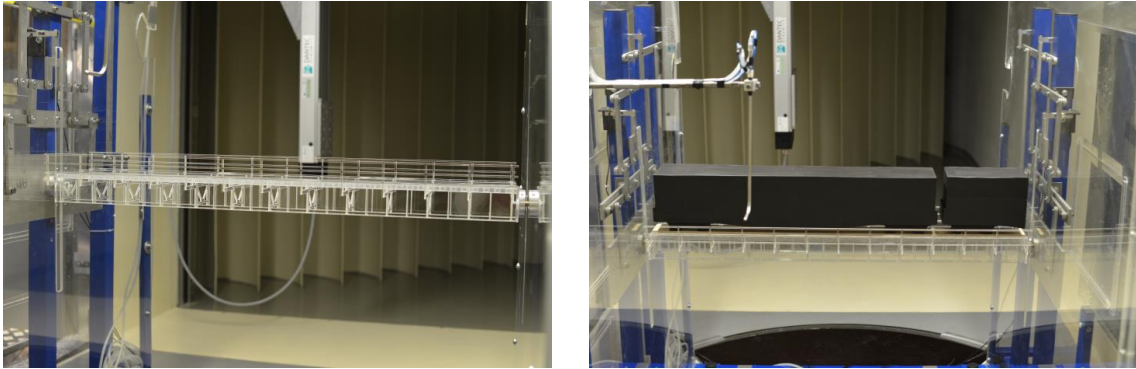


Figure 5.12: Bridge B2 – Aerodynamic model.

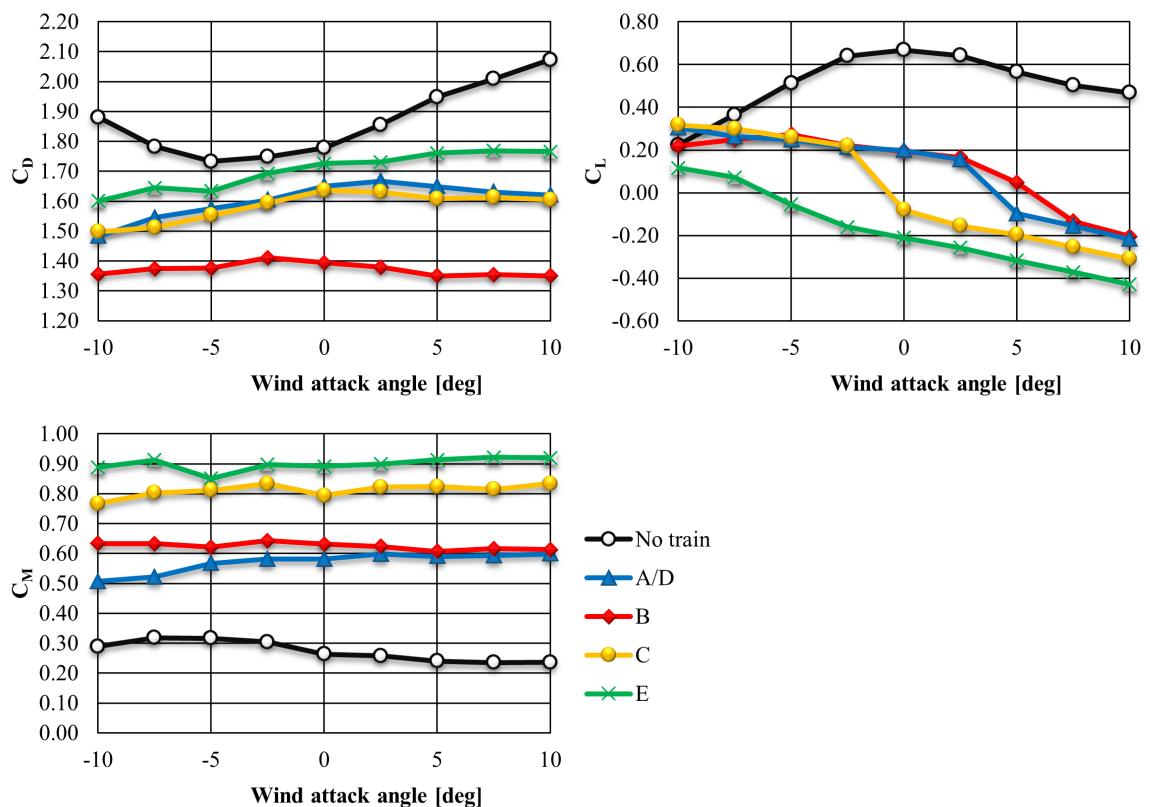


Figure 5.13: Bridge B2 – aerodynamic coefficients.

5.4.4 Bridge B3 – Plate Girder Bridge with Intermediate Bridge Deck

The aerodynamic model of the plate girder bridge with intermediate bridge deck was fabricated from plastic board in a scale of 1:25. See Figure 5.14 for model mounted in the aerodynamic scales. See Figure 5.15 for measured aerodynamic coefficients.

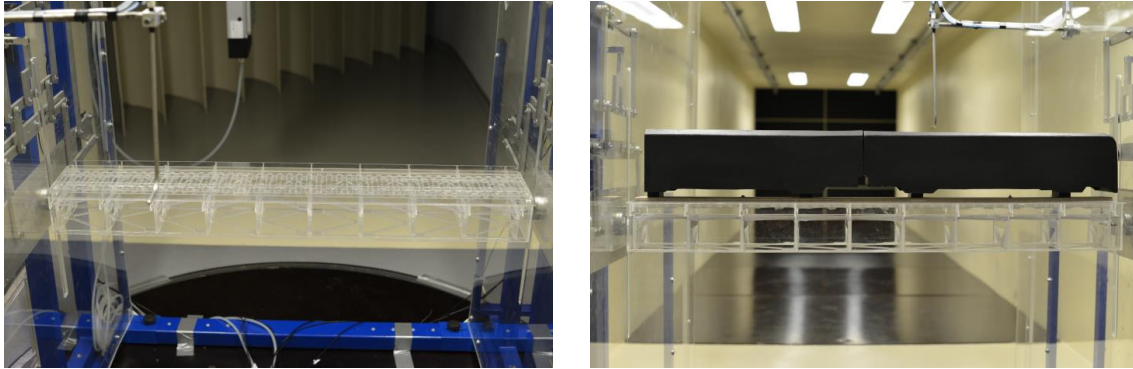


Figure 5.14: Bridge B3 – Aerodynamic model.

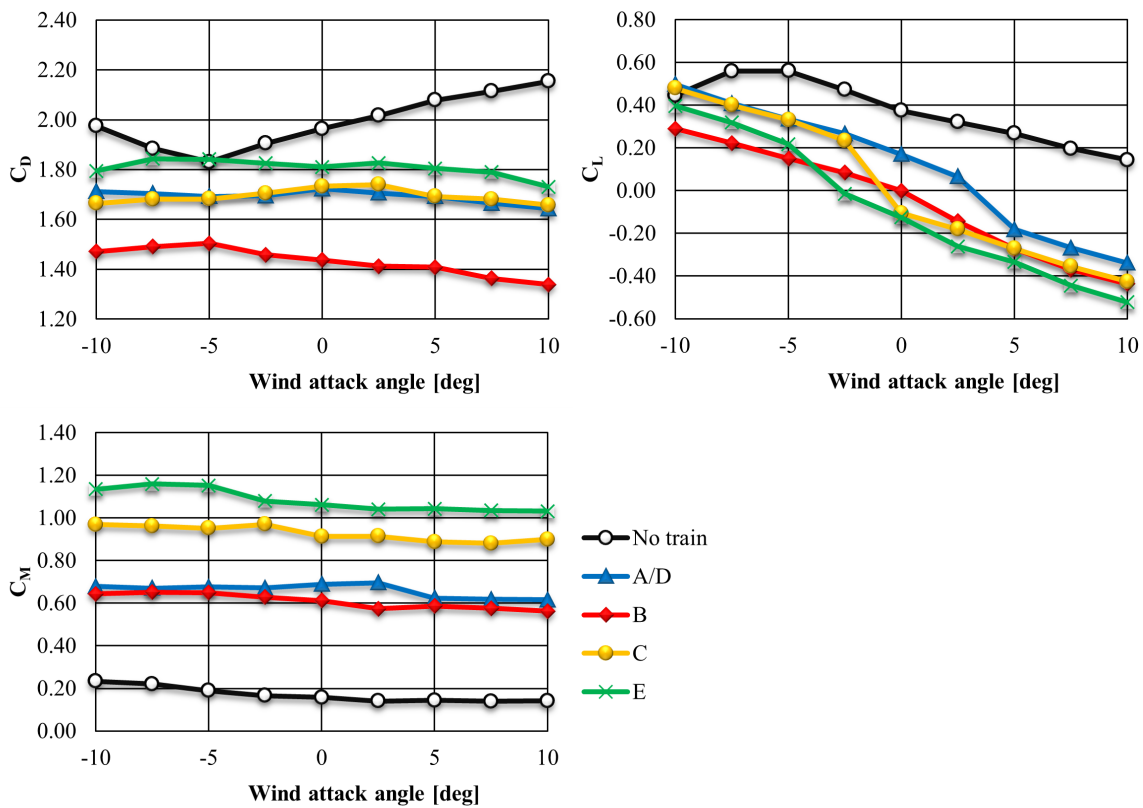


Figure 5.15: Bridge B3 – aerodynamic coefficients.

5.4.5 Bridge B4 – Plate Girder Bridge with Lower Bridge Deck

The aerodynamic model of the plate girder bridge with lower bridge deck was fabricated from plastic board in a scale of 1:25. See Figure 5.16 for model mounted in the aerodynamic scales. See Figure 5.17 for measured aerodynamic coefficients.

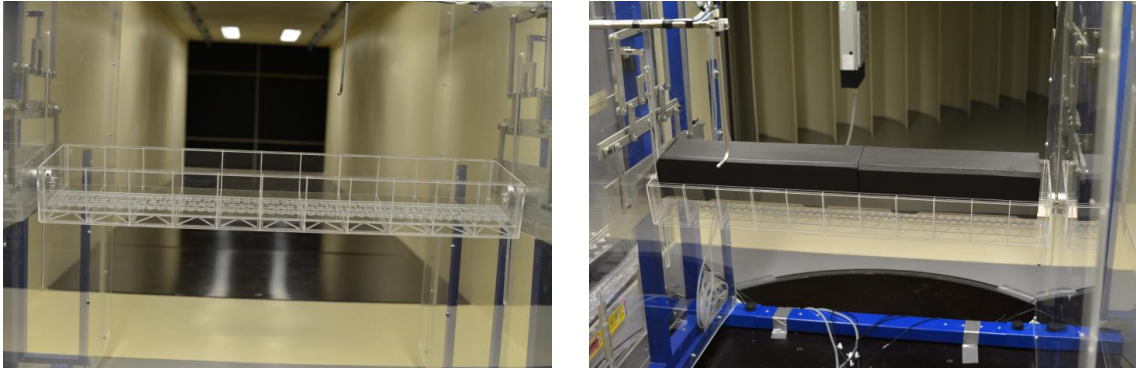


Figure 5.16: Bridge B4 – Aerodynamic model.

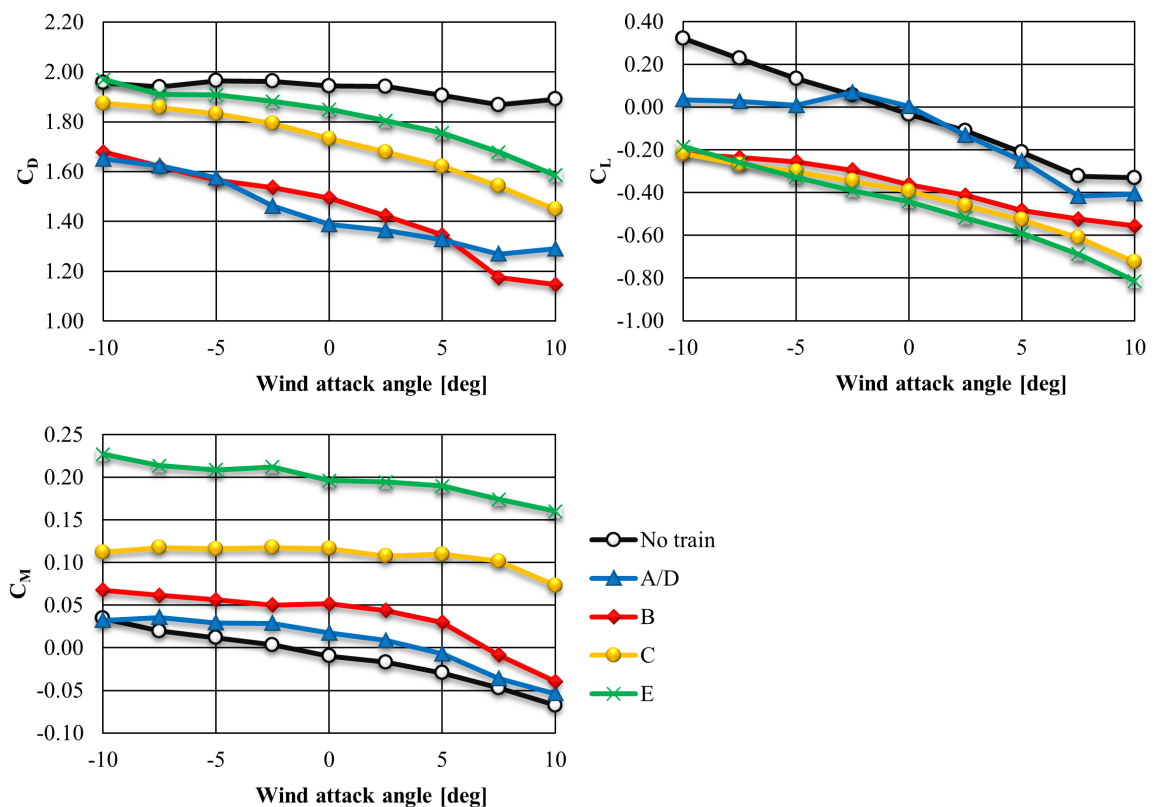


Figure 5.17: Bridge B4 – aerodynamic coefficients.

5.4.6 Bridge B5 – Truss Girder Bridge with Upper Bridge Deck and Ballast Bed

The aerodynamic model of the truss girder bridge with upper bridge deck and ballast bed was fabricated from plastic board in a scale of 1:60. See Figure 5.18 for model mounted in the aerodynamic scales. See Figure 5.19 for measured aerodynamic coefficients.

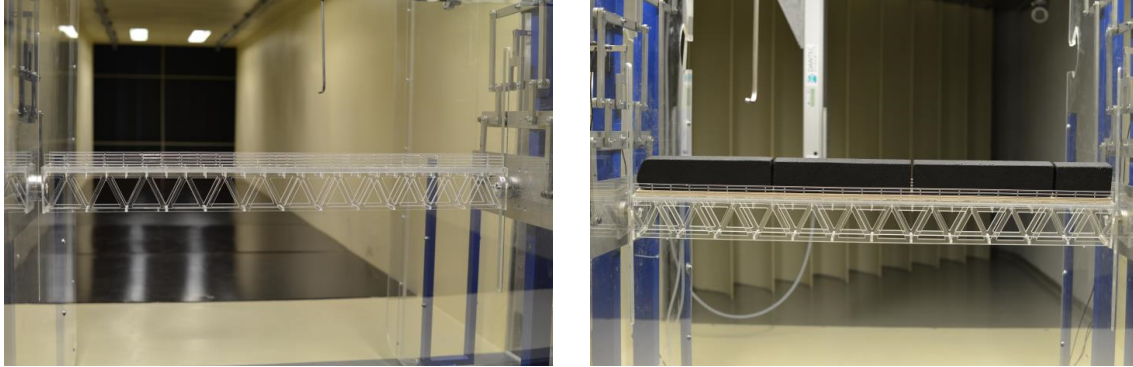


Figure 5.18: Bridge B5 – Aerodynamic model.

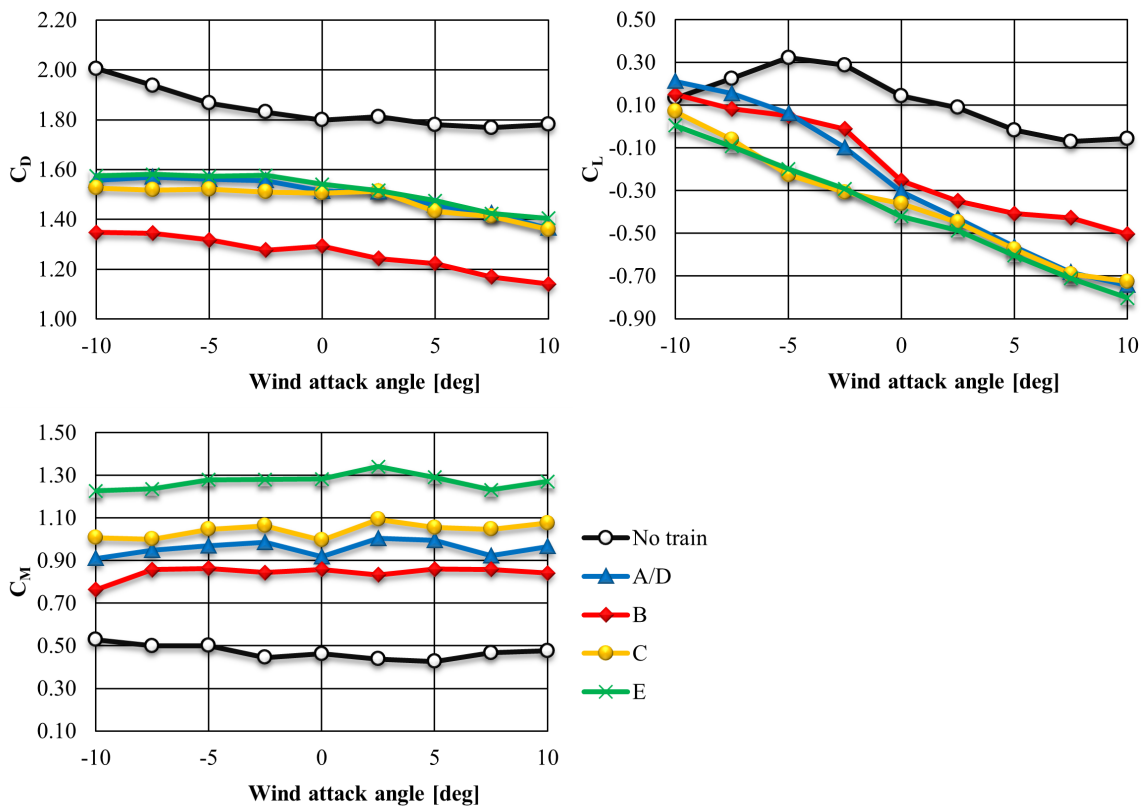


Figure 5.19: Bridge B5 – aerodynamic coefficients.

5.4.7 Bridge B6 – Truss Girder Bridge with Upper Bridge Deck

The aerodynamic model of the truss girder bridge with upper bridge deck was fabricated from aluminum in a scale of 1:30. This model was borrowed from TOPCON and this was the only model measured in the climatic chamber of the wind tunnel, see Figure 5.20. See Figure 5.21 for model mounted in the aerodynamic scales. See Figure 5.22 for measured aerodynamic coefficients.

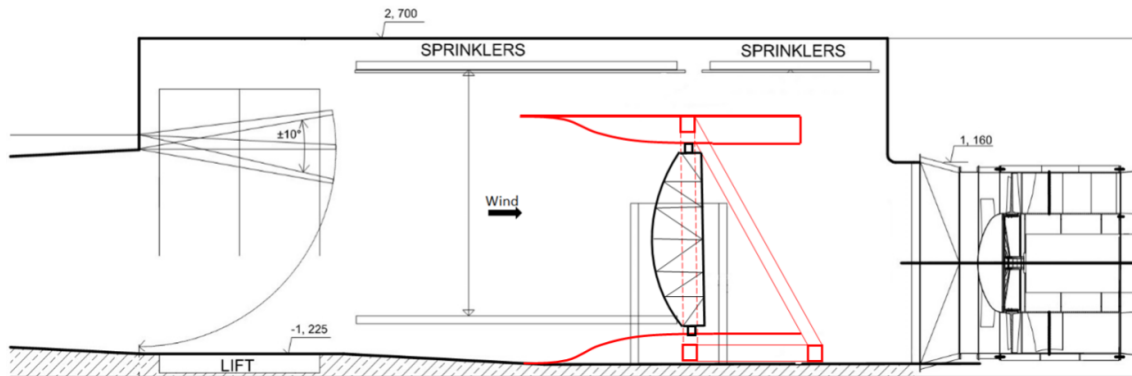


Figure 5.20: Diagram of the climatic section of the tunnel with bridge placement.

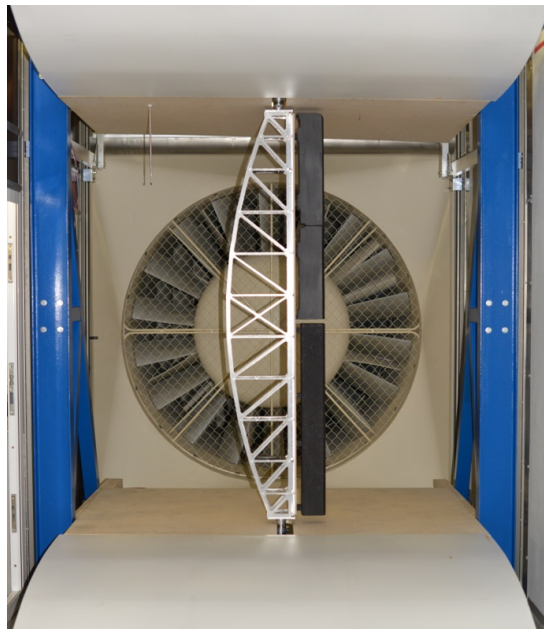


Figure 5.21: Diagram of the climatic section of the tunnel with bridge placement.

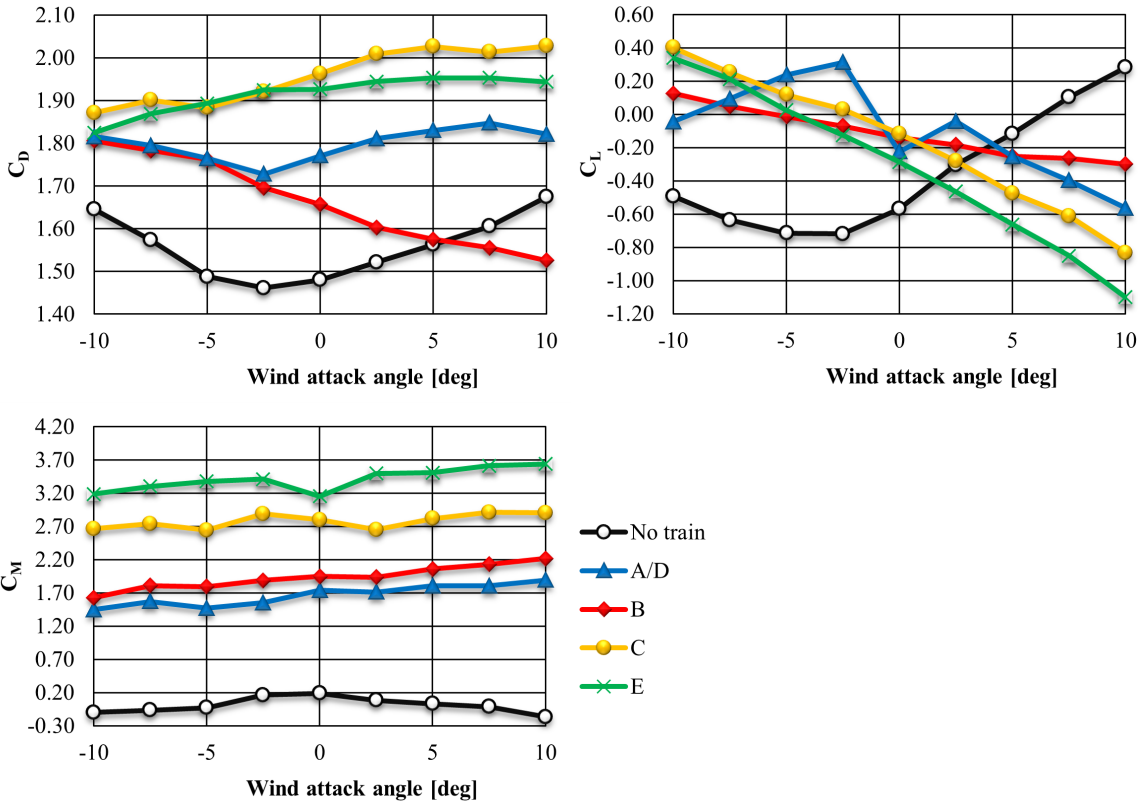


Figure 5.22: Bridge B6 – aerodynamic coefficients.

5.4.8 Bridge B7 – Truss Girder Bridge with Intermediate Bridge Deck

The aerodynamic model of the truss girder bridge with intermediate bridge deck was 3D printed in a scale of 1:25. See Figure 5.23 for model mounted in the aerodynamic scales. See Figure 5.24 for measured aerodynamic coefficients.

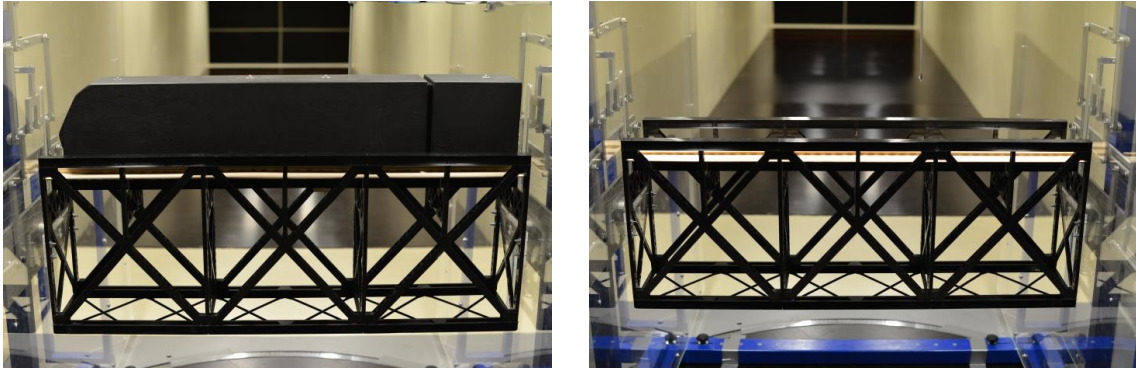


Figure 5.23: Bridge B7 – Aerodynamic model.

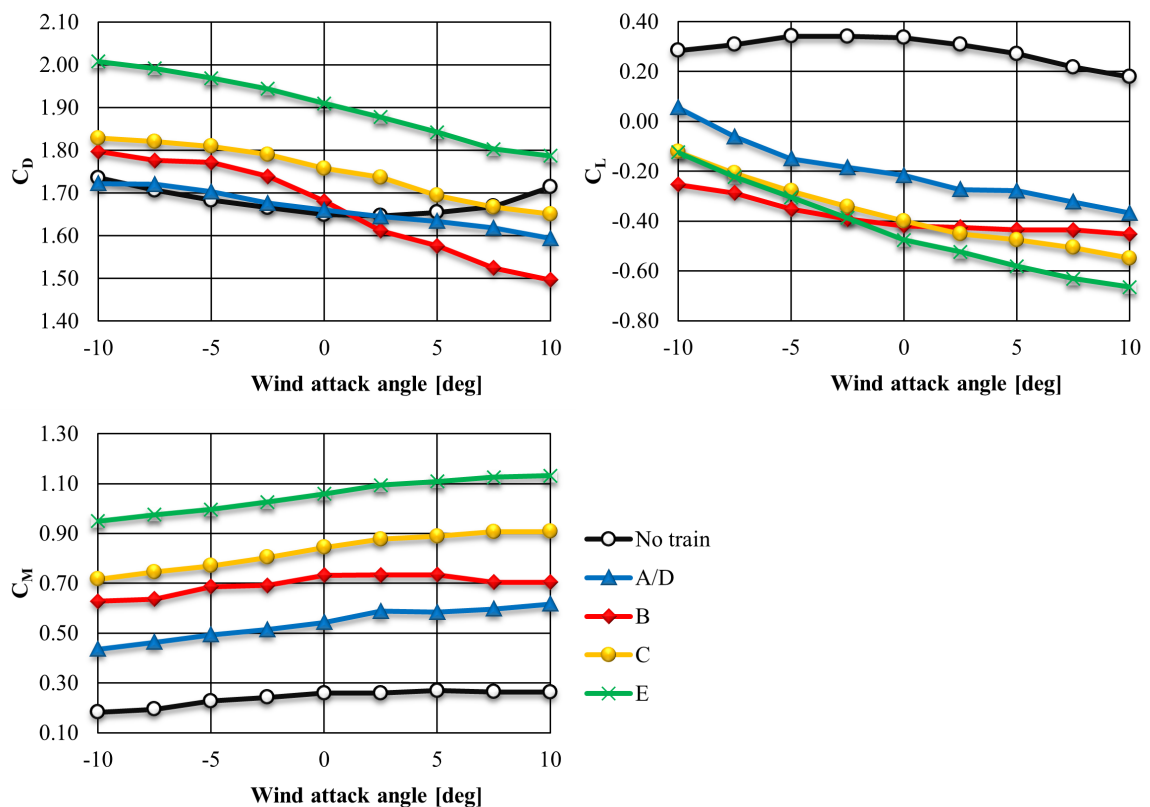


Figure 5.24: Bridge B7 – aerodynamic coefficients.

5.4.9 Bridge B8 – Truss Girder Bridge with Lower Bridge Deck

The aerodynamic model of the truss girder bridge with lower bridge deck was 3D printed in a scale of 1:25. See Figure 5.25 for model mounted in the aerodynamic scales. See Figure 5.26 for measured aerodynamic coefficients.

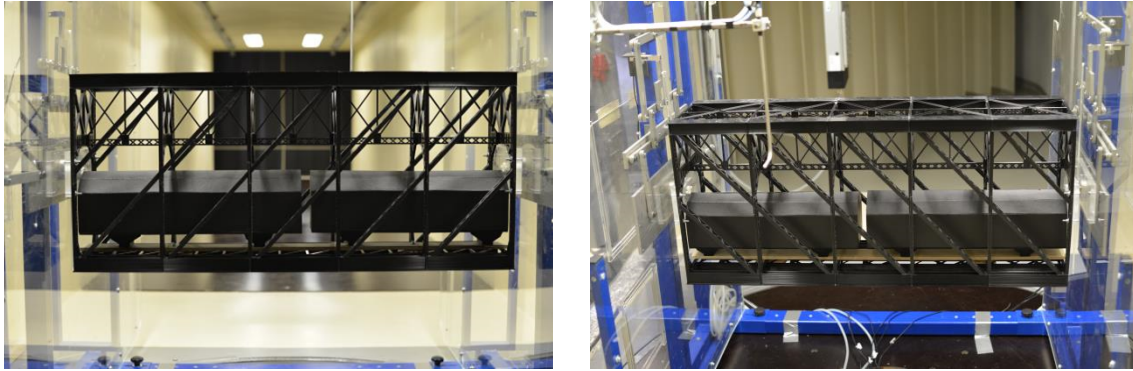


Figure 5.25: Bridge B8 – Aerodynamic model.

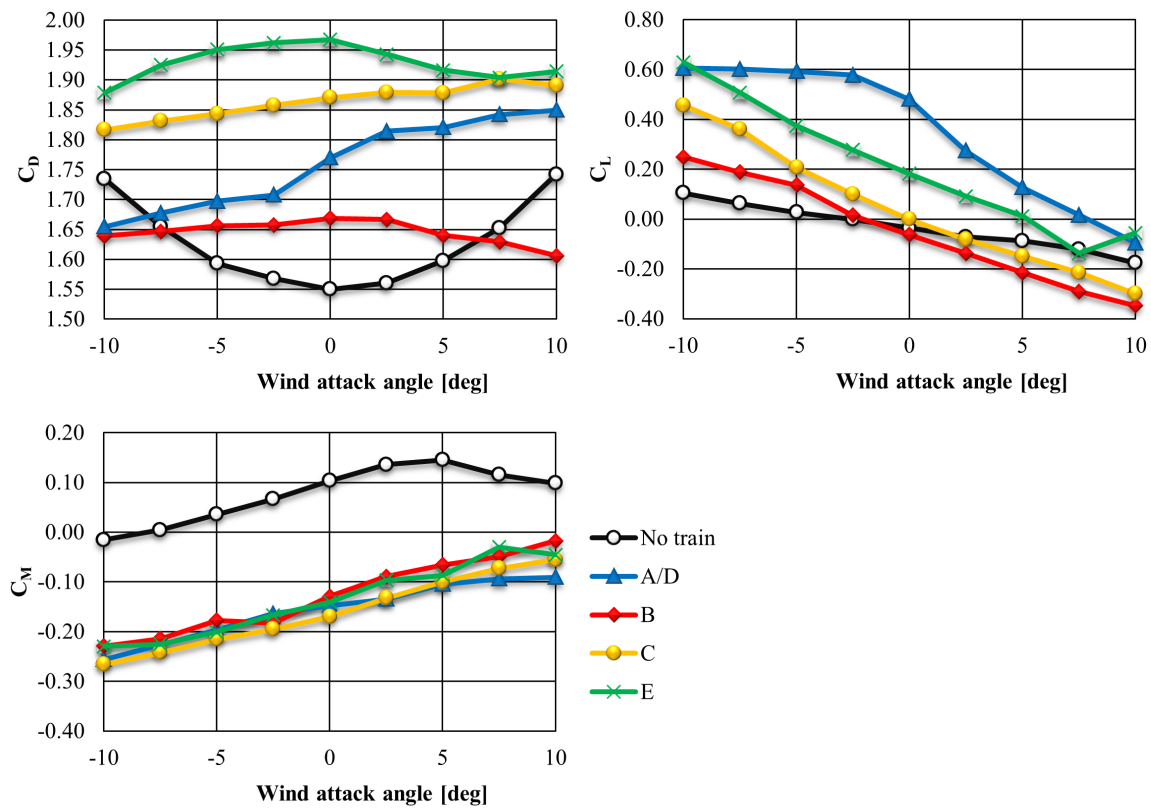


Figure 5.26: Bridge B8 – aerodynamic coefficients.

5.5 Results of Specific Measurements

In this section, the results for following specific measurement are presented: a) the effect of turbulent airflow; b) the effect of ground distance from the bridge; and c) the investigation of the interaction of the windward and leeward parts of the truss girders. The analysis investigates what is the effect of on the aerodynamic coefficients. Reduced number of measurements was performed on the bridges B2, B7 and B8 without traffic or with Class A/D train.

5.5.1 Effect of Turbulence on Aerodynamic Coefficients

The section models were tested for two cases of airflow with different turbulence intensity, which has a significant effect on the values of aerodynamic coefficients. Due to the nature of the tests, it was not necessary to model the atmospheric boundary layer in both cases. The velocity and turbulence intensity profile along the tunnel height was realized as constant. The actual flow velocity was measured using a Prandtl-Pitot tube and a CTA probe. Both probes were placed at a sufficient distance from the model to avoid distortion of the measured velocity due to blocking of the airflow by the model. The CTA method was also used to measure the turbulence intensity of the airflow. The turbulence intensity without the turbulence generator was $I_u = 0.73\%$. The integral scale values were obtained by tuning the normalized power spectrum distribution of the longitudinal airflow velocity component to the theoretical Fichtl-McVehil model. This type of airflow was considered as laminar. A wooden grid was used to obtain higher turbulence intensity. The grid was placed at a distance of 2 m from the aerodynamic chamber. According to the CTA measurements, generated a turbulence intensity of approximately $I_u = 9.05\%$ with an integral length of $L_u = 0.105\text{ m}$.

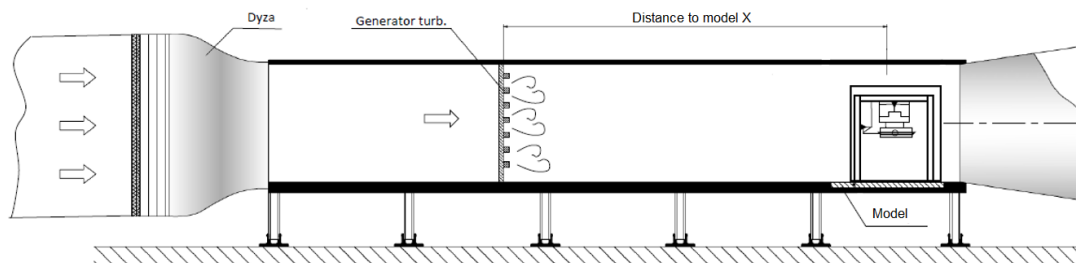


Figure 5.27: Experiment setup with turbulence generator in the aerodynamic section.

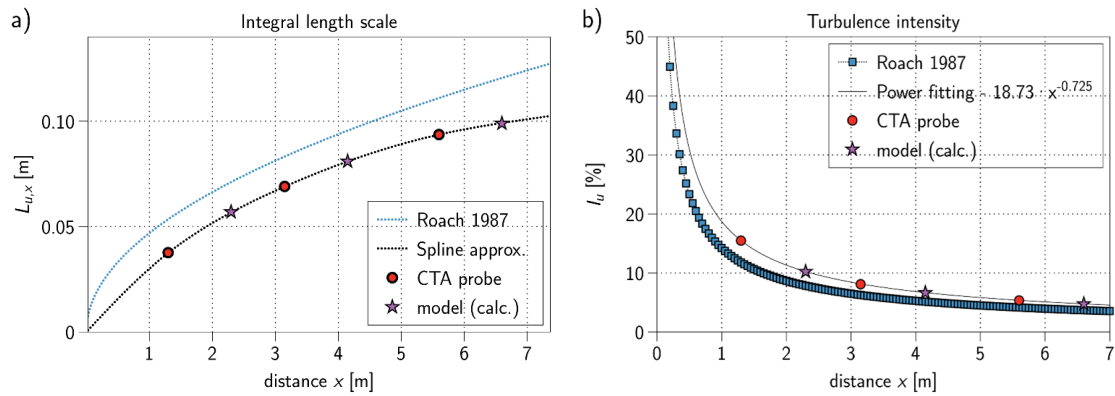


Figure 5.28: Experimental relationship between turbulence intensity and the distance to the test site.

Figure 5.28 a) shows the tendency of the turbulence length integral scale $L_{u,x}$ to increase with increasing distance from the turbulence generator. The values of the turbulence length integral scale measured in the tunnel are given together with the theoretical values according to Roach (Roach, 1987). The dependence of the turbulence intensity has the opposite trend and as the distance from the grid increases, the value of turbulence intensity of the airflow decreases as shown in Figure 5.28 b). The intensity and integral length scale values of turbulence were calculated according to the current position of the model.

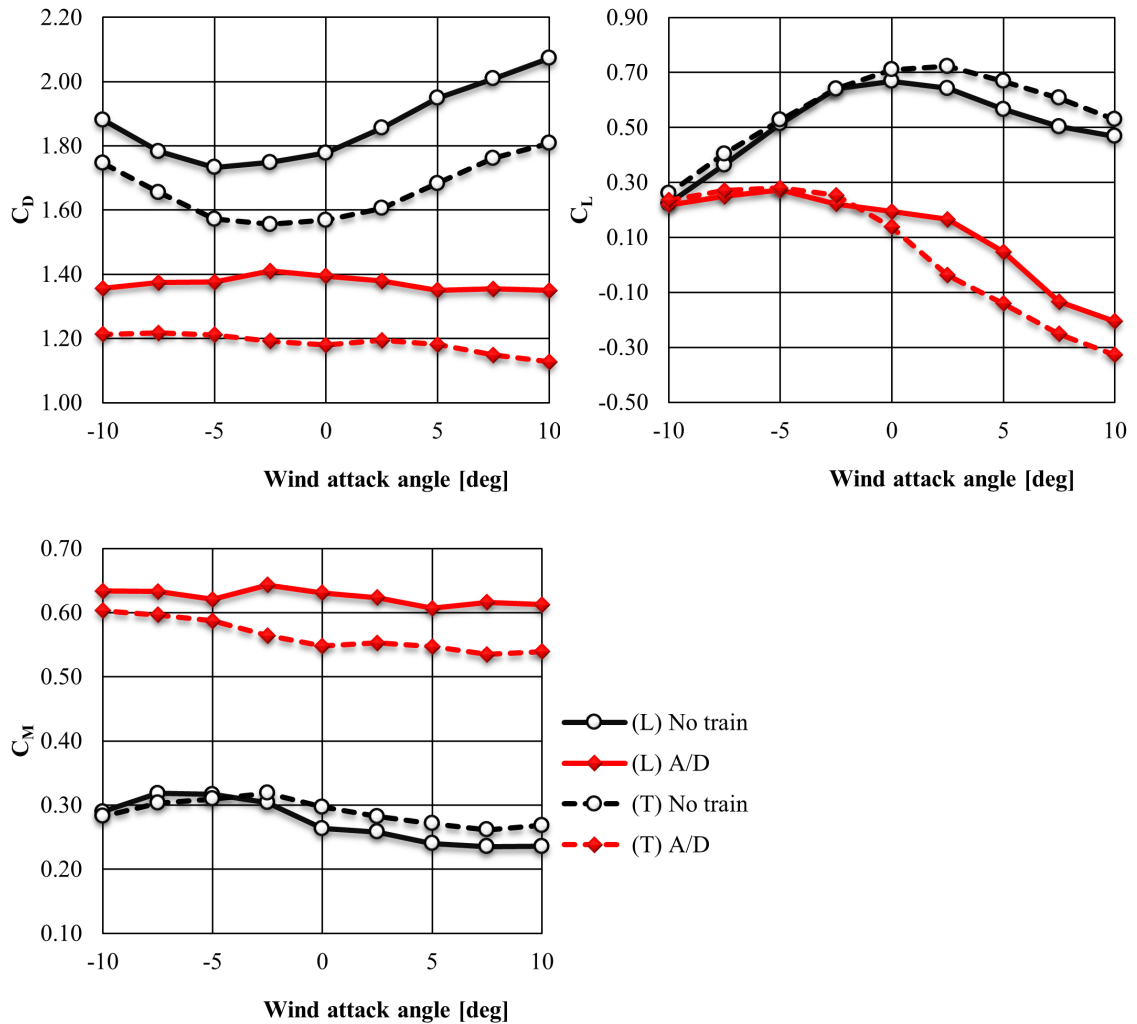
Bridge B2**Description:** Plate girder bridge without bridge deck**Scale:** 1:25

Figure 5.29: Bridge B2 – Comparison of force and moment coefficient values for laminar (L) and turbulent (T) airflow.

Bridge B7

Description: Truss girder bridge with intermediate bridge deck

Scale: 1:25

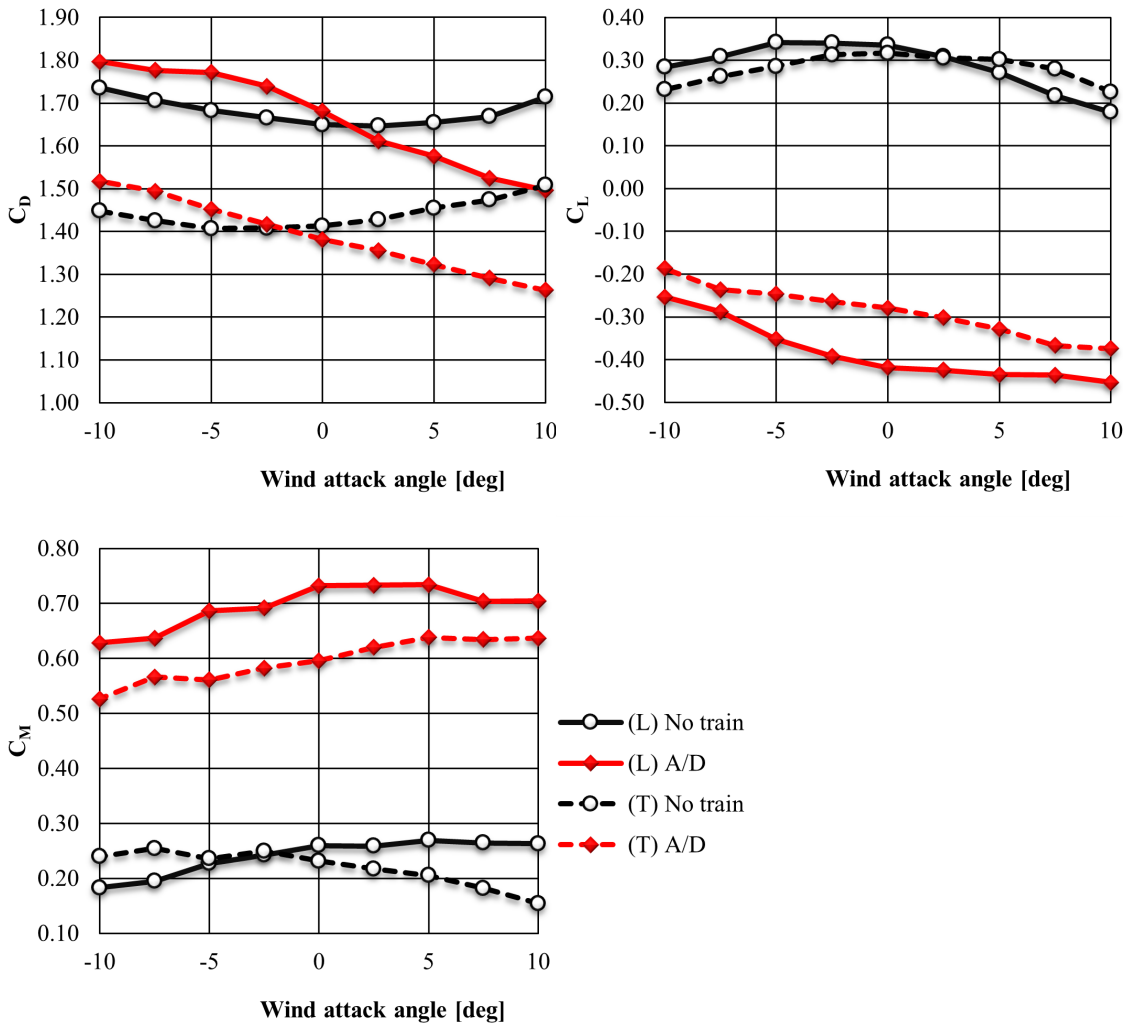


Figure 5.30: Bridge B7 – Comparison of force and moment coefficient values for laminar (L) and turbulent (T) airflow.

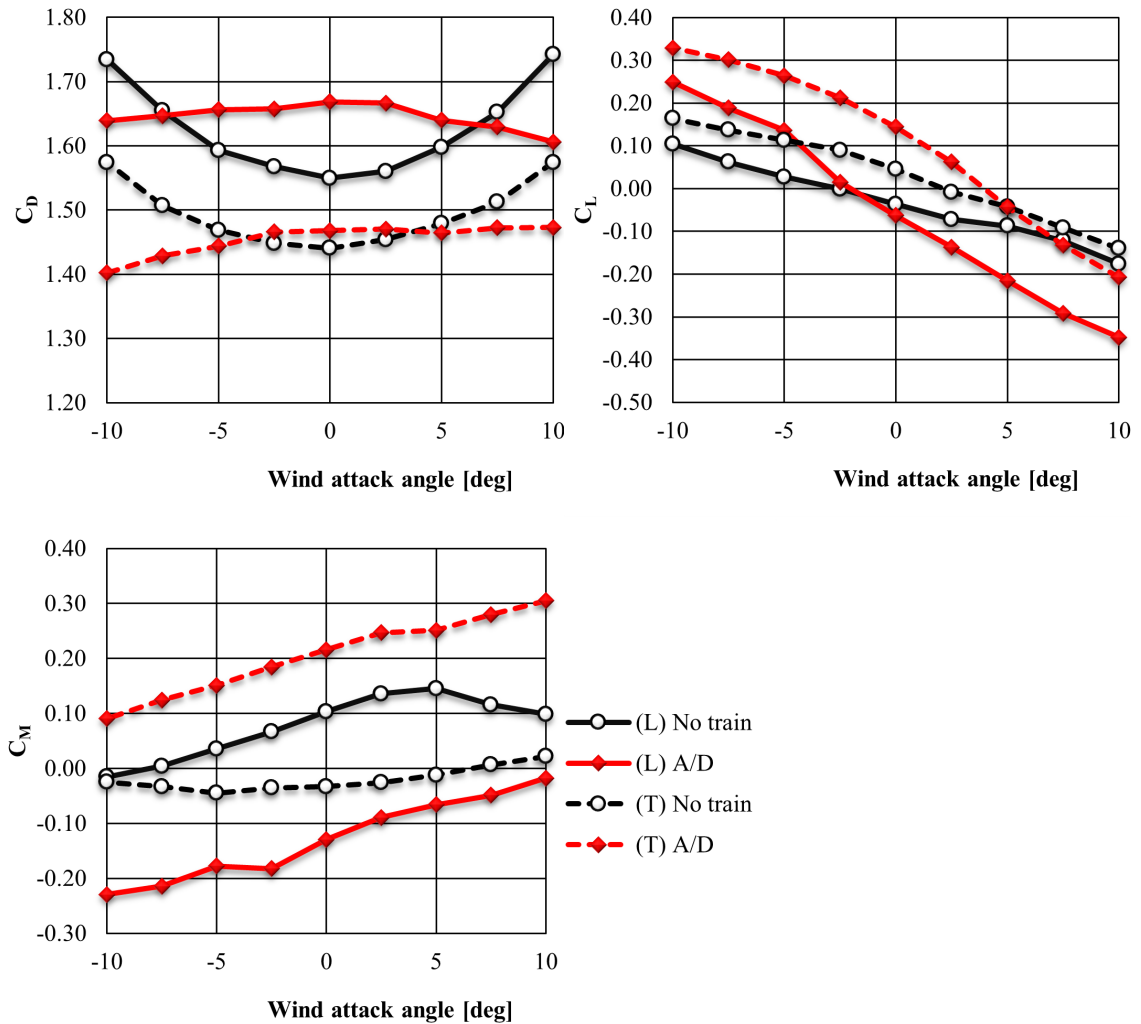
Bridge B8**Description:** Truss girder bridge with lower bridge deck**Scale:** 1:25

Figure 5.31: Bridge B8 – Comparison of force and moment coefficient values for laminar (L) and turbulent (T) airflow.

From the experimental results it can be concluded that the turbulence intensity has a significant impact on the aerodynamic coefficients. The difference is maintained for different values of wind attack angle. For all three bridges the drag coefficient C_D was on average 14 % lower for the turbulent airflow compared to the laminar. The coefficients of lift C_L and moment C_M for bridge B2 remain unchanged and independent of the airflow mode. Similar effect can be observed for the bridge B7 without traffic, with the class A train the values dropped by 25 % and 17 % respectively. However, for bridge B8 there is a quite dramatic increase, 50 % on average, for lift and moment coefficient. Therefore, for truss girder bridges the position of the bridge deck has an effect on the lift and moment aerodynamic coefficients. More conservative laminar airflow results for C_D were considered in the remaining analysis.

The way the airflow flows through bridge B8 was further investigated using the Particle Image Velocimetry (PIV) method. PIV is a non-intrusive method based on laser illumination and camera airflow sensing. It is used to measure wrapping around structures, monitor vorticity, etc (Kat and Oudheusden, 2012). Equipment from Dantec and Litron Lasers was used for the PIV measurements. The particle flow field was captured using a Dantec FlowSense EO camera at 2048x2048 pixel resolution. The flow field was illuminated with an A pulsed Nd:YAG laser. A fogging device was placed in the climatic part of the wind tunnel, the device was placed in front of the propeller so there is no effect on the airflow mode in the wind tunnel in any way. The fog generator was always started only for a moment before the actual measurement was made. Sufficient time (about 5 minutes) was allowed for the smoke particles to disperse sufficiently to create a homogeneous particle field in the tunnel.

Fifty pairs of frames were always recorded at a frequency of 10 Hz for each measurement. The time interval between each frame was 200 μ s. The air velocity in the wind tunnel was fixed at 2.9 m/s. The Reynolds number in the PIV experiment was $Re = 1.6 \cdot 10^4$. The images were subsequently analyzed using Dantec DynamicStudio software (version 5.01). To obtain the local velocity vectors, the adaptive correlation technique was used. The size of the investigated area was set to 64 pixels using three iterative steps. The resulting array of vectors was refined with a 3x3 moving projection filter.

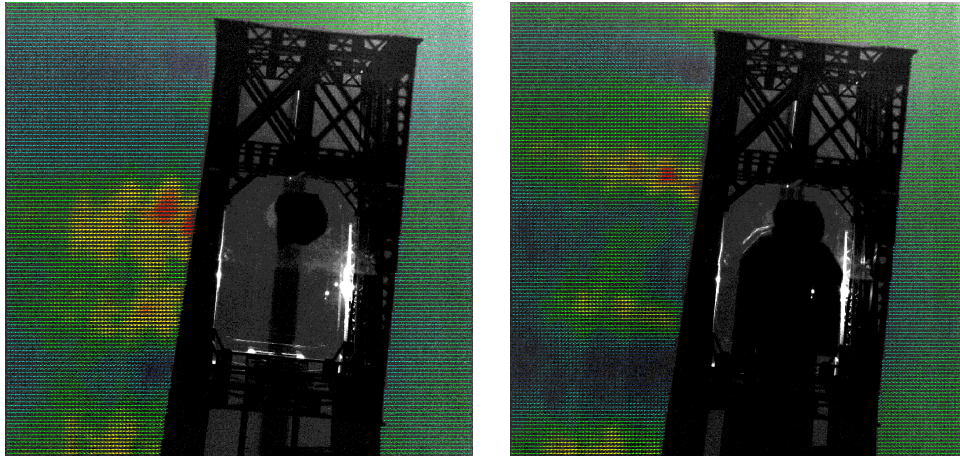


Figure 5.32: PIV visualization of Bridge B8 without and with Class A train.

Figure 5.32 shows the intensity of airflow through the bridge B8, higher intensity with towards red and lower intensity towards blue color spectrum. On the left picture it can be observed that the air flows mainly through the middle of the truss girder, it flows less in the upper part due to the intermediate truss. In the second picture the main airflow path was blocked by the Class A train model and therefore, majority of the airflow was diverted through the less permeable section of the truss causing higher uplift and moment.

5.5.2 Terrain Effect on Aerodynamic Coefficients

Series of experiments was carried out to investigate the effect of the proximity of the ground level below the bridge on the aerodynamic characteristics (wind forces and moment). For this purpose, a triangular ramp was fabricated to reduce the airflow profile in front of the bridge in the aerodynamic chamber. The plate was made of Plexiglas and fixed to a stand with a aerodynamic scales. The height of the ramp was adjustable through threaded rod to simulate different distance between bridge and ground level h . Bridges B2, B7 and B8 were measured without traffic and with Class A/D train. The intensity of the turbulence was $I_u = 0.73\%$ (laminar) for all measurements.

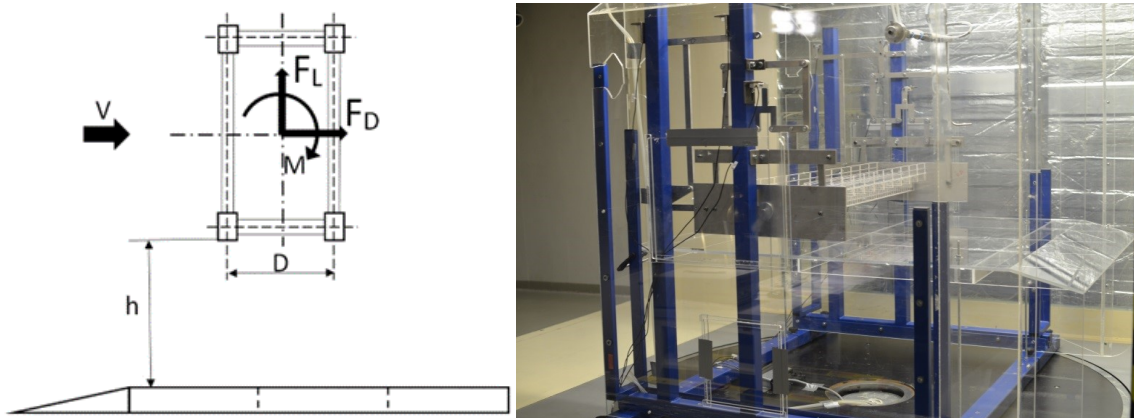


Figure 5.33: The experiment setup to investigate the effect of ground level distance from the bridge.

From the measurement results it can be concluded that a low height above the terrain has impact on the aerodynamic coefficients of the bridge as the airflow between the terrain and the bridge accelerates which causes a change in the aerodynamic characteristics. In most cases the aerodynamic coefficients of drag, lift and moments were on average 10% higher for the minimum distance $h = 100$ mm which corresponds to approximately 2.5 m in the real scale. The experiment suggests that an increase in wind loads should be expected when designing bridges with a low height above the terrain. However, it should be noted that in the case of such low heights, the roughness of the terrain already plays a significant role. The effect of roughness is opposite as it decelerates the air flow.

Bridge B2

Description: Plate girder bridge without bridge deck

Scale: 1:25

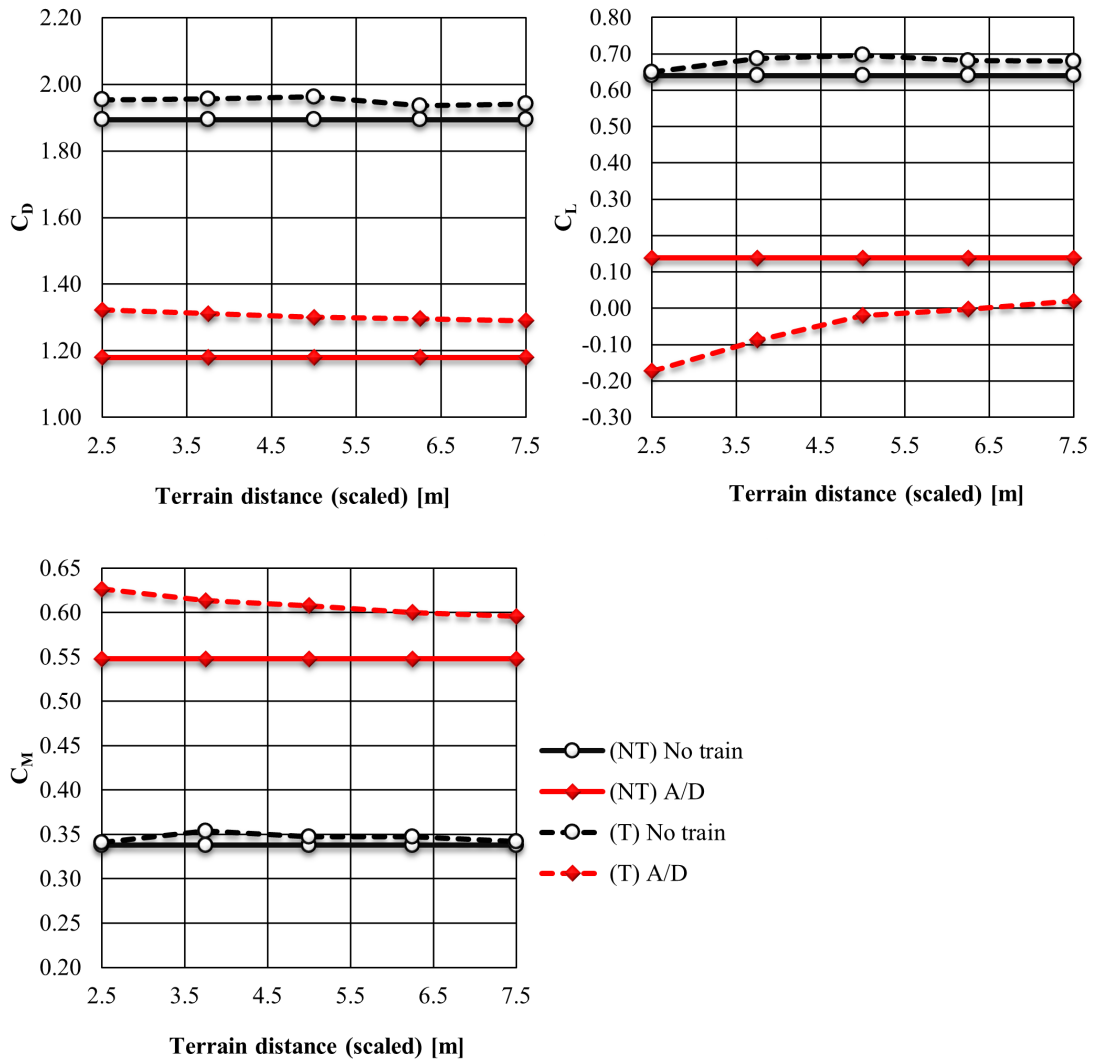


Figure 5.34: Bridge B2 – Effect of terrain on aerodynamic coefficients, (NT) = No terrain, (T) = terrain.

Bridge B7

Description: Truss girder bridge with intermediate bridge deck

Scale: 1:25

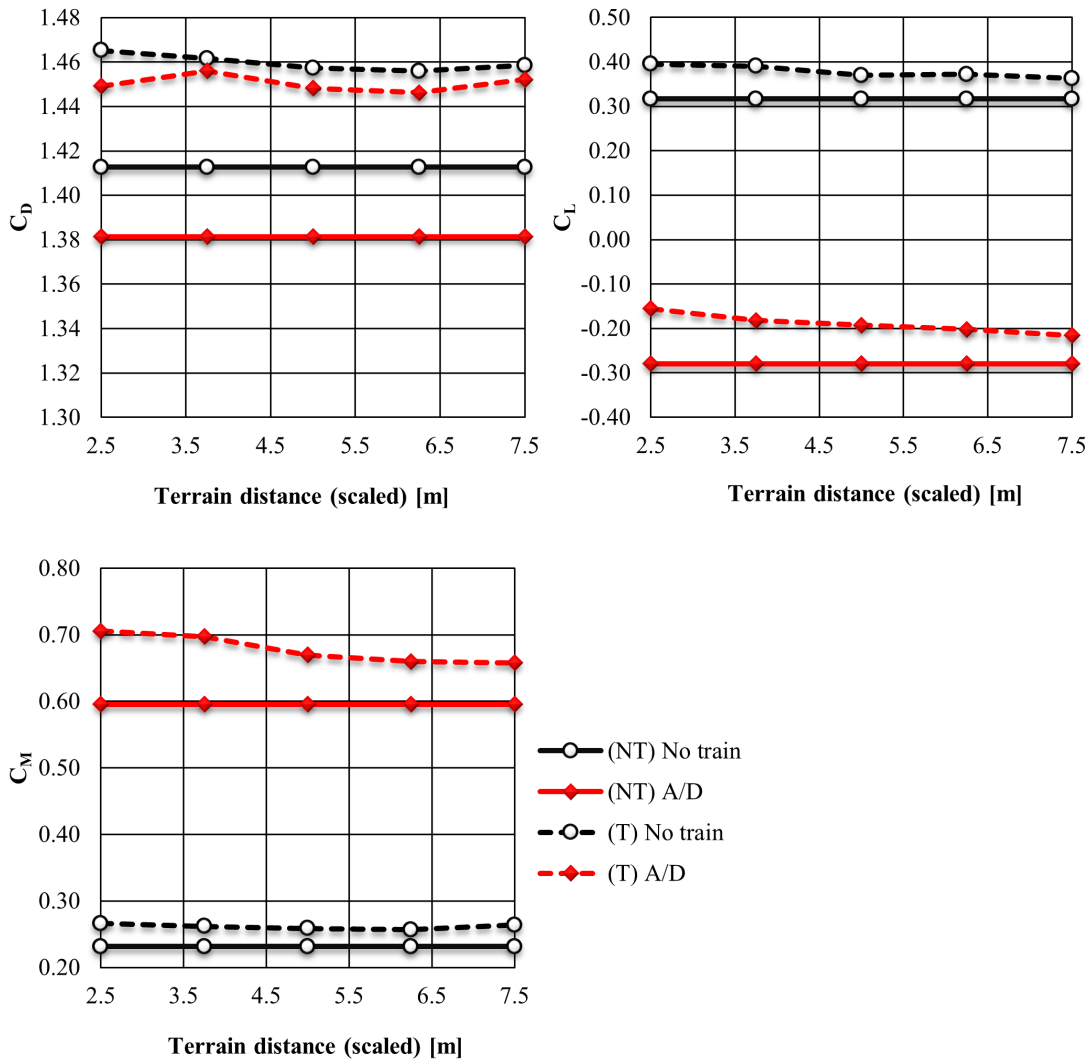


Figure 5.35: Bridge B7 – Bridge B2 – Effect of terrain on aerodynamic coefficients, (NT) = No terrain, (T) = terrain.

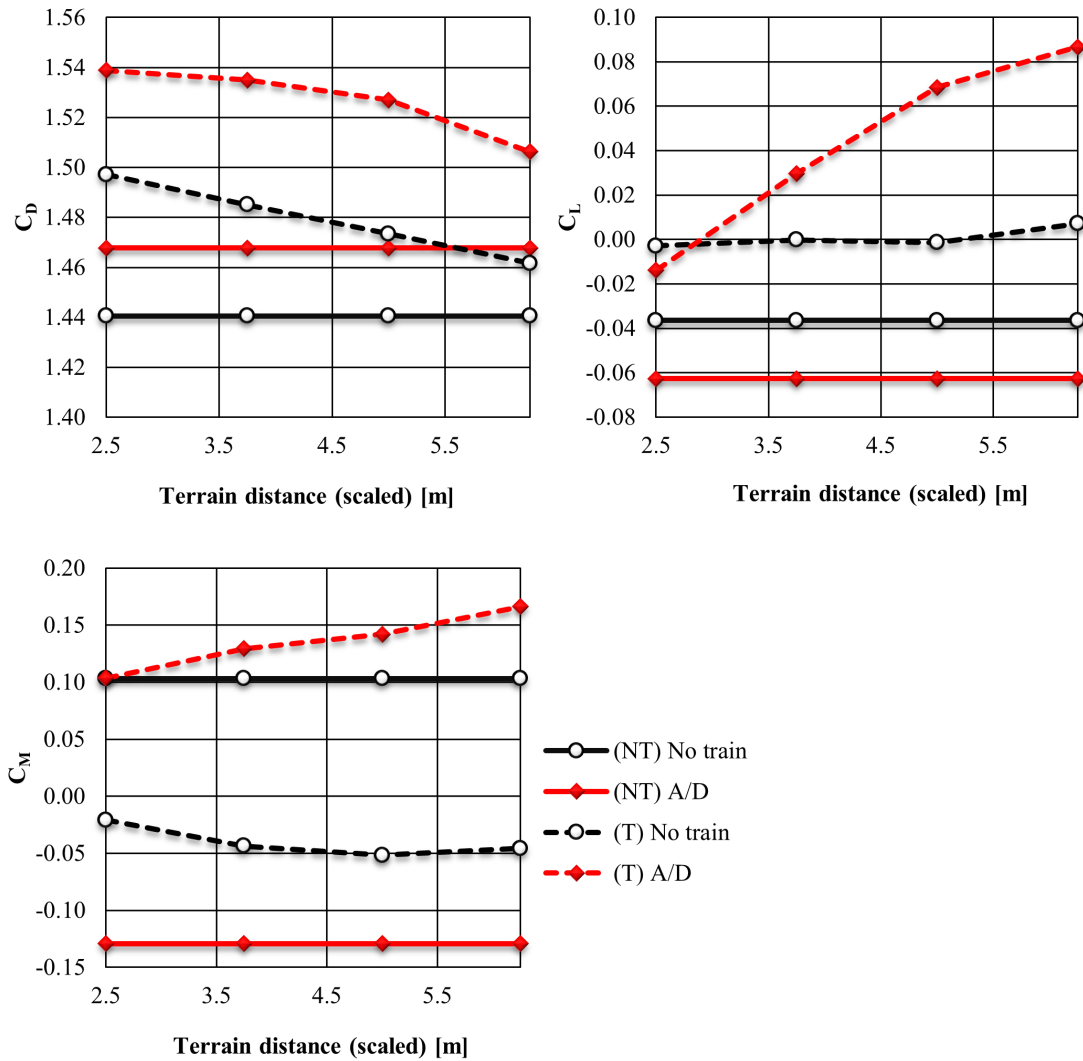
Bridge B8**Description:** Truss girder bridge with lower bridge deck**Scale:** 1:25

Figure 5.36: Bridge B8 – Bridge B2 – Effect of terrain on aerodynamic coefficients, (NT) = No terrain, (T) = terrain.

5.5.3 Effect of Truss Girder Spacing on Leeward Truss Girder Coefficients

The aim of this experiment was to verify the methodology of calculation of aerodynamic coefficients for truss bridge structures. EN 1991-1-4 suggests to determine the reference area A_{ref} of a truss girder bridge as the sum of areas of unobstructed trusses and a bridge deck. However, for determination of aerodynamic coefficients for trusses there are three methods; a) one coefficient for special truss girder; b) one coefficient for planar truss girder applied to all of them; c) determines a aerodynamic coefficient on each truss girder member separately. Pair of a single planar truss models based on geometry of bridge B8 truss was developed. The experiment was carried out for three configurations; **I** windward truss alone; **II** leeward truss behind the windward truss with variable spacing; **III** both trusses connected together with variable spacing, see Figure 5.37. The distance between trusses D varied from 150 mm to 300 mm (corresponding to real scale spacing of 3.75 m to 7.5 m. The measurements have been performed with different values of Re to determine it the mode of airflow wrapping has an impact on the aerodynamic coefficients.

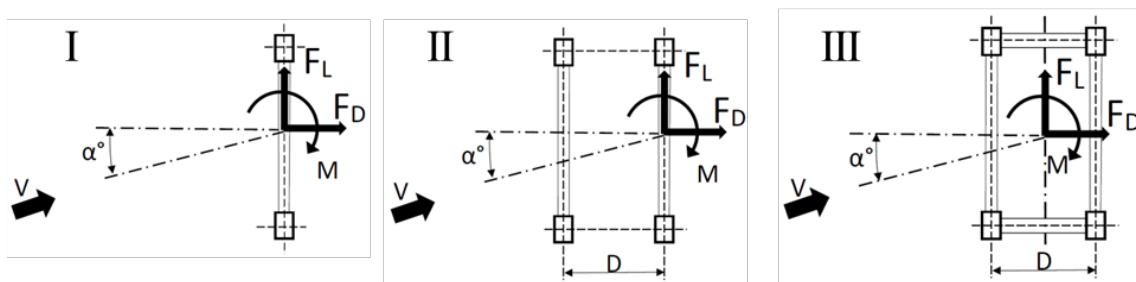


Figure 5.37: Experiment setup for determination of leeward truss girder aerodynamic coefficients.

The plots in Figure 5.39 show the ratio between leeward and windward truss girder drag coefficient dependent on variable distance D and variable Re number. The Re number has virtually no effect on the airflow wrapping, as confirmed by the small variability of the coefficients for different values of Re . The effect of the distance D and the wind attack angle is much more significant. The results in Figure 5.40 show that the most accurate method is the "I + II" method, which is the sum of the measurements for the windward and leeward side. In practical application, the measurements for both trusses together can be used, which corresponds in principle to the measured aerodynamic coefficient presented in Section 5.4. At the same time, it can be observed that the Eurocode assumption of equal loading of all trusses is unrealistic in some cases while the method given in BS 5400 using the shielding factor for leeward truss based on solidity ratio (ratio of truss projected area

to boundary area) is more realistic. The load on the leeward girder, depending on the relative distance, inclination and turbulence, ranges from about 40 to 70 % of the load on the windward girder.

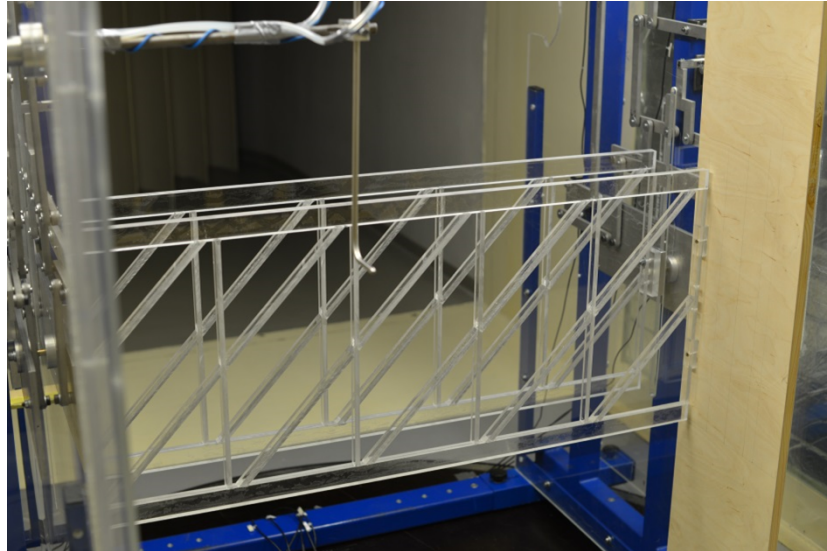


Figure 5.38: Model of bridge B8 main truss girders separated to leeward and windward truss.

Bridge B8

Description: Truss girder bridge with lower bridge deck

Scale: 1:25

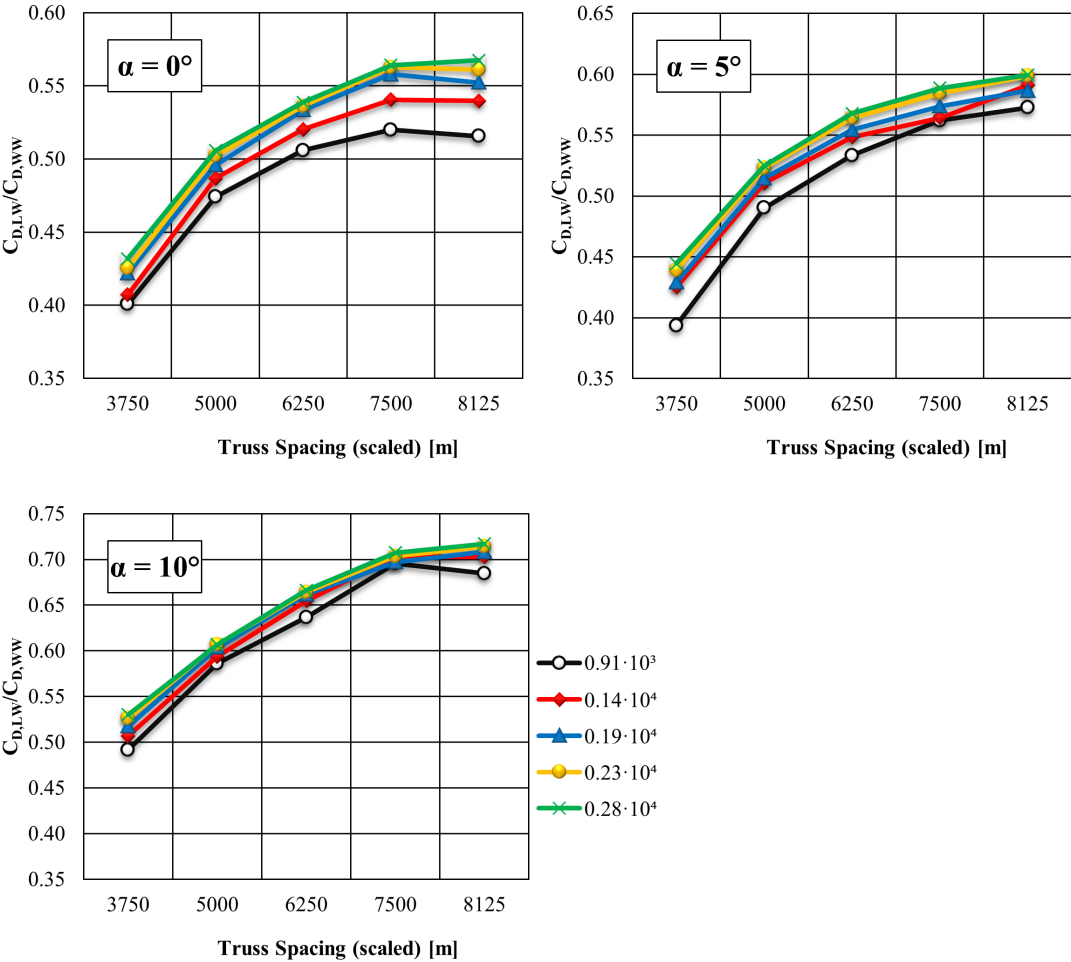


Figure 5.39: Bridge B8 – Ratio of leeward against windward aerodynamic drag coefficient.

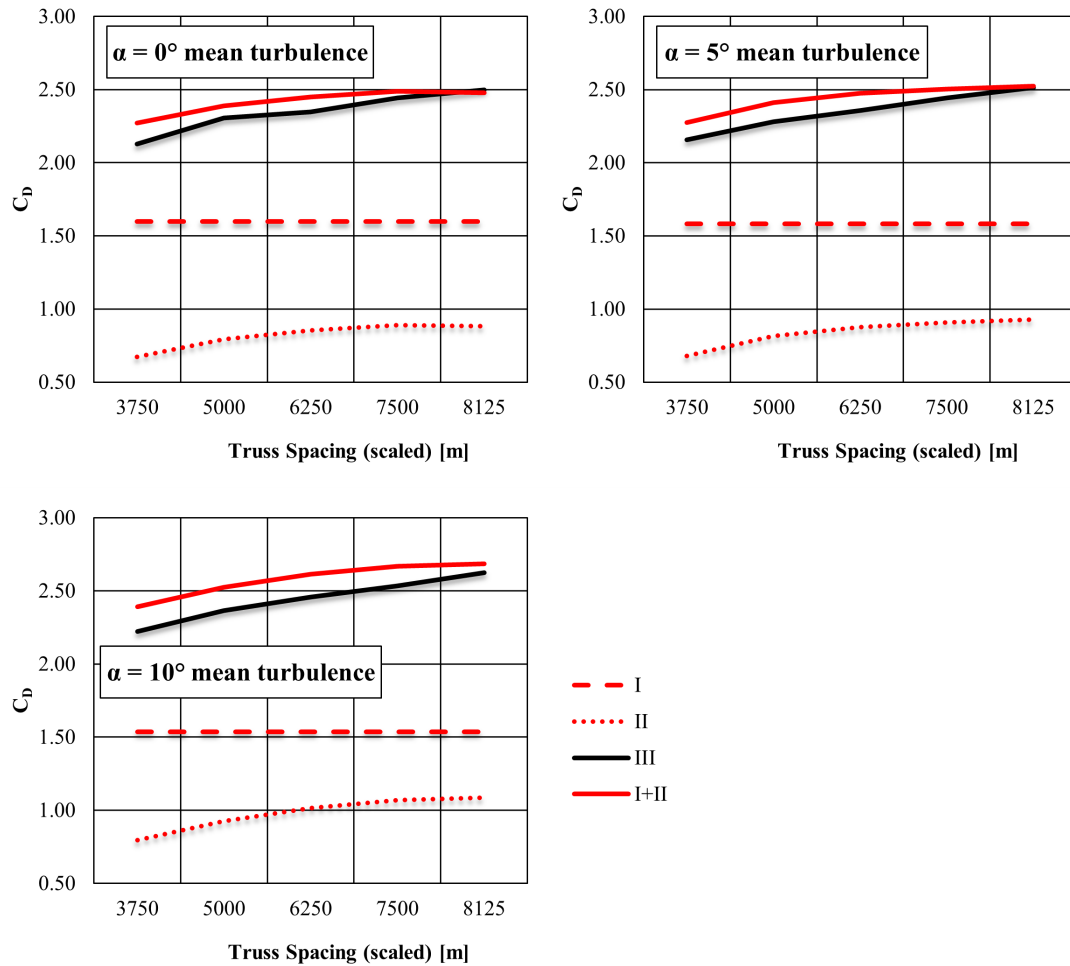
Bridge B8**Description:** Truss girder bridge with lower bridge deck**Scale:** 1:25

Figure 5.40: Bridge B8 – Drag coefficient for all model setups based on variable (scaled) truss girder spacing.

Chapter 6

Evaluation of Experimental Results

6.1 Wind Load according to EN 1991-1-4

In general the wind load acting on structures according to EN 1991-1-4 is calculated as follows:

$$F_W = q_p(z_e) \cdot \sum C_i \cdot A_{ref,i} \quad (6.1)$$

where q_p is the peak velocity pressure at reference height of external wind action z_e , C is the wind load factor on bridges and A_{ref} is the reference area.

The peak velocity pressure is determined according to Chapter 4 of EN 1991-1-4. The basic wind velocity v_b depends on the fundamental value of the basic wind velocity $v_{b,0}$, which is obtained from the wind velocity map for given location and wind zone, and the wind directional factor c_{dir} and the seasonal factor c_{season} . According to national Annex for the Czech Republic both these coefficients shall be $c_{dir} = 1.0$ and $c_{season} = 1.0$.

$$v_b = v_{b,0} \cdot c_{dir} \cdot c_{season} \quad (6.2)$$

The mean wind velocity $v_m(z)$ at height z above the terrain depends on the terrain roughness factor $c_r(z)$ the orography factor $c_o(z)$ and the base wind velocity v_b . Where orography (e.g. hills, cliffs etc.) increases wind velocities by more than 5 %, the effects should be taken into account using the orography factor c_o according to Appendix A otherwise can be taken as 1.0.

$$v_m(z) = c_r(z) \cdot c_o(z) \cdot v_b \quad (6.3)$$

$$c_r(z) = k_r \cdot \ln\left(\frac{z}{z_0}\right) \quad (6.4)$$

$$k_r = 0.19 \cdot \left(\frac{z_0}{z_{0,II}}\right)^{-0.07} \quad (6.5)$$

where k_r is the terrain factor, z_0 is the roughness length according to assumed terrain category and $z_{0,II}$ is the roughness length for terrain category II.

The turbulence intensity $I_v(z)$ depends on the standard deviation of the turbulence σ_v and the mean wind velocity $v_m(z)$. The turbulence factor k_l is assumed to be 1.0 according to the National Annex.

$$\sigma_v = k_r \cdot v_b \cdot k_l \quad (6.6)$$

$$I_v(z) = \frac{\sigma_v}{v_m(z)} \quad (6.7)$$

The peak dynamic pressure $q_p(z)$ depends on the turbulence intensity $I_v(z)$, the mean wind velocity $v_m(z)$ and the air density ρ (recommended value is 1.25 kg/m^3).

$$q_p(z) = [1 + 7 \cdot I_v(z)] \cdot \frac{1}{2} \cdot \rho \cdot v_m(z)^2 \quad (6.8)$$

The wind load factor C on bridges is described in Chapter 8 of EN 1991-1-4 as force coefficient in x-direction $c_{f,x}$ (drag coefficient) and force coefficient in z-direction $c_{f,z}$ (lift force). Longitudinal wind is described in the code as well. However, it was not a subject of the wind tunnel experiments.

For plate girder bridges and bridge decks of truss girder bridges, the force coefficient $c_{f,x}$ is determined according to EN 1991-1-4, Figure 8.3, depending on the ratio of the width and height of the structure b/d_{tot} . If traffic is present on the bridge the height of the train should be added to the overall height d_{tot} , the height of train is defined as 4 m above the top of the rail in EN 1991-2. The reference area for the calculation of the wind load is considered as the projection of the whole plate girder bridge or bridge deck including traffic.

The wind code provides limited guidance on how to determine the force coefficient $c_{f,x}$ on truss girder bridges. Per EN 1991-1-4 Chapter 8.3.1 the force coefficient shall be determined separately for bridge deck with or without the traffic and separately for the truss girders. However, to determine wind load acting on truss girders, three different

approaches are described in EN 1991-1-4 Chapter 7 and none of them is preferred in the code.

1. Method M1 – the force coefficient $c_{f,x}$ is separately evaluated for bridge deck with or without traffic according to Chapter 8.3.1 of EN 1991-1-4 and separately for the whole spatial truss girder structure with angle members. The force coefficient is determined according to Figure 7.34 of EN 1991-1-4 as a function of the solidity ratio φ of the truss girder. The reference area of the truss is determined as its projection in the plane. The leeward side of the structure is ignored as it is already taken into account in the force coefficient.
2. Method M2 – the force coefficient $c_{f,x}$ is separately evaluated for bridge deck with or without traffic according to Chapter 8.3.1 of EN 1991-1-4 and separately for each planar truss girder structure with angle members. The force coefficient is determined according to Figure 7.33 of EN 1991-1-4 as a function of the solidity ratio φ of the truss girder. The reference area of the truss is determined as its projection in the plane. The leeward part of the structure is included in the reference area of the truss. According to this method both windward and leeward truss girder have the same force coefficient and are both loaded by equal wind load.
3. Method M3 – the force coefficient $c_{f,x}$ is separately evaluated for bridge deck with or without traffic according to Chapter 8.3.1 of EN 1991-1-4 and separately for each member of the truss girder structure. The force coefficient is determined according to Figure 7.23 of EN 1991-1-4 based on the height to thickness ratio of each sharp-edge truss girder member. The reference area is calculated for each member separately from its length and dimension perpendicular to the wind direction. The leeward truss members are included in the reference area. According to this method both windward and leeward truss girder members have the same force coefficient and are all loaded by equal wind load.

The force coefficient in the vertical direction $c_{f,z}$ is determined regardless of bridge type. The reference area being equal to the vertical projection of the bridge in plan. Vertical wind force component occurs due to variability of the wind attack angle which is mainly dependent on the orography conditions or superelevated geometry of the bridge deck. For flat, horizontal terrain or for hilly terrain where the bridge deck is at least 30 m above ground the angle α can be taken as $\pm 5^\circ$ due to turbulence. The height of d_{tot} can be limited to the height of the bridge superstructure independent of traffic and any bridge

equipment. The value of $c_{f,z}$ may be conservatively taken as $\pm 0,9$ or alternatively the coefficient can be determined according to Chart 8.6 of EN 1991-1-4.

6.2 Comparison of Wind Tunnel Results to EN 1991-1-4

6.2.1 Horizontal Wind Load – Plate Girder Bridges

For plate girder bridges the values of drag coefficient measured in the wind tunnel C_D can be directly compared to the force coefficient $c_{f,x}$ determined per Chapter 8.3.1 of EN 1991-1-4. Figure 6.1 shows all measured drag coefficients for bridges B1 thru B4 plotted into Figure 8.3 from EN 1991-1-4 based on the model's b/d_{tot} , red data points show the drag coefficient for the bridges without traffic and blue data points for bridges with traffic.

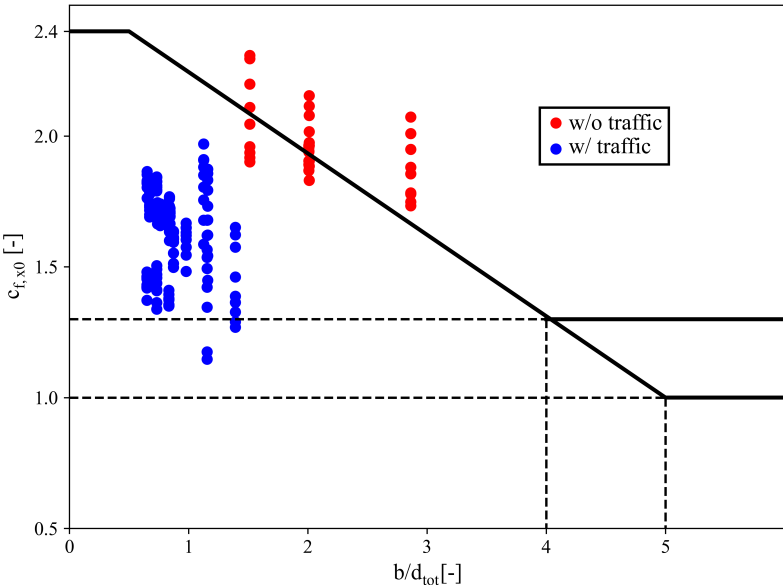


Figure 6.1: Force coefficient Figure 8.3 per EN 1991-1-4 with plotted wind tunnel drag coefficients C_D for bridges B1 thru B4 without and with traffic.

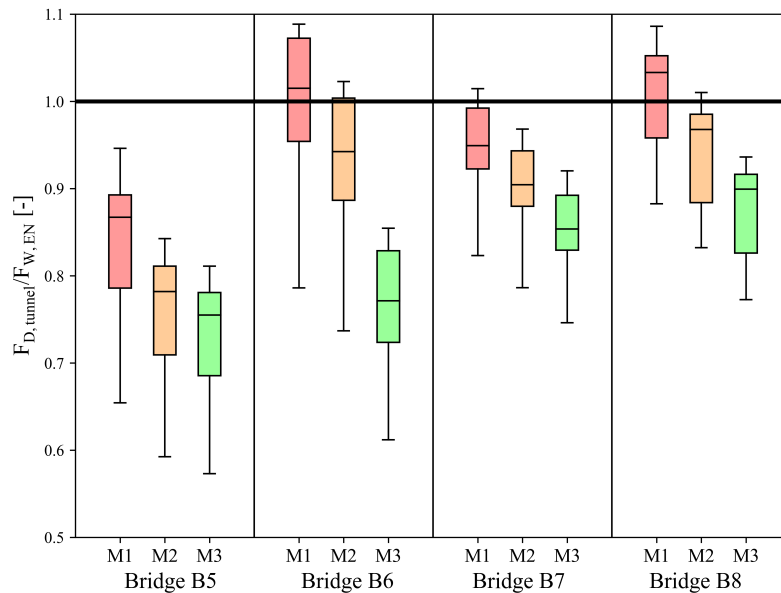
Based on the comparison, the Eurocode slightly underestimates the force coefficient for bridges without traffic, which is rarely the controlling design case for railway bridges. However, for bridges with traffic the Eurocode is conservative for all configurations of bridges and trains. Table 6.1 shows the maximum measured drag coefficient for each configuration compared to force coefficient determined per EN 1991-1-4 assuming 4 m train height per EN 1991-2.

Class	B1	B2	B3	B4
No train	1.13	1.26	1.14	1.04
A/D	0.65	0.63	0.66	0.79
B	0.76	0.75	0.76	0.78
C	0.78	0.73	0.77	0.88
E	0.81	0.79	0.81	0.93

Table 6.1: Ratio of $C_{D,tunnel}$ and $c_{f,x0,EN}$ for plate girder bridges.

6.2.2 Horizontal Wind Load – Truss Girder Bridges

For truss girder bridges B5 thru B8 the drag coefficient cannot be compared directly with the values per Eurocode as the force coefficient is determined separately for bridge deck with traffic and separately for truss girders per Method M1 thru M3. Therefore the wind force calculated according to Equation 6.1 was compared. Figure 6.2 and 6.3 shows the box plot of the ratio of drag coefficients measure in the wind tunnel $F_{D,tunnel}$ and the wind force calculated per EN 1991-1-4 Method M1 thru M3 $F_{W,EN}$. Figure 6.2 shows the ratio of $F_{W,EN}$ calculated for height of Class A thru E trains are shown. Figure 6.3 shows the ratio of $F_{W,EN}$ calculated for 4 m train height per EN 1991-2 are shown.

Figure 6.2: Box plot of the ratio of $F_{D,tunnel}$ and $F_{W,EN}$ for truss girder bridges B5 thru B8. $F_{W,EN}$ calculated for height of Class A thru E trains.

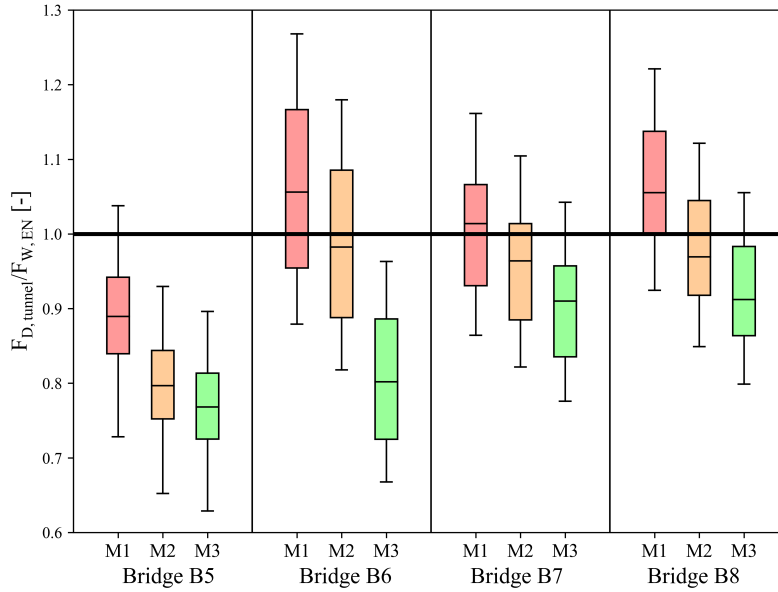


Figure 6.3: Box plot of the ratio of $F_{D,tunnel}$ and $F_{W,EN}$ for truss girder bridges B5 thru B8. $F_{W,EN}$ calculated for 4 m train height per EN 1991-2.

Based on Figure 6.2, right plot, it can be concluded that the drag forces measured in the wind tunnel match the wind forces calculated according to Method M2 in the most cases. Therefore this method should be preferred in the code to determine the wind actions on truss girder bridges and is used in the remaining part of the dissertation. Due to the fact that the most fitting Method M2 was selected to compare with the wind tunnel measurements and that almost all classes of railway vehicles have significantly larger height than 4 m according to EN 1991-2, the comparison leads to both overestimated and underestimated wind load effects based on the assumed railway vehicle class. Table 6.2 shows the maximum measured drag force for each configuration compared to wind force determined per EN 1991-1-4 assuming 4 m train height per EN 1991-2.

Class	B5	B6	B7	B8
No train	1.14	1.09	1.14	1.13
A/D	0.77	0.97	0.99	0.93
B	0.80	0.91	0.91	0.95
C	0.85	1.08	1.03	1.04
E	0.93	1.18	1.10	1.12

Table 6.2: Ratio of $F_{D,tunnel}$ and $F_{W,EN}$ for truss girder bridges.

6.2.3 Vertical Wind Load

For vertical wind load effect, the lift force coefficient measured in the wind tunnel $C_{L,tunnel}$ can be directly compared to the force coefficient in the vertical direction $c_{f,z}$ determined per EN 1991-1-4 Section 8.3.3. Figure 6.4 shows all measured lift force coefficients for bridges B1 thru B8 plotted into Figure 8.6 from EN 1991-1-4 based on b/d_{tot} according to the model, red data points show the lift force coefficient for the bridges without traffic and blue data points for bridges with traffic.

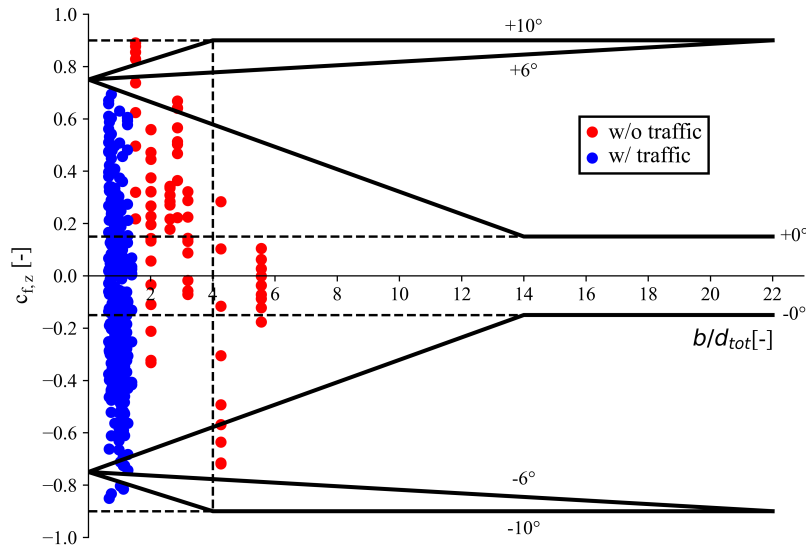


Figure 6.4: Lift force coefficient Figure 8.6 per EN 1991-1-4 with plotted wind tunnel lift force coefficients C_L for bridges B1 thru B8 without and with traffic.

For majority of the experimental results Eurocode overestimates the lift force coefficient for bridges without traffic and with traffic, Table 6.3 shows the maximum measured lift force coefficient for each configuration compared to lift force coefficient determined per EN 1991-1-4.

Class	B1	B2	B3	B4	B5	B6	B7	B8
No train	0.99	0.74	0.62	0.37	0.36	0.80	0.38	0.20
A/D	0.74	0.30	0.48	0.62	0.56	0.33	0.50	0.39
B	0.77	0.34	0.55	0.46	0.83	0.63	0.41	0.67
C	0.65	0.35	0.53	0.81	0.81	0.93	0.61	0.51
E	0.73	0.48	0.58	0.91	0.89	0.95	0.74	0.70

Table 6.3: Ratio of $C_{L,tunnel}$ and $c_{f,z,EN}$ for all bridge types.

6.3 Force Coefficients in EQU

In Equilibrium Limit State (EQU), the overturning wind moment does not solely depend on the drag force, but the lift force and moment measured in the wind tunnel have impact as well. The force coefficient calculated from the wind tunnel measurements shall be calculated per following equation:

$$c_{f,EQU,tunnel} = \left(F_D \cdot h_{bot} + F_L \cdot \frac{b}{2} + F_M \right) / \left(\frac{1}{2} \cdot \rho \cdot v^2 \cdot A_{ref} \cdot z_w \right) \quad (6.9)$$

where F_D , F_L and F_M denote the drag, lift and torsion forces, respectively, measured in the wind tunnel tests; h_{bot} is the height of the point of fixity during tests to the bottom chord; b is the width of the bridge; and z_w is the distance of the centroid of the reference area to the center of rotation, see Figure 6.5.

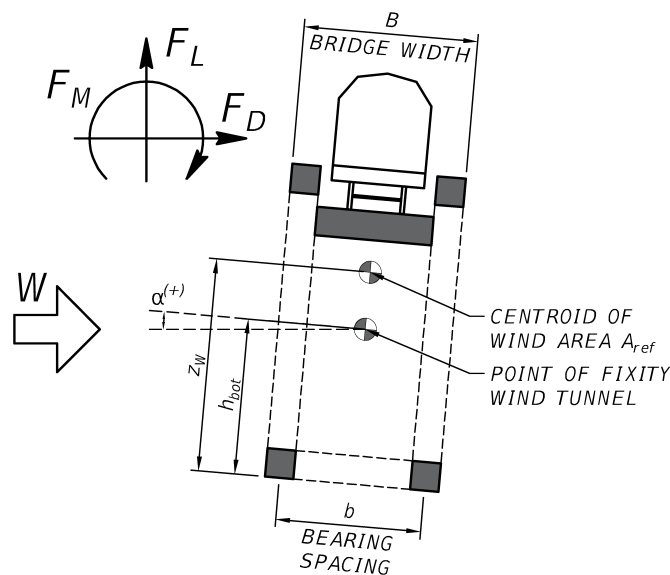


Figure 6.5: Designation of variables in Eq. 6.9.

The force coefficient for plate girder bridges and truss girder bridges according to approach M2 determined for the whole bridge while taking into account the geometry of the unloaded train shall be calculated per following equation:

$$c_{f,EQU,M2} = F_w \cdot z_w / \left(\frac{1}{2} \cdot \rho \cdot v^2 \cdot A_{ref} \cdot z_w \right) \quad (6.10)$$

where F_w is the wind force according to EN 1991-1-4.

The ratio of the force coefficients for all bridges obtained in the wind tunnel to those estimated by EN 1991-1-4 are displayed in Figure 6.6. The graph for each bridge shows the distribution of the force coefficient for all wind attack angles and train classes. Only the most conservative value for each train class was used in the EQU reliability verification. The graph also depicts if the bridge satisfies the equilibrium condition per EN 1990.

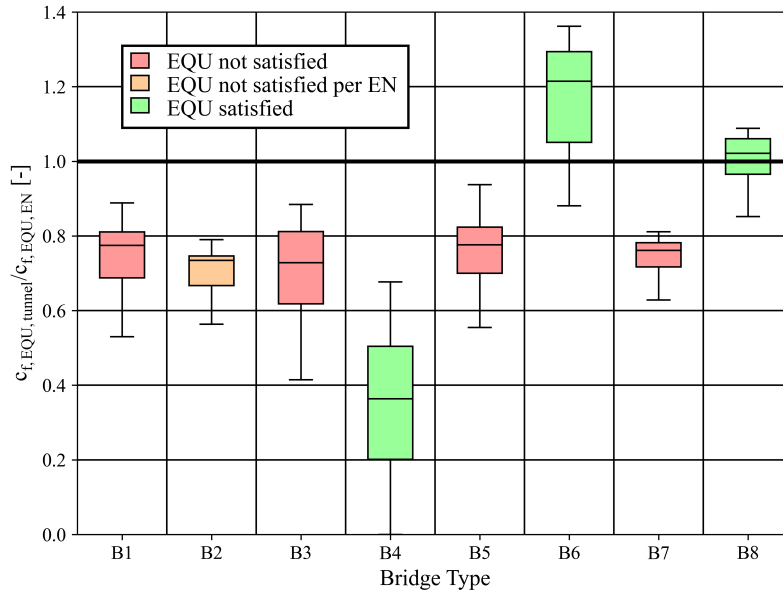


Figure 6.6: Box plot of the ratio of $c_{f,EQU,tunnel}$ and $c_{f,EQU,EN}$ for all bridge types.

The comparison of force coefficients obtained in the wind tunnel for various vehicle types reveals that the ratio $c_{f,EQU,tunnel}/c_{f,EQU,EN}$ ranges typically between 0.6-0.9 for bridges not satisfying EQU verification, see Table 6.4. It is emphasized that these results apply to EQU, thereby to the global wind effect. It is interesting to compare these biases with the study by (Hansen et al., 2015) focused on buildings – they concluded: “The Eurocode global wind action often overestimates the wind action measured in the wind tunnel. Often the overestimation is of an order of at least 40 %.”

Class	B1	B2	B3	B4	B5	B6	B7	B8
A/D	0.64	0.59	0.58	0.40	0.68	0.93	0.69	0.90
B	0.80	0.78	0.85	0.64	0.94	1.20	0.80	1.08
C	0.82	0.79	0.84	0.52	0.82	1.36	0.80	1.03
E	0.89	0.77	0.88	0.68	0.83	1.32	0.81	1.09

Table 6.4: Ratio of $c_{f,EQU,tunnel}$ and $c_{f,EQU,EN}$ for all bridge types.

Chapter 7

Wind Pressure Model

7.1 Wind on Bridges

Wind is defined as the movement of air that is caused by changes in atmospheric pressure. These are the result of the different heating of the Earth's surface by sun radiation. Areas with high and low pressure are referred to as high pressure and low pressure zones. Naturally, air tends to flow from an area of high pressure to an area of low pressure, but the curvature of the Earth and its rotation around its own axis mean that the resulting wind direction is more or less perpendicular to its expected flow direction. The direction of the wind therefore approaches the direction of the isobars, curves connecting points with the same air pressure value, in each point. The speed of the wind then depends on the distance between these isobars (pressure gradient) and is higher the closer the isobars are to each other and the larger the pressure gradient (Humphreys, 1964). With a large distance between isobars, wind characteristics are influenced by local factors, such as coastal winds (breezes) or valley winds.

In the middle geographical latitudes, the distribution of atmospheric pressure almost never repeats, with wind return periods often measured in years or even decades. This means that wind loading is a highly variable quantity that differs significantly from place to place and day to day. The frequency, strength, and duration of windstorms can vary each year. For buildings and structures, the most dangerous windstorm scenario is associated with a large low-pressure system, with atmospheric pressure far below its normal value and isobars crowded close together. Large low-pressure systems can result in extreme windstorms, such as cyclones, tornadoes, or hurricanes, but thankfully these extreme storms only occur in some parts of the world (Hay, 1992).

Bridge structures are often exposed to significant wind loads due to their position,

location and shape. As bridge engineering and bridge spans evolved over history, the requirements for adequate load-bearing capacity and stability of structures to withstand wind storms also increased. The need to develop methodology to account for wind loads on bridges was facilitated by several tragic events in the past. The most notable was the collapse of the Tay railway bridge in Scotland in 1879, just 18 months after its opening, when a train was crossing it (Prebble, 1979). According to modern interpretations, wind gusts reached 40 m/s at the time of the catastrophe and the bridge broke in the middle and fell into the river along with the passing train. None of the passengers survived. This disaster influenced bridge engineering for several decades. The commission investigating the accident set the wind pressure for the design of new bridges at 2.7 kN/m^2 . For example, when designing one of the historical landmarks of bridge engineering, the Firth of Forth bridge in Scotland, the concept of suspended bridge was abandoned and the truss bridge structure was built. Later, after the introduction of new theories for structure analysis, it was found to be significantly overdesigned. Another major milestone in the approach to wind loads on bridges occurred in the 20th century after the collapse of the Tacoma Narrows Bridge and excessive vibration of the Golden Gate Bridge, which pointed to the danger of dynamic wind loads on bridges, even at lower wind speeds.

7.2 Wind Speed

The direction and speed of wind are not constant quantities but change randomly over time. The flow of wind is divided into laminar and turbulent. Sudden changes in wind speed are called gusts or lulls and form the fluctuating component of wind loading. In a certain period of time, we can observe that a certain direction prevails and is associated with a certain wind strength, which can then be defined by the instant or average speed in all directions. For meteorological purposes, the vertical component of wind is neglected and direction and speed of wind are determined only from horizontal components. The instrument measuring these quantities is called an anemometer. Since wind speed changes with height, it is internationally established that all meteorological stations measure wind speed at a height of 10 m at ground level. The intensity of turbulence is defined as the ratio of the standard deviation to the own value of speed (Davenport, 1960). The measured values from meteorological stations are used to determine the size of wind loading. In EN 1991-1-4, the average wind speed over a ten-minute interval at a height of 10 m above the ground, in the terrain without obstacles and with an annual probability of exceedance $p = 0.02$ (1x in 50 years) is used. This speed corresponds to synoptic storms, thunder-

storms, or generally maximum wind gusts are not taken into account (Kral, 2010). On the other hand, some international standards, such as BS 5400, or the withdrawn Czech standard CSN 73 0038, consider wind loading based on maximum wind gusts (Shellard, 1963). The maximum wind speeds, regardless of whether they include wind gusts, are processed into a map of ten-minute average speeds with a return period of 50 years. In the Czech Republic, this map was created based on data from 46 Czech Hydrometeorological Institute's synoptic and climatological stations. To determine the annual maximums, the period from 1961 to 2000 was selected and the Gumbel distribution was used. The speeds were corrected so that all of them correspond to terrain roughness category II (areas with low vegetation and isolated obstacles) (Kral, 2010). The map was divided into five regions with boundary speeds of 22.5 - 25.0 - 27.5 - 30.0 - 36.0 m/s, see Figure 7.1.

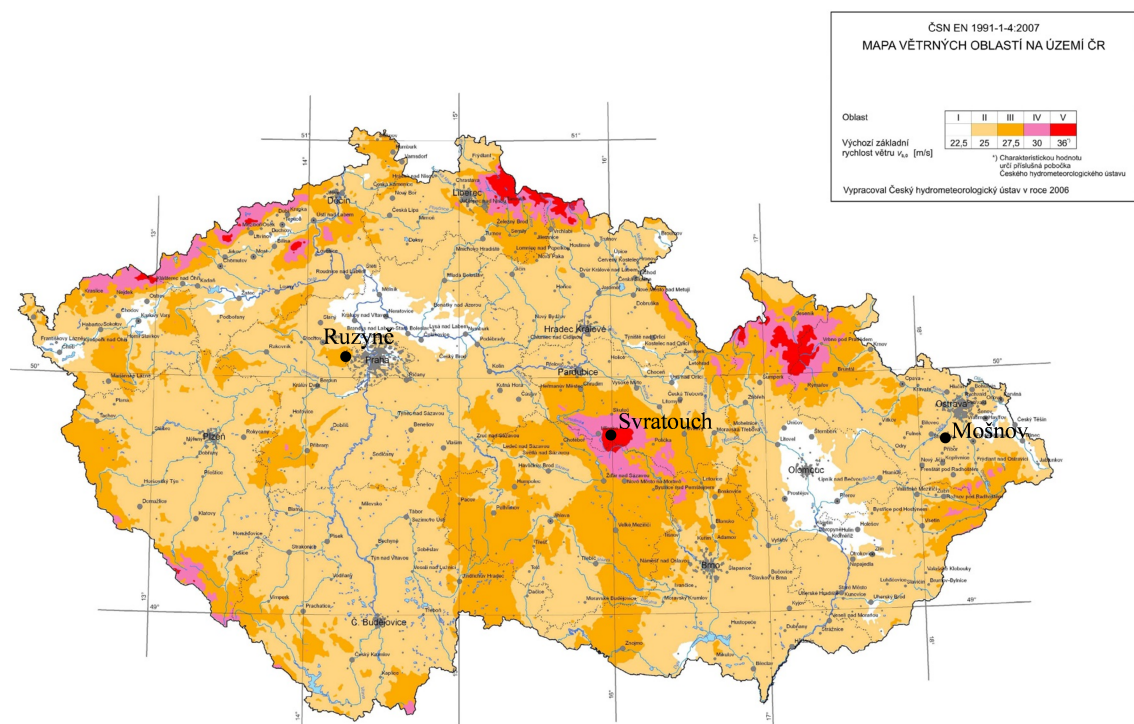


Figure 7.1: Wind map of the Czech Republic (EN 1991-1-4).

7.3 Windstorms

The most unfavorable wind load scenario for a bridge is a windstorm, which is defined by JCSS Probabilistic Model Code (JCSS PMC, 2021) as a situation where the average speed exceeds 10 m/s for a "certain period of time". For Central Europe, the number of windstorms per year can be estimated to be $n_W \approx 50$. The average duration of a storm

is 8 hours. [Kasperski \(2009\)](#) analyzed wind speeds at the Düsseldorf airport, Germany, and concluded that a storm could be defined by wind speed exceeding 14 m/s with a representative duration of three hours, based on analysis of correlations between strong wind speeds. [Baravalle and Kohler \(2018\)](#) proposed to fit a Gumbel distribution to the tail of a wind speed distribution, considering the highest 30 % of wind speeds in the data set. They then focused on wind speeds exceeding approximately 20 m/s in areas with high wind speeds, with mostly $v_{b,k} > 30 \text{ m/s}$.

The characteristics describing the duration and intensity of storms can be commonly considered as statistically independent. A range of statistical distributions was considered to model wind speeds during extreme events (such as those describing annual maxima). The most popular model seems to be a Gumbel distribution for maxima, considered by the [JCSS PMC](#), [EN 1991-1-4](#), and [ASCE/SEI 7-16](#) for the minimum design loads and associated criteria for buildings and other structures. Both [JCSS PMC](#) and [EN 1991-1-4](#) consider also a Weibull distribution. Research studies observed that in some situations, e.g. Generalised Extreme Value or Generalised Pareto distribution might provide a better fit ([Kruger et al., 2013](#); [Niemann and Diburg, 2013](#); [Holmes, 1998](#)). The background document for Eurocodes considered Gumbel, three-parameter lognormal or Weibull distributions for extreme wind speeds in Europe ([Formichi et al., 2016](#)). Studies by the Klokner Institute focused on the Czech climate conditions suggested that a suitable theoretical model could be a three-parameter lognormal distribution LN, or the Gumbel distribution ([Rozsas et al., 2016](#); [Holicky and Sykora, 2016](#)). Considering the studies providing background to the Eurocodes and focused on the Czech conditions, a Gumbel distribution seems to generally provide a reasonable fit to wind speed records.

The most destructive windstorm recorded in the Czech Republic in recent years was Hurricane Kyrill. On January 18 and 19, 2007, a cold front accompanied by a pressure low passed over the Czech Republic, resulting in a storm with winds reaching hurricane force. This storm affected the entire territory of the Czech Republic, the strongest wind gusts were recorded mainly at mountain meteorological stations, such as Sněžka or Milešovka. The maximum recorded 10-minute average wind speed reached 23.3 m/s (approximately the 10-year maximum) and the maximum wind gust was 34.5 m/s (approximately the 5-year maximum). Four stations recorded higher 10-minute maximums than the 50-year return statistical estimate. Five stations recorded higher wind gusts than the 50-year return statistical estimate. The passage of Hurricane Kyrill generally confirmed the characteristic wind speeds in the Czech wind map ([Kral, 2010](#)).

7.4 Wind Zone Models

The wind pressure models for each wind zone are based on detailed wind speed records for three hydrometeorological stations, see 7.1 for their locations marked in the wind map of the Czech Republic. 10-minute mean wind speed records were used for wind zone II, III and V.

- Wind Zone II – Mošnov (257 m MSL, 1957-2016, >400,000 data points,
 $v_{b,0} = 25 \text{ m/s}$.)
- Wind Zone III – Ruzyně (380 m MSL, 1957-2016, >700,000 data points,
 $v_{b,0} = 27.5 \text{ m/s}$.)
- Wind Zone V – Svratouch (734 m MSL, 1977-2017, >185,000 data points,
 $v_{b,0} = 36 \text{ m/s}$.)

Hydrometeorological stations Mošnov and Ruzyně are located in the proximity of airports with probably the best quality data taken for air traffic management purposes, well representing areas with heavy rail traffic. Svratouch station is in the area with rail traffic and it is the area with the highest characteristic wind speed in the Czech Republic. Data are available at variable intervals – after six hours at the beginning of the monitored period to after half an hour at the end of the period.

The JRC report by [Formichi et al. \(2016\)](#) presents common methods for estimating the parameters of probability distributions from data: a) method of moments; b) least squares method; c) maximum likelihood method. Information on application of these methods is given in [Holický \(2015\)](#). The JRC report by [Formichi et al. \(2016\)](#) suggests that the differences in the estimates of the characteristic values (98% of the quantiles of the annual maxima) are insignificant. Further analysis relies on the method of moments.

The JRC report by [Formichi et al. \(2016\)](#) lists the following distributions as suitable for annual wind speed maxima: Weibull, Gumbel and lognormal. The [JCSS PMC](#) considers the Gumbel distribution for annual maxima. The values of the unbiased estimates of the sampling skewness in [Table 7.1](#) suggest that the Gumbel distribution with a constant skewness of 1.12 is a suitable model for the annual maxima for the Mošnov and Ruzyně stations, while for Svratouch station the negative skewness could be described by a three-parameter lognormal distribution ([Holický, 2015](#)). However, for Svratouch, observations may be affected by measurement errors, to which skewness is the most sensitive of the observed statistical characteristics. Therefore, skewness is ignored for Svratouch when choosing the appropriate distribution and the Gumbel distribution is considered for all three stations, see [Figure 7.2](#). [Table 7.1](#) shows the characteristics of basic wind speed.

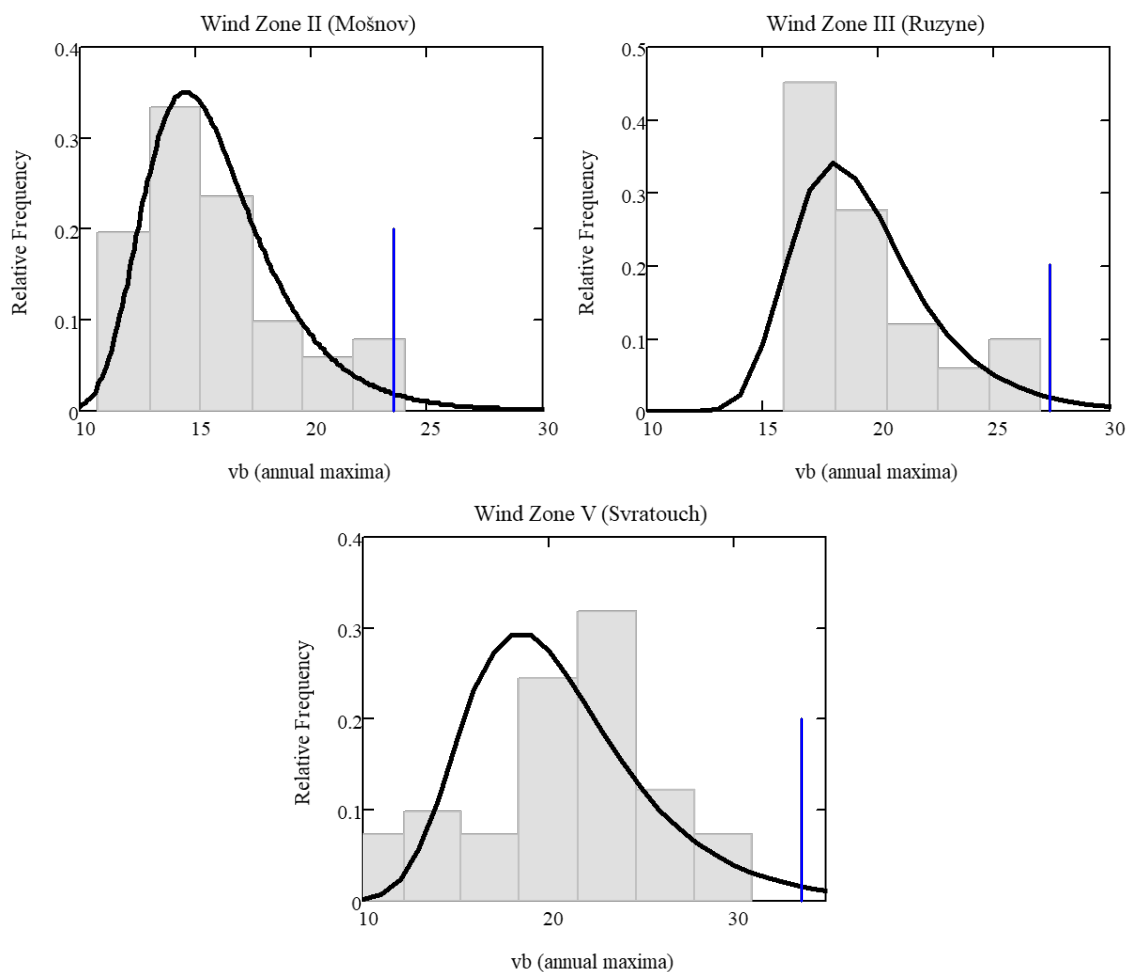


Figure 7.2: Histogram of annual maxima of wind speed in m/s, probability density function of Gumbel distribution and characteristic value determined as 98% quantile of the annual maxima.

Station	Mean annual maxima μ in [m/s]	Variation coefficient V	Skewness w	Characteristic wind speed 98% quantile [m/s]
Mošnov	15.9	0.19	0.95	23.3 (25)
Ruzyně	19.5	0.16	1.08	27.4 (27.5)
Svratouch	20.7	0.24	-0.53	33.7(36)

Table 7.1: Basic wind speed characteristics.

As described in Chapter 7.3 only the strong wind scenario is relevant for the bridge design. A Gumbel distribution was found to provide a suitable model for wind speeds during strong wind events, which are defined as storms where wind speeds exceed 10 m/s. Figure 7.3 provides the comparison of the empirical upper fractiles (considering measurements

with $v_b \geq 10 \text{ m/s}$ only) with those of the fitted Gumbel distribution of $v_{b, \text{strong}}$ (red dots). Note that the dots aligned with the black line would indicate a perfect fit. The statistical characteristics of the Gumbel distribution were obtained using the Least Square Method and Table 7.2 shows the mean value μ_v , standard deviation σ_v describing the tail of the distribution of wind speeds $\geq 10 \text{ m/s}$ and skewness $\tilde{\mu}_3$. Wind zone I and IV pressure models are approximated based on 3-second gust wind speed records. Note that analysis of the effect of climate change on wind load effects is beyond the scope of this contribution; for details see Orcesi et al. (2022).

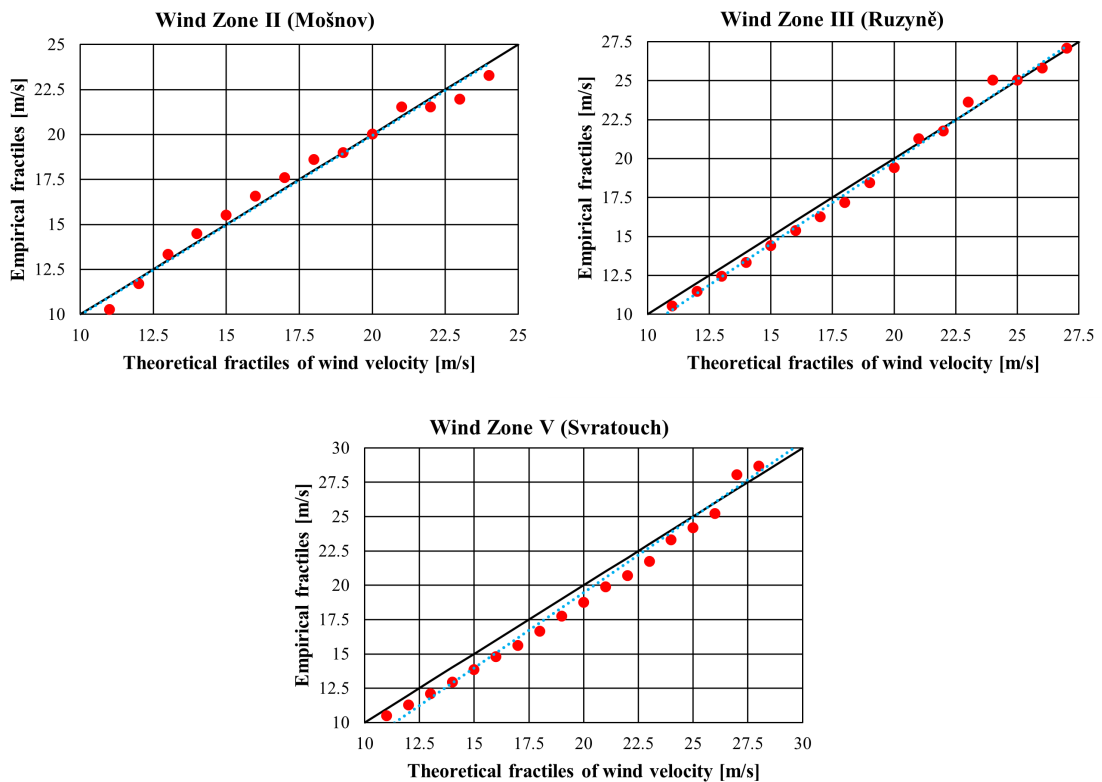


Figure 7.3: Q-Q diagnostic plot for wind speeds $\geq 10 \text{ m/s}$.

Wind Zone	$v_{b,k}$ [m/s]	Relative exceedance time 10 m/s ^{a)}	μ_v [m/s]	σ_v [m/s]	$\tilde{\mu}_3$
I	22.5	0.67 % (2.4 days/year)	9.90	2.20	-
II	25	1.21 % (4.4 days/year)	9.82	2.44	0.25
III	27.5	2.31 % (8.4 days/year)	10.74	2.37	0.22
IV	30	3.70 % (13.5 days/year)	10.60	2.65	-
V	36	10.8 % (39 days/year)	11.06	3.02	0.27

^{a)} The JCSS PMC (2021) gives an estimate of 16.7 days/year.

Table 7.2: Results of the analysis of high wind speeds – upper tail fit.

7.5 Notes on Wind Load Model

The notes are based on consultations with Ing. Král (Klokner Institute of CTU, Czech representative for EN 1991-1-4 and leading experts on structural reliability and wind loading from the Netherlands – Prof. Raphaël Steenbergen (TNO Delft, TU Ghent) and Prof. Ton Vrouwenvelder (TNO Delft).

1. The wind map in ČSN EN 1991-1-4 is processed so that the annual maxima of mean wind velocities have a probability of occurrence of 0.02. For approximately 5% of the territory of the Czech Republic, the values were corrected and higher mean wind speeds were used; related increases remain unknown.
2. The model in ČSN EN 1991-1-4 is processed for extreme wind speeds observed for synoptic storms. Thunderstorms and generally maximum wind gusts were not considered in the development of the wind map unless they were directly recorded by the meteorological stations.
3. The model in ČSN EN 1991-1-4 may not accurately reflect situations such as when two opposing trains pass by on a bridge during strong winds. Immediately after passing, an additional gust occurs in the open space between the trains, which may result in additional stress on the bridge.
4. For lower wind speeds (for load combination purposes) or wind speeds caused by thunderstorms, the Eurocode model may underestimate wind speeds at low heights above the terrain due to an overestimated orography effect.
5. It is assumed that the characteristic wind speeds cannot be reduced all over the Czech Republic. While the wind map might be conservative in most locations due to simplifications and zoning, higher values may be justified in some areas. If a detailed assessment is needed, it is recommended to request records from the Czech Hydrometeorological Institute, which can consider local information not used in the development of the wind map (additional wind speed measurements, terrain influence, mathematical flow models, etc.).
6. In combinations of the wind load with other variable loads, the values of load combination factors may need to be updated. It is recommended to consider limiting transport during strong winds – the crossings of strong synoptic storms are known

sufficiently in advance and are accompanied by tree falls. For structures whose reliability is significantly affected by wind loads, recommendations can be made for what wind speed it is recommended to limit or exclude transport.

From the above notes, it is concluded and considered in the following reliability analysis that the Eurocode model may underestimate the effects of wind loading. It is important to note that many studies focused on the reliability and calibration of individual coefficients point to hidden safety in the wind loading model (Soerensen and Hansen, 2016; Hansen et al., 2015; Holicky et al., 2016). For example, a recent study by Hansen et al. (2015) states: "The Eurocode model for verifying global effects often overestimates the effects observed in wind tunnels; this overestimation can exceed 40%." We note that calibrations of individual coefficients for various types of variables, including climatic loads, are currently being conducted.

A detailed analysis of these effects is beyond the scope of the dissertation. In the further analysis, these facts will be taken into account at least indirectly – in the case of ambiguous statistical data, more conservative estimates will be chosen. The characteristic value provided in the wind map is verified on the basis of available wind speed data.

Chapter 8

Light-weight Traffic Model

8.1 Traffic Load Models based on Traffic Records

According to EN 1991-2 Traffic load on bridges Section 6.3.4, the unloaded train load model is specified as 10 kN/m uniformly distributed load. According to EN 1991-1-4 Section 8.3.1, the height of railway vehicle shall be assumed as 4 m above the top of rail. Uniformly distributed load from the unloaded train load model and wind load shall be applied on the whole length of the bridge.

Based on research of railway vehicles operated in the railway network of the Czech Republic it is expected that particularly for local railway lines, this model is overly conservative (Ryjacek et al., 2017). To verify this assumption, the database of all trains in the Czech railway network was compiled in cooperation with the Czech railway authority – management of railways SŽ (Správa železnic) and main Czech operators. The railway managers recommended that it would be sufficient to base detailed analyses on the data for May and November, which should represent the two months with the highest train frequencies through the year.

Railway traffic data seem to have been mostly utilized in the previous studies focused on fatigue verification (Li et al., 2015; Lukacevic et al., 2014), and occasionally on dynamic effects (Jung et al., 2019; James, 2003) and ULS strength-related assessments (O'Connor et al., 2009). No investigations into EQU verification, and related measurements, and detailed analysis of data regarding the light-weight traffic – unloaded trains – have been presented as yet, according to the best knowledge of the author.

In the absence of experience with railway traffic measurements, findings obtained for road traffic and weight-in-motion data are utilized here to indicate a sufficient length of records. For instance, the sensitivity analysis by Sifre and Lenner (2021) demonstrated

that statistical uncertainty in predicted extreme road traffic load and related partial factor drops significantly when half-month records are available and insignificant reductions of the uncertainty are achieved for longer measurements. This is in broad agreement with [Steenbergen et al. \(2012\)](#) who concluded that approximately three weeks are usually representative for the traffic distribution and are thus sufficient for reliability assessment. Similarly, the final report of [ARCHES \(2009\)](#) required at least one week of heavy traffic and [O'Brien et al. \(2015\)](#) two weeks of heavy traffic.

Two months of measurements are deemed to be sufficient to establish a representative probabilistic model for unloaded trains considering the recommendations of railway authority experts and based on the following arguments:

1. In comparison to road traffic, railway traffic exhibits normally lower variability and even lower variability is characteristic for unloaded trains ([Lukacevic et al., 2014](#)). The low variability results from:
 - (a) Well-controlled loads in railway lines where all vehicles need to be permitted and controlled.
 - (b) All travels being organized through time schedules.
2. The leading variable action effect – wind pressure is associated with much larger uncertainty than that due to weight of unloaded trains, G_{train} ; thus a small error in estimating statistical characteristics of G_{train} (possibly associated with a limited length of records) is likely to have a negligible effect on the resulting reliability level. Similarly, an accompanying action G_{train} is in EQU verification typically represented by fractiles corresponding to approximately a characteristic (unfactored) value, thus approximately an extreme value with return periods of about 10 to 50 years. In contrast, the design (factored) value of wind pressure may correspond to return periods of hundreds of years ([JRC, 2023](#)).
3. No seasonal patterns can be assumed for unloaded trains – the records taken in May and November should be sufficiently representative.

8.2 Available Data for Traffic Model Specification

The light-weight traffic distribution was determined based on data sets provided from following railway operational databases.

ISOR (Accessed 2016) is a central dispatching system created by Oltis Group, serving rail infrastructure managers. The basic data object in the system database is a TRAIN, and the following is recorded in the system for this object:

- Specific active driving vehicles of the train and their location in the train.
- Total number of vehicles in the train as the sum of all tractive and driving vehicles.
- Total number of train axles as the sum of all tractive and driving vehicles.
- Total weight of the train as the sum of all tractive and driving vehicles.
- Total length of the train as the sum of all tractive and driving vehicles.
- Maximum train speed given by the technical capabilities of the vehicles in the train, or reduced speed due to current restrictions on the train (exceptional shipments, insufficient braking).
- Time position of the train between monitored traveling transit points (bridges are not transit points).
- Type of carrier and train.

The ISOR database contains the most complete set of data on transport in the Czech railway network, mostly complete data of all Czech carriers. Trains of international carriers often have incomplete information about the composition of the train in the database, but at least information that the train passed through the track node at that moment and what type of train it was, is found in the database. For trains with missing detailed information about their composition, the information for the given track node was supplemented as an average value for trains of the same type for the given month.

COMPOST (Accessed 2016) data system is designed to track information about train composition and primarily serve as a data communication channel between the railway management and the information systems of individual carriers in the Czech Republic. The system should contain the following information about the train in a specific section of the track:

- Train type (distinction between normal train and locomotive train).
- Total weight of the train including driving vehicles.
- Total length of the train including driving vehicles.
- Number of vehicles in the train.
- Number of axles in the train.
- List of driving units.
- Maximum speed of the train.
- Braking mode (P = passenger, G = freight).

However, the information in this system is incomplete. For example, data from the car-

rier ČD, which operates up to 80% of all passenger trains, is missing from 2015. ČD Cargo adds data to the system, but their accuracy is not guaranteed due to deviations in transportation planning.

REVOZ (Accessed 2016) information system contains records of locomotives series, special vehicles, passenger and freight cars, and individual vehicles including their technical parameters. The system primarily contains the following information about locomotives:

- Serial number of locomotives and special vehicles.
- Serial number of passenger and freight cars.
- Record of locomotives and special vehicles, including their technical parameters.
- Central serial number of train controllers and radio stations.
- Vehicle technical parameters.
- Territorial approval of vehicle – record of approved track sections for each vehicle.
- Load tables.
- Tractive, energy and current characteristics.

Operational load is one of the main markers of railway traffic intensity on a particular railway line and is expressed in millions of gross tons per year [mil. gross tons/year]. According to this criterion, the railway network in the Czech Republic is divided into six zones. Figure 8.1 shows the division of the Czech railway network. The railway network is divided into following six railway line classes:

1. more than 47.450 mil. gross tons/year
2. 29.201 - 47.450 mil. gross tons/year
3. 14.601 - 29.200 mil. gross tons/year
4. 7.301 - 14.600 mil. gross tons/year
5. 1.825 - 7.300 mil. gross tons/year
6. less than 1.825 mil. gross tons/year

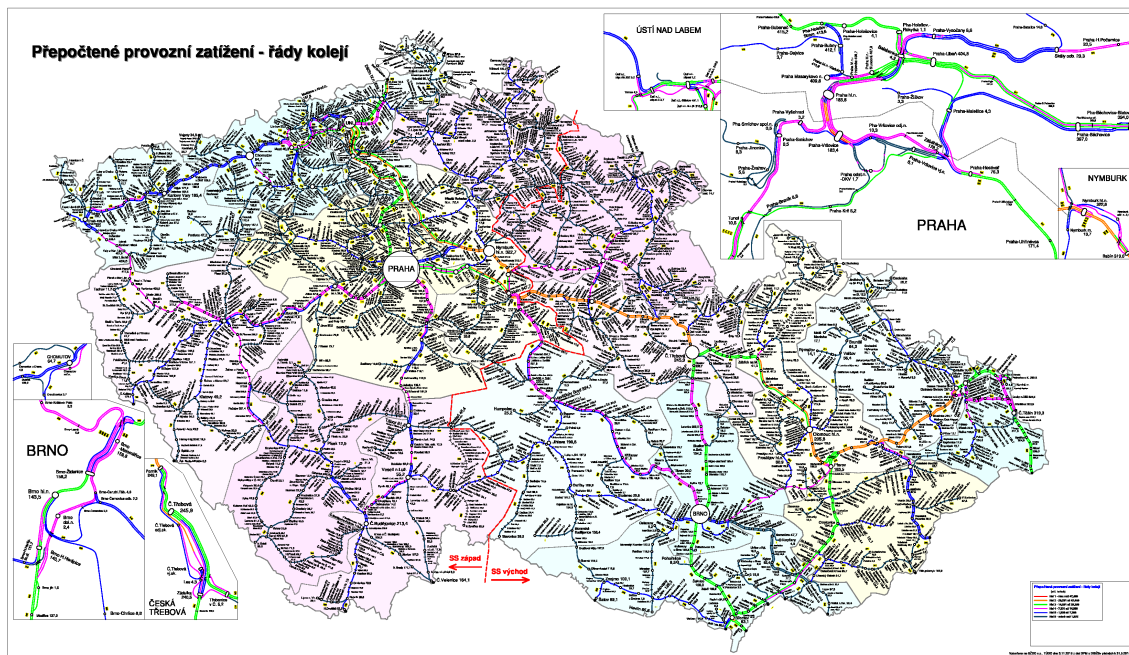


Figure 8.1: Operational load map.

8.3 Unloaded Train Distribution

Three representative railway lines have been selected to model the distribution of unloaded trains:

- High-intensity line in Class 2 (Český Brod), mainly for public transportation trains;
- Medium-intensity line in Class 4 (Most), with a high frequency of freight train traffic;
- Low-intensity line in Class 5 (Holubov), a local railway line only with specific public transportation train traffic.

A detailed statistical analysis of train weight was performed for these three railway lines. The database does not contain information on the types of train cars (except for locomotives), so it is impossible to link train weights with heights unless it is a standardized public transportation train system (Class B and E). The observed train weights were divided into five Classes A to E and assigned the train height and wind load properties relevant to each train Class per Section 5.4. Trains with weights exceeding 2 t/m are not considered in the EQU verification. Only the weight of the train cars was considered in the evaluation while the weight of the locomotive was conservatively ignored. Data from the months of May and November were used as recommended by the operator to reasonably

well characterize traffic flow. Figures 8.2, 8.3 and 8.4 show the unloaded train distribution and Table 8.1 provides the tabulated summary of train frequency n , mean weight of the unloaded train μ in t/m and standard deviation σ in t/m.

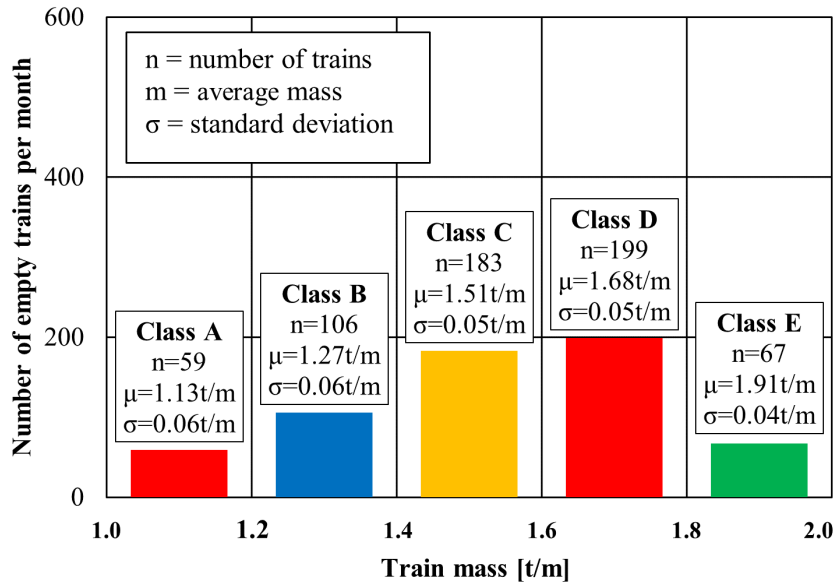


Figure 8.2: Unloaded train distribution – high-intensity line (Class 2).

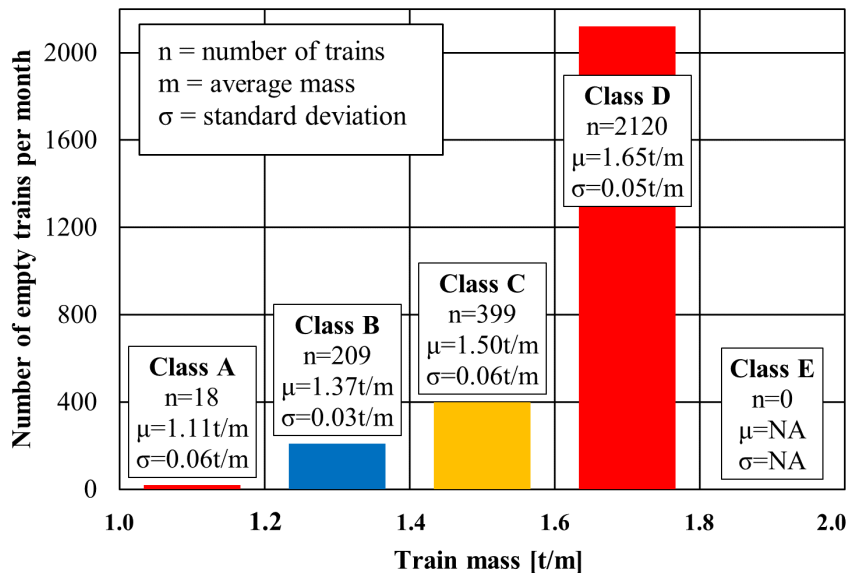


Figure 8.3: Unloaded train distribution – medium-intensity line (Class 4).

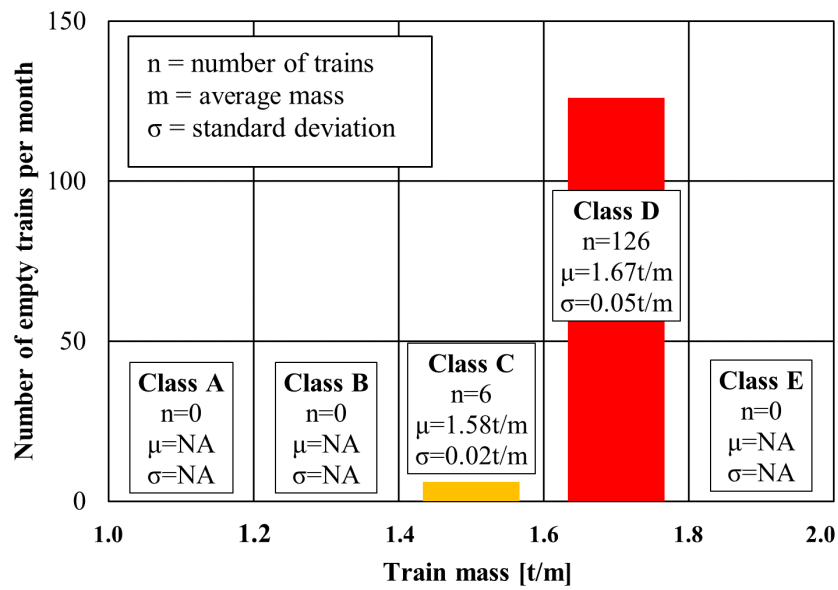


Figure 8.4: Unloaded train distribution – low-intensity line (Class 5).

Class/ Station	High-intensity line			Medium-intensity line			Low-intensity line		
	n	μ	σ	n	μ	σ	n	μ	σ
A	59	1.13	0.06	18	1.11	0.03	-	-	-
B	106	1.27	0.06	209	1.37	0.03	-	-	-
C	183	1.27	0.06	399	1.50	0.06	6	1.58	0.02
D	199	1.68	0.05	2120	1.65	0.05	126	1.67	0.05
E	67	1.91	0.04	-	-	-	-	-	-

Table 8.1: Unloaded train distribution.

Chapter 9

Reliability Verification

9.1 Basic Assumptions

Probabilistic methods provide appropriate operational tools for assessing the safety and reliability of existing bridges since they take into account the inherent uncertainties and variability in the load effects on bridges and the resistance of the bridge components.

The loads on bridges, such as traffic loads and environmental loads, are inherently random and variable. In addition, the resistance of bridge components, such as the strength of the steel or concrete, can also be variable due to factors such as construction quality, geometrical imperfections and material degradation over time. These uncertainties and variabilities lead to uncertainty in the assessment of the safety and reliability of bridges.

Probabilistic assessment uses statistical methods and probability theory to model and quantify relevant uncertainties in reliability assessment of existing bridges. Therefore, it can provide more accurate and comprehensive assessments of the safety and reliability of bridges than traditional methods, which often rely on simplified assumptions and deterministic analyses.

Probabilistic assessment helps to avoid unnecessary conservatism in EQU verification based on the partial factor method, including improved modeling of site-specific wind speeds, description of wind-on-light-weight train situations, and modeling of the effects of actual geometry and weight of a bridge (Zitny et al., 2023).

The assessment by the partial factor method and probabilistic approach aims to verify reliability of the bridge in the case with respect to the EQU limit state under the following assumptions:

1. The main variable action is the wind pressure.

2. The force coefficients for wind pressure obtained from the wind tunnel tests are taken into account. For the sake of comparison, the EN 1991-1-4 force coefficients according to the M2 method are also applied, with a more conservative bias and larger uncertainty.
3. The effects of orography and terrain roughness are considered in accordance with EN 1991-1-4.
4. The probabilistic models for the basic wind speeds are based on the meteorological records obtained and evaluated for the reference stations in wind zones I-V. The records of 10-minute mean wind speed are considered, irrespective of wind direction and time of year, at a height of 10 m above ground level in flat open country terrain. The upper tail of the wind speed distribution is used in the reliability verification, only wind speeds exceeding 10 m/s.
5. Probability of simultaneous occurrence of strong wind and light-weight train crossing the bridge is estimated based on the databases for wind speeds and traffic flows. Important is the assumption that railway traffic is interrupted when wind speed exceeds 30 m/s, $v_{b,lim}$, DB Richtlinie 807.04, (Fujii et al., 1999) and higher wind speeds are thus ignored in the probabilistic assessment. Example of the method of traffic operation control under high wind speeds in Japan is provided in (Fujii et al., 1999). Note that EN 1991-1-4, Section 8.1(5) provides a different limit on wind speed for the combination of traffic and wind loads; however, it is ignored here due to a difficulty to interpret this limit (referring to fractiles of wind speed distribution) in a probabilistic analysis. As various approaches are adopted to control railway traffic safety and avoid derailments due to excessive wind speeds, the importance of an adopted wind speed limit on reliability of bridges is further investigated. The limiting wind speed, $v_{b,lim}$, is considered as a study parameter in the probabilistic assessment.
6. Classes A thru E of light-weight train distributions according to Chapter 8 are considered.
7. The parameters describing geometry of the whole bridge are considered as deterministic – they are verified in-situ with negligible uncertainty.

While some of these assumptions are bridge- and EQU verification-specific, the approach to reliability analysis remains general and subsequent studies focused on other limit states

and other types of bridges can be inspired by both adopted procedure and numerical results.

9.2 Partial Factor Method

The partial factor method is a fundamental method used to verify the reliability of structural designs. It is specified in the Eurocodes and ISO standards. The partial factors, combination factors, and other reliability elements used in this method have been calibrated using probabilistic methods and taking into account previous standards and experiences. Using the partial factor method, the bridge is assumed to satisfy the EQU limit state when the design value of the destabilizing moment of wind pressure, M_{Wd} , is less than the design value of the stabilizing moments due to permanent actions on the bridge and weight of an unloaded train, M_{Gd} .

$$M_{Wd}(\gamma_W; v_{b,k}) / M_{Gd}(\gamma_{G,inf}; G_{bridge}; G_{train}) \leq 1.0 \quad (9.1)$$

where $\gamma_W = 1.5$ and $\gamma_{G,inf} = 0.95$ are the partial factors for wind pressure and favorable permanent actions, respectively, for EQU according to EN 1990.

In accordance with Reliability background to the Eurocodes (JRC, 2022), the wind pressure is obtained as:

$$w = c_f c_g c_r^2 \theta \rho v_b^2 = 0.5 C \rho v_b^2 \quad (9.2)$$

where c_f = force coefficient; c_g = gust factor; c_r^2 = roughness factor; θ = wind load uncertainty; ρ = air density; v_b = basic wind speed (10-minute mean wind speed); and $C = c_f c_g c_r^2 \theta$ denotes the time-invariant component of wind pressure. The notation of basic variables is provided in Table 9.1 and 9.2.

Symb.	Basic variable X	Dist. $_a$	μ_X/X_k	V_X	Note
G_{bridge}	Permanent actions bridge	N	1	0.04	Eurocode background documents (JRC, 2022; CEN/TC250, 1996; Gulvanessian et al., 2012)
G_{train}	Light-weight train	N	1.11-1.91 $_b$)	<0.05	Based on traffic flow data (Table 8.1)
C	Time invariant comp. - EN 1991-1-4 - wind tunnel	LN0	0.32-1.09 0.8	0.26 0.16	Detailed parameters in Table 9.2
$v_{b, strong}$	Wind speed during storm	Gum	0.31-0.44 $_c$)	0.22-0.27 $_d$)	Based on strong wind distribution (Table 7.2)

$_a$) N – normal, LN0 – lognormal with the origin at zero, Gum – Gumbel (maxima). Mean value μ_X , characteristic value X_k and coefficient of variation V_X .

$_b$) peak values of light-weight train distribution, Class A thru Class E, $X_k = 1.0t/m$.

$_c$) $\mu_v/v_{b,k}$

$_d$) σ_v/μ_v

Table 9.1: Probabilistic models of basic variables in Eq. 9.1.

Symb.	Factor	μ_X/X_k	V_X	Note
c_f	Force - EN 1991-1-4 - wind tunnel	0.4-1.32 $_a$) 1	0.1 0.05	$c_{f,EQU,M2}$ - bias for M2 (Table 6.4). $c_{f,EQU,tunnel}$ See Section 9.3.2.
c_g	Gust	1	0.1	Same for wind tunnel and EN 1991-1-4.
c_r^2	Roughness	0.8	0.1	Same for wind tunnel and EN 1991-1-4.
θ	Load eff. unc. - EN 1991-1-4 - wind tunnel	1 1	0.2 0.05	- See Section 9.3.2 for more details.

$_a$) Class A thru E, respectively.

Table 9.2: Probabilistic models of factors affecting the time-invariant component of wind pressure.

9.3 Probabilistic Model

9.3.1 Limit State Function

Considering crossing of a particular type of the light-weight train, probabilistic verification is based on the following limit state function:

$$Z_{t_{ref},i}(\mathbf{X}) = G_{bridge} \frac{b}{2} - \max_{j=1..n(t_{ref})} \left(CA_{ref} 0.5 \rho v_{b,strong}^2 z_w - G_{train,i,j} \frac{b}{2} \right) \quad (9.3)$$

where i denotes the type of a train (Table 4.2); b is the bearing spacing; z_w is the distance of the centroid of the reference area to the center of rotation, see Figure 6.5; and $n(t_{ref})$ is the number of load events as discussed in the following text. The notation and probabilistic models of the basic variables are provided in Table 9.1. Failure probability is then evaluated from Eq. 9.3 for a particular type of train “ i ” as:

$$P_{f,t_{ref},i} = P[Z_i(\mathbf{X}) > 0] \quad (9.4)$$

and reliability index is obtained as:

$$\beta_{t_{ref},i} = -\Phi^{-1} \left[P_{f,t_{ref},i} \right] \quad (9.5)$$

where $\Phi^{-1}(\cdot)$ is the inverse cumulative distribution function of the standardized normal variable.

9.3.2 Basic Variables

Self-weight of the bridge and other permanent actions such as bridge equipment, G_{bridge} , are based on the bridge documentation, visual inspections, and measurements. This is why the characteristic value is considered to be unbiased and low coefficient of variation (“CoV”) is considered. Further information about probabilistic modeling of permanent actions on railway bridges can be found in (O’Connor et al., 2009; Moreira et al., 2016); general principles are then provided by the JCSS PMC (2021). The model of weight of light-weight trains, G_{train} , is based on the analysis traffic data presented in Section 8. The biases above unity indicated in Table 9.1 for the Class A thru E vehicles reveal that verification based on characteristics of light-weight trains will likely lead to more favorable results in comparison to verification based on the generalized (conservative) EN 1991-2 unloaded train model. As expected, weight of light-weight trains exhibits lower variability, $< 5\%$, than that considered for railway traffic load effects with CoV around 10% (Wisniewski et al., 2009; Moreira et al., 2016).

Uncertainty in load effect of the stabilizing actions is considered to be small and it is ignored in reliability analysis. In contrast, uncertainty in the destabilizing load effect, θ , is explicitly included in the following probabilistic model of the time-invariant component, C , of wind pressure; in Eq. 9.2:

$$C = \theta c_f c_g c_r^2 \quad (9.6)$$

The notation and probabilistic models of the factors in Eq. 9.6 are provided in Table 9.2;

a lognormal distribution is assumed (LN0).

The values of biases and CoVs in Table 9.2 are based on **JCSS PMC**, with the following additional considerations:

- CoV of the load effect uncertainty, $V_\theta = 0.05$, for the models based on wind tunnel tests accounts for significantly reduced uncertainty in comparison to the generic **EN 1991-1-4** model for which $V_\theta = 0.2$. Further, the reduced CoV is based on the assumptions adopted in the draft of the **fib Model Code 2020** where $V_\theta = 0.075$ is generally considered for ULS verification. However, the Model Code indicates that $V_{\theta E} < 0.075$ may apply for simple static systems with well-defined boundary conditions where load effects can be determined without uncertainties and considers in such cases $V_{\theta E} = 0.025$. This is why $V_\theta = 0.05$ is considered for the load effect based on wind tunnel tests.
- The bias of force coefficient, cf , for the **EN 1991-1-4** model is based on the comparison with wind tunnel tests; no systematic bias is assumed for the model based on wind tunnel test results. CoV for **EN 1991-1-4** is based on the recommendations of **JCSS PMC** while for wind tunnel tests, a reduced value, $V_{cf} = 0.05$, is assumed to account for uncertainty due to improved knowledge in comparison to the generalized **EN 1991-1-4** model, the values is based on information provided in Background to Eurocodes **JRC (2022)** for load coefficient measured in wind tunnel for local effects on buildings. The reduced value of CoV seems to be in broad agreement with uncertainties in wind tunnel testing indicated in (**Kasperski, 2003**).

Further information is provided by (**fib bulletin 80, 2016; Sykora, Holicky, Jung and Diamantidis, 2016; Baravalle et al., 2017; Nadolski et al., 2019; Cardoso et al., 2019; Kasperski, 2009**).

9.3.3 Evaluation of Failure Probability

Monte Carlo simulation has been used to evaluate the limit state function based on variable distribution and uncertainties shown in Table 9.1. The Monte Carlo method is a statistical technique that uses random sampling to simulate real-world processes and estimate results. The Monte Carlo method works by generating a large number of random samples from a probability distribution, and using those samples to estimate results that would be difficult or impossible to determine analytically. It quantifies uncertainty and account for the randomness inherent in many real-world processes (**Binder, 1979**). Following is the flowchart of the algorithm.

Algorithm 9.1 Monte Carlo simulation of limit state function Eq. 9.3.

```

1:   $n_{sim}$                                 #number of simulations
2:   $n_{LC}$                                   #no. of strong wind-on-light-weight train events
3:   $n_f \leftarrow 0$                         #number of failures
4:  for  $i \in 1..n_{sim}$ 
5:     $x_1 \leftarrow \text{norm}(\text{rand}, \mu_{G_{bridge}}, \sigma_{G_{bridge}})$ 
6:     $x_2 \leftarrow 0$ 
7:    for  $j \in 1..n_{LC}$ 
8:       $x_2 \leftarrow \max[x_2, \text{lognorm}(\text{rand}, \mu_C, \sigma_C) \cdot \text{gum}(\text{rand}, \mu_{v_{b,strong}}^2, \sigma_{v_{b,strong}}) -$ 
9:         $\text{norm}(\text{rand}, \mu_{G_{train}}, \sigma_{G_{train}})]$ 
10:    $n_f \leftarrow n_f + \text{if}(x_1 - x_2 < 0, 1, 0)$ 
11:   $P_f \leftarrow n_f/n_{sim}$                 #probability of failure

```

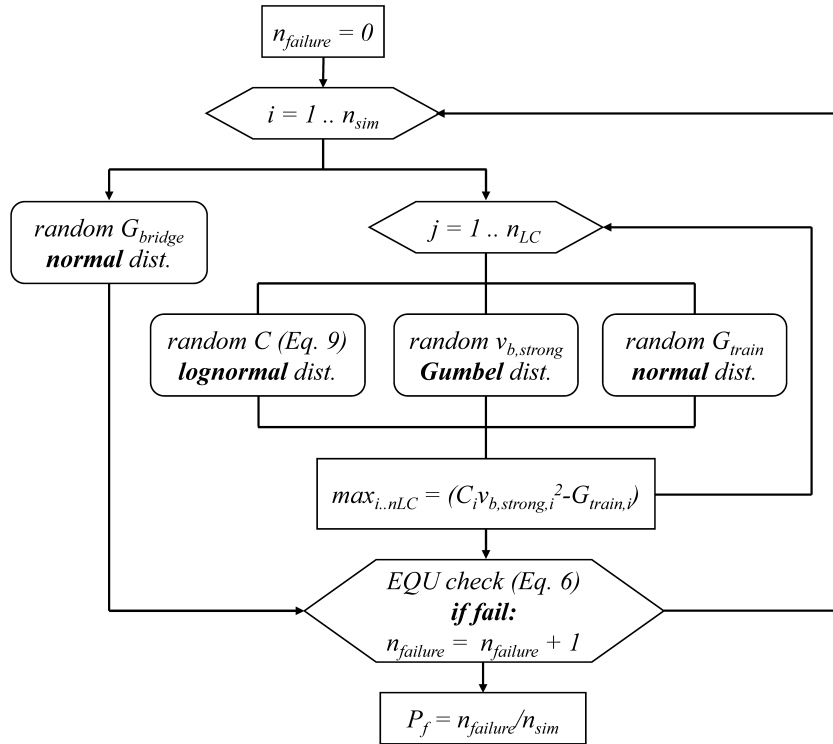


Figure 9.1: Monte Carlo simulation of limit state function Eq. 9.3.

Due to the high computational demands of the Monte Carlo method, it was used only to verify the several design combinations of bridge type, wind zone and light-weight train distribution. For the remaining calculations the numerical integration method was used according to Holicky [Holicky \(2009\)](#). The weight of the bridge G_{bridge} and weight of the train G_{train} have been considered only by mean values due to their insignificant variability

in comparison to the remaining variables, C and $v_{b,strong}$.

$$P_{f,t_{ref}} = \int_0^{\mu_C + 10\sigma_C} \mathbf{gum} \left(\sqrt{\frac{\mu_{G_{bridge}} + \mu_{G_{train}}}{c}}, \mu_{v_{b,strong}}, \sigma_{v_{b,strong}} \right)^{n_{LC}} \cdot \mathbf{lognorm}(c, \mu_C, \sigma_C) dc \quad (9.7)$$

9.4 Target Reliability

Reliability indices $\beta_{bridge,1}$ obtained by the probabilistic analysis need to be compared with a target level adequate for (i) EQU limit state and (ii) existing railway bridges. Regarding (i), the target levels specifically derived for the EQU verification are unavailable and they are scarcely discussed in the scientific literature. **Holicky and Sykora (2009)** studied the reliability levels associated with the EQU design according to Eurocodes. Focusing on a cantilevered beam exposed to a destabilizing imposed load and motorway gantry exposed to wind pressure, they found a target level of $\beta_{t,50} \approx 3$ for a 50-year reference period. This design reliability level should correspond to the annual $\beta_{t,1} \approx 3.6 - 4.0$ (**Holicky et al., 2018**). The beam and gantry are assumed to be classified in the middle failure consequence class – CC2 according to **EN 1990**.

As to (ii), the target reliability of existing structures is subject of ongoing discussions of researchers, practitioners, and code makers. At present, broad consensus on the target reliabilities for existing structures is missing throughout the world, but also among European countries. The recent report on reliability background of the Eurocodes **JRC (2022)** indicates that the target reliability levels for new structures can in most cases be considered conservative for the assessment of existing structures. The economic, societal, and sustainability arguments may help to substantiate a lower assessment level.

Following the guidance of the new **fib Model Code 2020** and **Baravalle and Kohler (2018)** indicates that considering an annual reference period for assessment could be beneficial as:

- Changing a reference period from e.g. 50 years to 1 year decreases the scatter of reliability levels for different loaddynamics ratios.
- Target levels need not be recalculated for existing structures with different service lives.
- An annual format is more consistent with regulations and acceptance criteria related to life safety.
- An annual format is more suitable for rapid deterioration e.g. due to fatigue or corrosion. Averaging over e.g. 50 years makes little sense when failure is likely in

the last few years of the considered service life.

Annual target reliability index should be fulfilled in each year of the service life of the structure. For further details see [Baravalle and Kohler \(2018\)](#).

EN 1990 is primarily intended for the design of new structures and thus the target levels therein are deemed to be inadequate for the assessment of existing railway bridges. Draft [fib Model Code 2020](#) indicates the annual target $\beta_{t,1} = 3.7$ for the ULS assessment of existing railway bridges classified in the highest consequence class CC3. This might be considered as well-matching the levels to EQU design for CC2 structures (3.6-4.0) – the assessment levels should be in principle lower than the design levels but CC3 structures should have higher target levels than CC2 structures. Based on these arguments, $\beta_{t,1} = 3.7$ is considered to provide an adequate target level for the EQU verification of existing railway bridges.

9.5 Probabilistic Assessment

Initially, reliability is analyzed for “n” loading events when a particular type of the light-weight train crosses the bridge during a strong wind event of mean duration of eight hours. To evaluate bridge reliability according to Eq. 9.3, number of such situations, $n_{t_{ref}}$, needs to be specified. Taking the light-weight train of Class C in Station S1 (Table 8.1) and Wind Zone II (Table 7.2) as an example, the following is obtained:

- Probability of wind speed over 10 m/s is estimated from the annual average of total duration of strong wind events – $P_{v_b \geq 10} \approx 106 h / (365.25 \times 24 h) = 1.21\%$ where 106 hours is the annual average duration of storms with wind speeds exceeding 10 m/s as obtained from meteorological measurements, see Table 7.2.
- Expected number of crossings of Class C trains (Station S1 distribution) during a storm per year is determined from the total number of crossings per year ($183 \times 12 = 2196$ from the traffic intensity database) and from $P_{v_b \geq 10}, n_{t_{ref}} \approx 2196 \times 0.0121 = 26.6 \approx 27$ crossings for $t_{ref} = 1 y$.

Using Eq. 9.3 and Eq. 9.4, Figure 9.2 portrays the variability of annual reliability index β_{1y} . (hereafter “ β_1 ”) with the limiting wind speed, $v_{b,lim}$, for crossings of all light-weight train types under consideration. Considering the wind pressure estimated on the basis of wind tunnel results, it appears that:

1. The limiting wind speed is governing reliability of the bridge in the EQU verification. When $v_{b,lim} < 23 m/s$, reliability index β_1 exceeds 5. When railway traffic is

operating at high wind speeds (with the danger of derailment), β_1 -values may drop below 4.

2. The type of train seems to be less important. The difference in terms of β_1 -values between the most unfavorable and most favorable types (Class C and Class B, respectively) is around 0.5.
3. Interesting to note is that focusing on Class C and Class D vehicles, lower reliability is obtained for heavier Class C for which higher wind pressures are predicted due to an unfavorable shape of the vehicle.

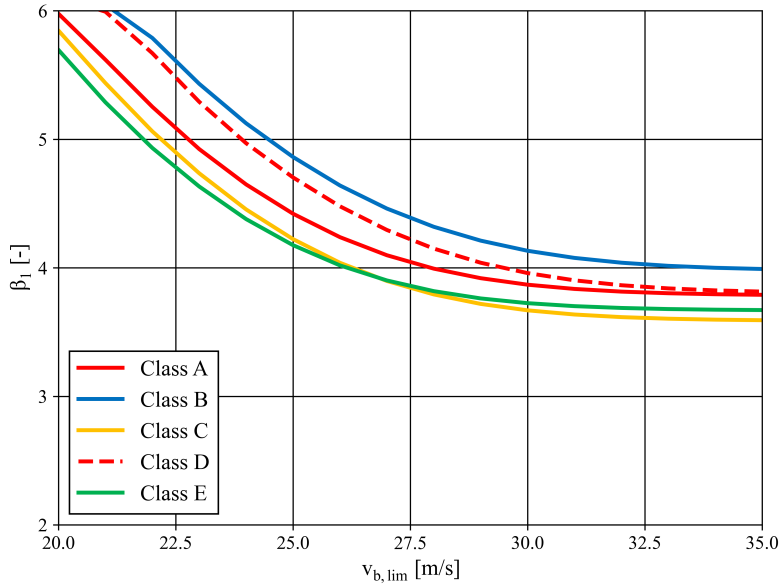


Figure 9.2: Annual reliability index β_1 for Classes A thru E as a function of limiting wind speed $v_{b,lim}$ (wind pressure based on wind tunnel tests).

The reliability indices in Figure 9.2 cannot be directly compared with the selected target index of 3.7. It remains to be taken into account that several types of trains cross the bridge, $i = 1..5$, and system reliability needs to be investigated – failure during the crossing of any type of light-weight train can be an EQU failure of the bridge:

$$P_{f,bridge,1} = P \left\{ U_{i=1}^5 [Z_{1,i}(\mathbf{X})] \right\} \quad (9.8)$$

where U denotes the union of events. As the events during which failure may occur are correlated (through the variables G_{bridge} and C) and five types of trains cross the bridge, failure probability in Eq. 9.8 can be evaluated with difficulty. For practical applications,

it is commonly sufficient to evaluate the bounds on system failure probability (Ditlevsen and Madsen, 1996):

$$\max_{i=1..5} P_{f,1,i} \leq P_{f,bridge,1} \leq \sum_{i=1}^5 P_{f,1,i} \quad (9.9)$$

The upper bound on failure probability corresponds to a lower bound on reliability index and vice versa. Figure 9.3 portrays lower and upper bound on annual system reliability index $\beta_{bridge,1}$ as a function of limiting wind speed $v_{b,lim}$ for wind pressure based on wind tunnel tests and EC1-4:

1. The lower and upper bounds on system reliability index provides a narrow interval indicating that uncertainty in system reliability is relatively small. For practical applications, it is likely often sufficient to consider the lower bound on $\beta_{bridge,1}$, hence upper bound on failure probability.
2. When comparing the results for EN 1991-1-4 and wind tunnel alternatives, the effect of uncertainties in c_f and θ reduced for the latter (Table 9.2) is significant:
 - (a) Reliability of the bridge can be considered sufficient for $v_{b,lim} \leq 26 \text{ m/s}$ when the probabilistic analysis is based on the wind tunnel results while bridge reliability is too low for $v_{b,lim} > 23 \text{ m/s}$ when the general EN 1991-1-4 model is taken into account.
 - (b) The difference in reliability levels between the wind tunnel and EN 1991-1-4 models vanishes with increasing $v_{b,lim}$ as in these cases variability of strong wind speeds dominates reliability.
3. The target reliability index is a key component of the reliability assessment – if it were decreased below 3.0, the bridge would satisfy the EQU verification for $v_{b,lim}$ up to 35 m/s (the operation of railway traffic at higher wind speeds being considered unsafe).

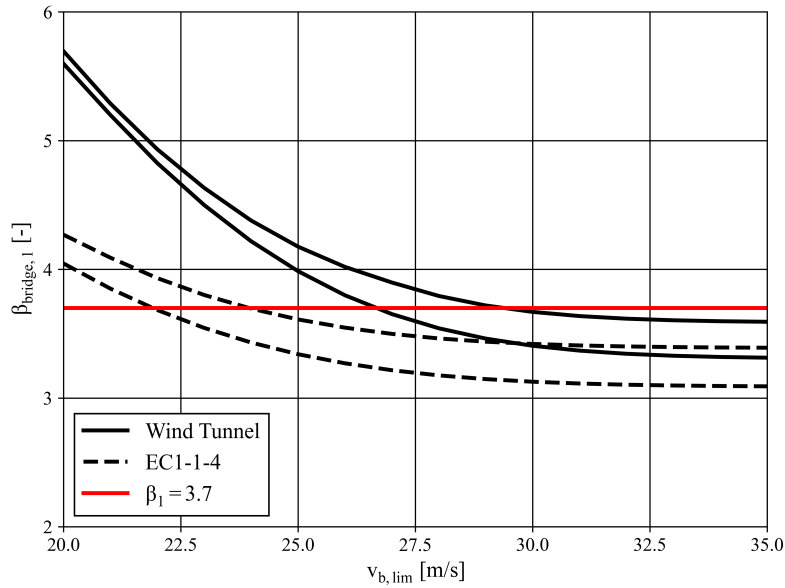


Figure 9.3: Lower and upper bound on annual system reliability index $\beta_{bridge,1}$ as a function of limiting wind speed $v_{b,lim}$ for wind pressure based on wind tunnel tests and EN 1991-1-4.

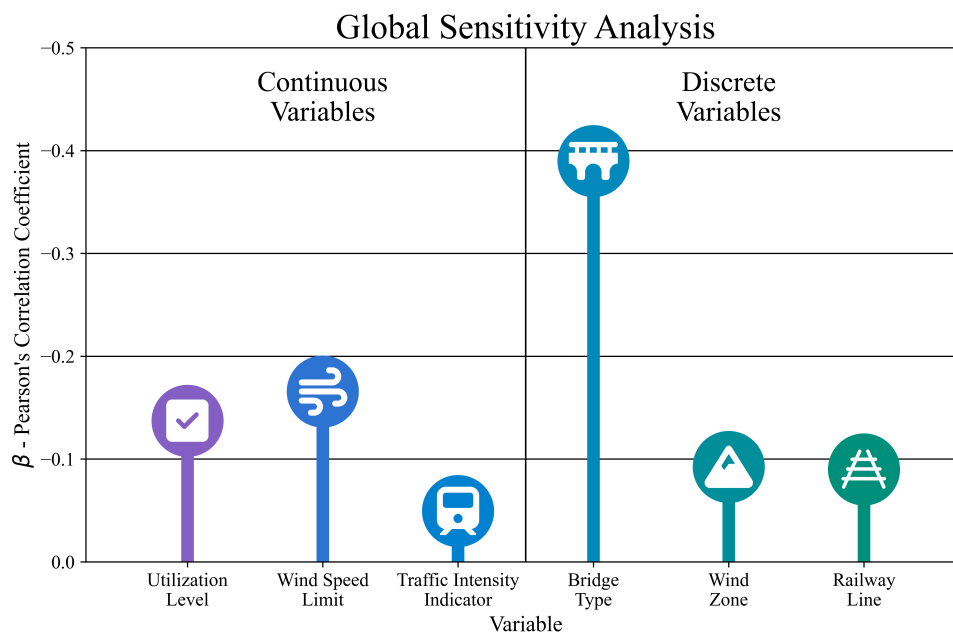
9.6 Sensitivity Analysis

Sensitivity analysis investigates how the uncertainty in the output of the probabilistic model can be appropriated to different sources of uncertainty in the model input (Saltelli, 2002). Sensitivity analysis is an integral part of the study of mathematical model properties. In this case Pearson's correlation coefficient is calculated. It is a statistical measure of the strength of linear relationship between paired data. It takes values from -1 to 1, closer to ± 1 shows how strong is the monotonic relationship (Saltelli, 2008). The sensitivity analysis is made for representative amount of data sets (10^5) generated in Design of Experiments (DoE) using Sobol sequence pseudo-random number generator (Sobol, 1967). See Table 9.3 for selected variables with lower and upper boundary selected for the DoE in the Global Sensitivity Analysis. The reliability index β is considered as the model output and the only cost function.

Variable	Type	Lower	Upper
EQU utilization level	Continuous	1.0	2.5
$v_{b,lim}$	Continuous	15	50
Indicator of local traffic intensity	Continuous	0.1	10
Bridge Type	Discrete	B1	B8
Wind Zone No.	Discrete	I	V
Railway Line No.	Discrete	S1	S3

Table 9.3: Global sensitivity analysis input.

Each continuous variable is related to one discrete variable. Utilization level expresses a quality of the bridge type; limiting wind speed relates to the wind zone wind speed distribution, suppressing any data above the wind speed limit to be assumed in the reliability analysis; and indicator of local traffic intensity relates to the station number decreasing or increasing the number of trains for given railway line. See Figure 9.4 for the results of the Global Sensitivity Analysis. It is to be noted that negative values of Pearson's correlation coefficients are typical for load effects – increasing load input decreases the reliability index β .

Figure 9.4: Global Sensitivity Analysis – Pearson's correlation coefficient related to reliability index β .

Additional sensitivity analysis is performed for all design cases using only the continuous variables. See Figure 9.5 for the average correlation coefficient for each bridge. This has proven that for all bridges the two most decisive variables are the wind speed limit and utilization level in EQU. Therefore, these two variables will be used for detailed probabilistic simulations to develop the wind speed limit to utilization relationships for all bridges.

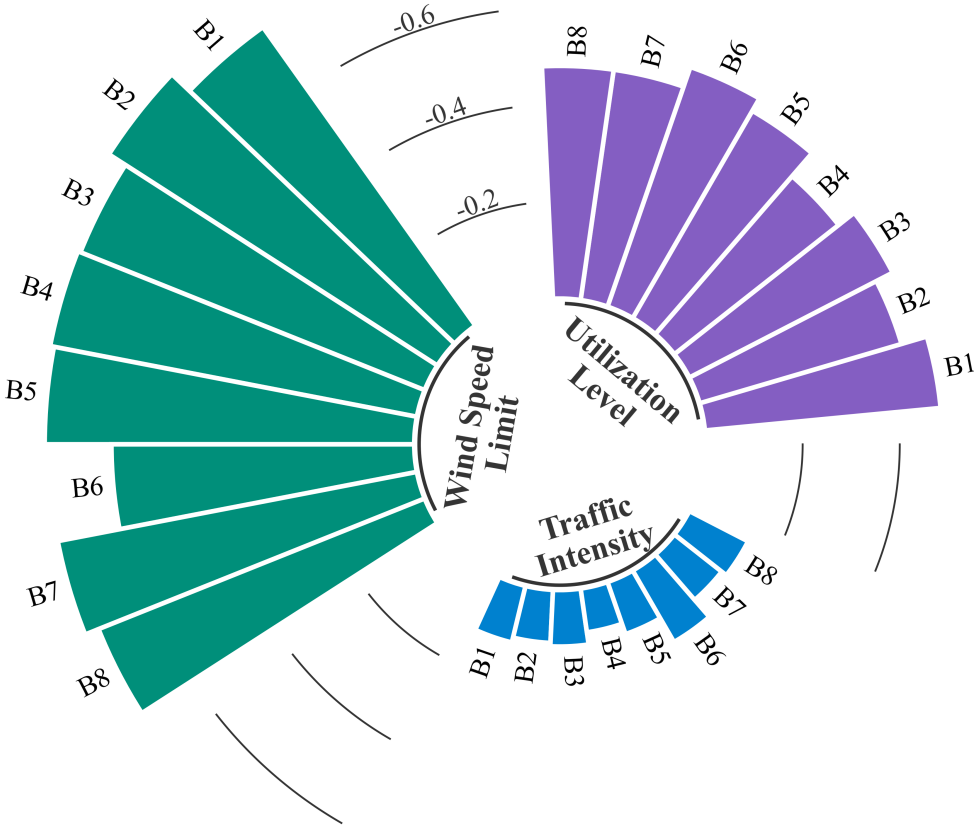


Figure 9.5: Global Sensitivity Analysis – Pearson’s correlation coefficient related to reliability index β .

The Global Sensitivity Analysis revealed following regarding the assumed probabilistic models presented in Section 9.3:

1. The bridge typology is the governing variable. No generalization can be made regarding the bridge type. The system reliability highly depends on the bridge properties (dimensions, weight and aerodynamic coefficients measured in the wind tunnel).

2. Second most important is the effect of local wind condition (wind speed limit and wind zone characteristics).
3. The least important appears to be the effect of light-weight traffic.
4. According to Figure 9.5 the trend is similar for all bridges B1 thru B8.

Following probabilistic analysis focuses on establishing a relationship between the utilization level in EQU and wind speed limit for selected bridge types.

9.7 Probabilistic Analysis

The goal of probabilistic analysis is to determine a relationship between the utilization level in EQU and wind speed limit for selected bridge types. The probabilistic simulation is using the probabilistic model proposed in Section 9.3 and the target reliability $\beta = 3.7$ proposed in Section 9.4. A simplified calculation approach described in Section 9.3.3 is used for the analysis of a large number of situations. The simulation is performed for all bridge types, all wind zones and all railway lines. As the railway line and indicator of local traffic intensity has the least importance according to the Global Sensitivity Analysis (Figure 9.4) the worst case data set for given bridge and wind zone is used only. Limiting wind speed $v_{b,lim}$ is simulated between 15-50 m/s. However, due to the value of characteristic wind speeds in the Czech Republic wind zones I thru V, only results for wind speeds ranging between 20-35 m/s are considered. The utilization level in EQU expresses the ratio $M_{W,d}/M_{Gd}$ ranging between 1.0-2.5. The various level of utilization was simulated by modifying the bridge weight G_{bridge} . The bridge weight is mainly dependent on the span length of the bridge and does not have any direct impact on the wind load. However, larger span does not have an impact only on the weight of the bridge but also on the dimensions which already have a direct impact on the wind load. Therefore, the limitation of applicability of the $v_{b,lim}$ to utilization level relationship should be the similarity of bridge dimensions b/d_{tot} . Figures 9.6 thru 9.13 display the relationship, each wind zone is represented by one curve and any combination of wind speed limit and utilization level below the curve has minimum target reliability $\beta = 3.7$. Two graphs for each bridge are shown, one represents the refined aerodynamic coefficients measured in the wind tunnel and the second the methodology according to EC11-4. Both models use the updated wind speed and light-weight traffic probabilistic models presented in this study.

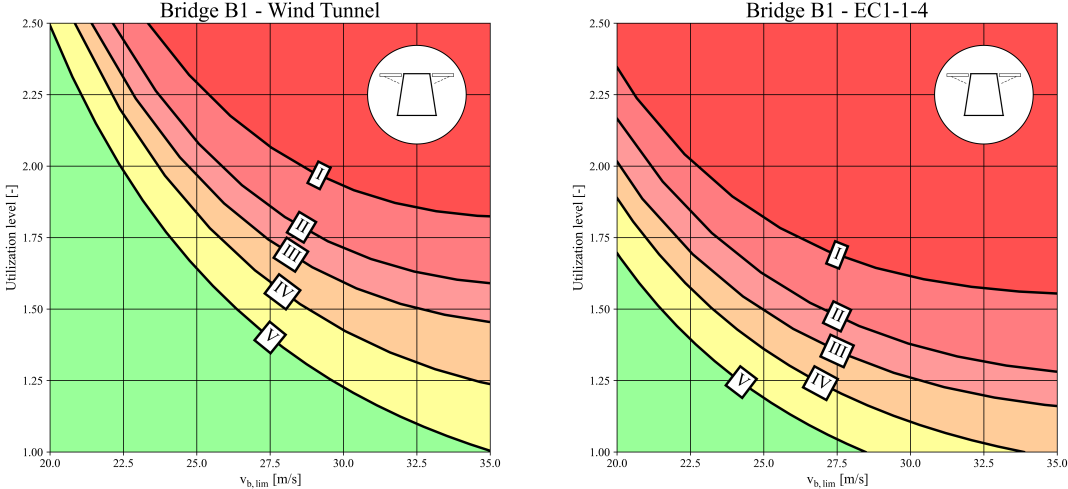


Figure 9.6: Bridge B1: $v_{b,lim}$ – Utilization Level, Wind tunnel (left), EN 1991-1-4 (right).

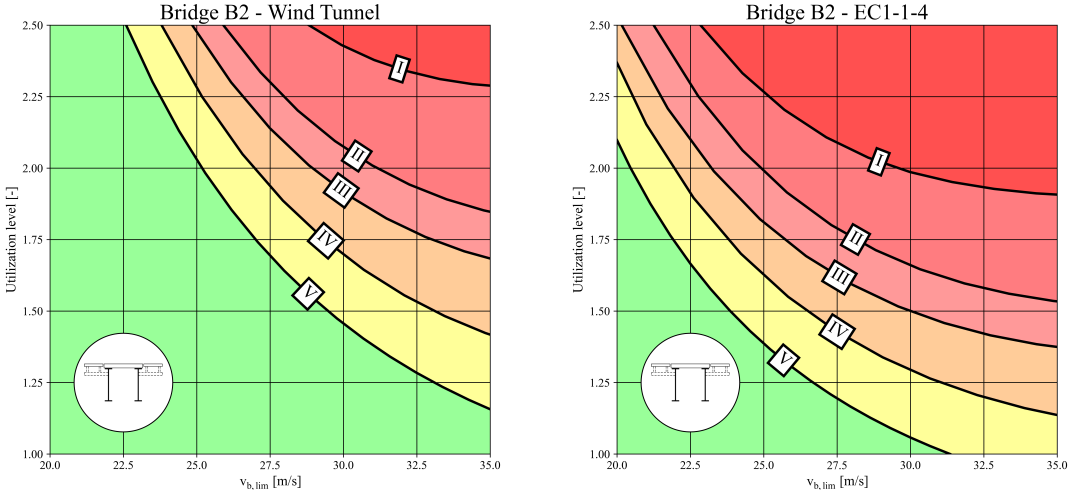


Figure 9.7: Bridge B2: $v_{b,lim}$ – Utilization Level, Wind tunnel (left), EN 1991-1-4 (right).

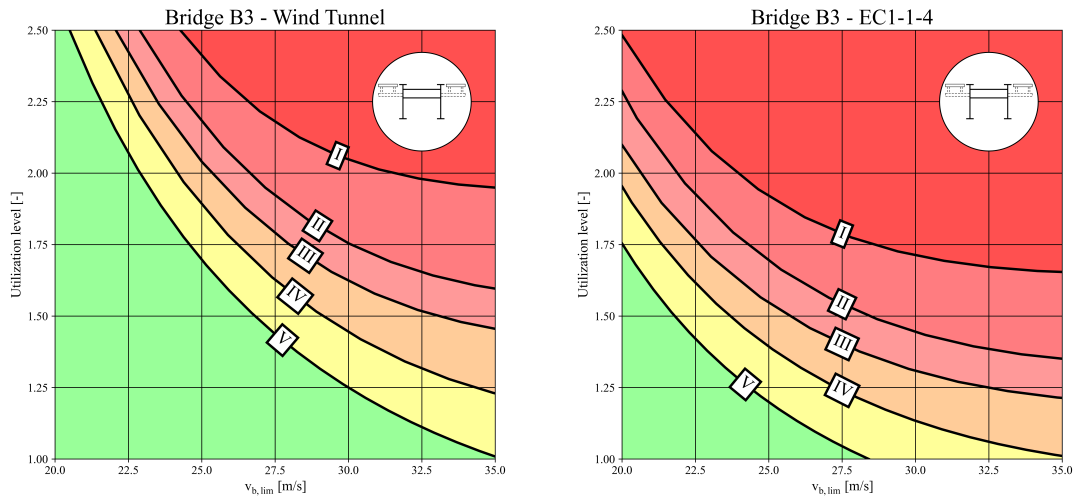


Figure 9.8: Bridge B3: $v_{b,lim}$ – Utilization Level, Wind tunnel (left), EN 1991-1-4 (right).

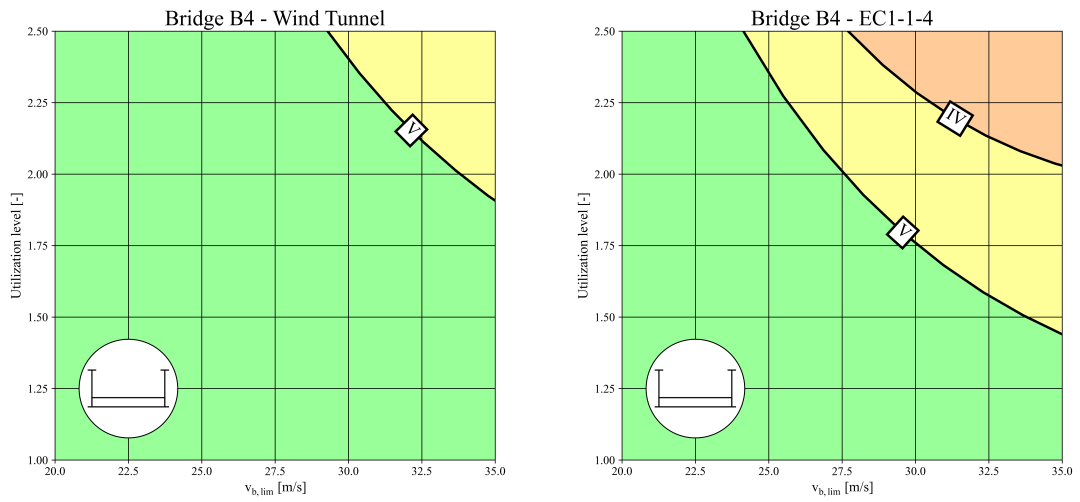


Figure 9.9: Bridge B4: $v_{b,lim}$ – Utilization Level, Wind tunnel (left), EN 1991-1-4 (right).

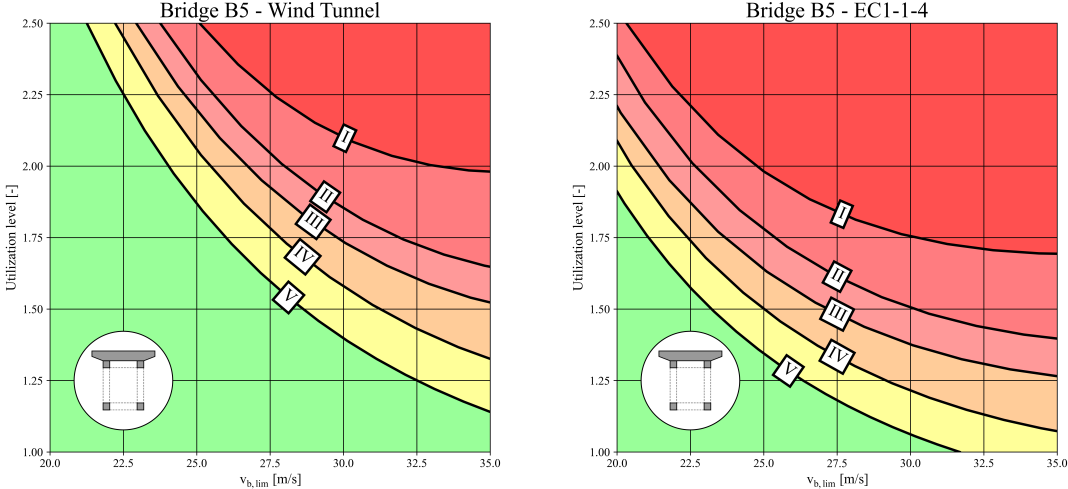


Figure 9.10: Bridge B5: $v_{b,lim}$ – Utilization Level, Wind tunnel (left), EN 1991-1-4 (right).

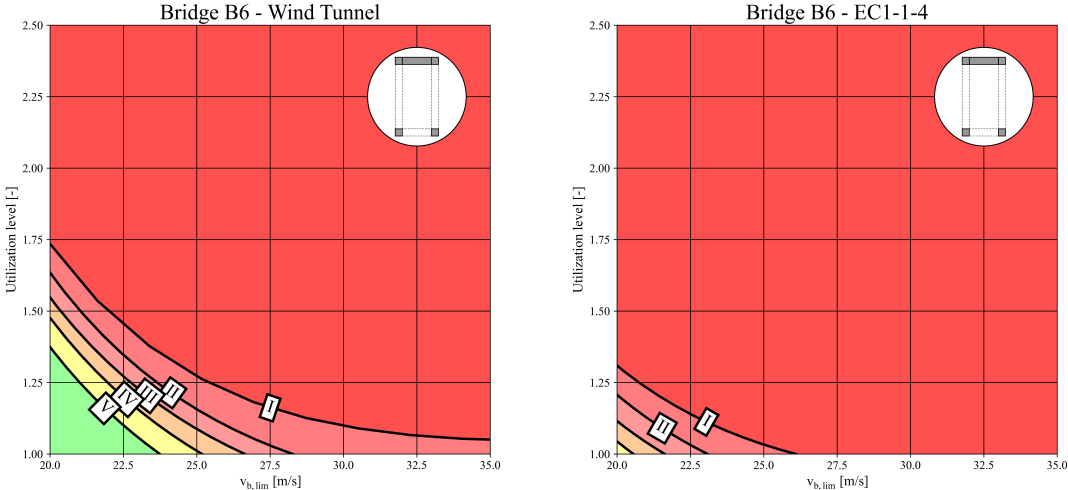


Figure 9.11: Bridge B6: $v_{b,lim}$ – Utilization Level, Wind tunnel (left), EN 1991-1-4 (right).

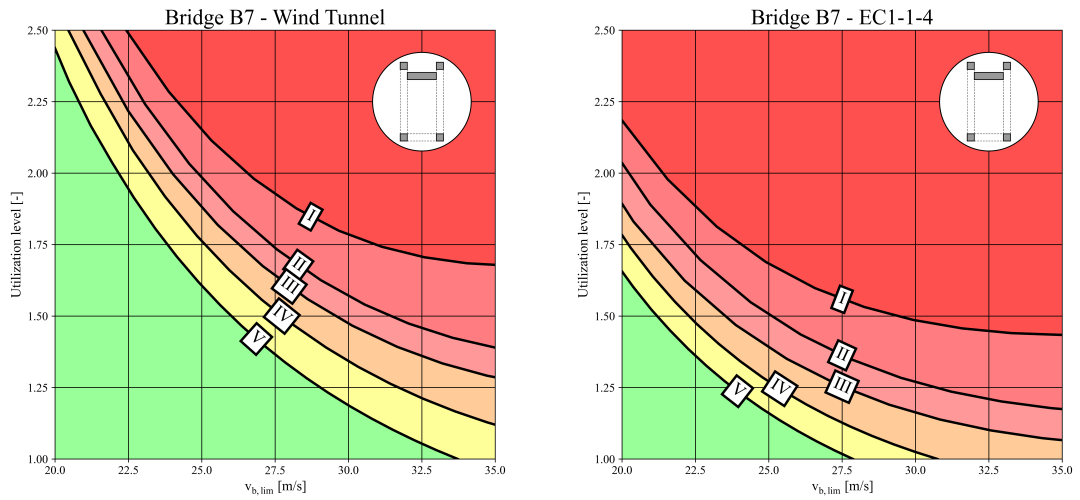


Figure 9.12: Bridge B7: $v_{b,lim}$ – Utilization Level, Wind tunnel (left), EN 1991-1-4 (right).

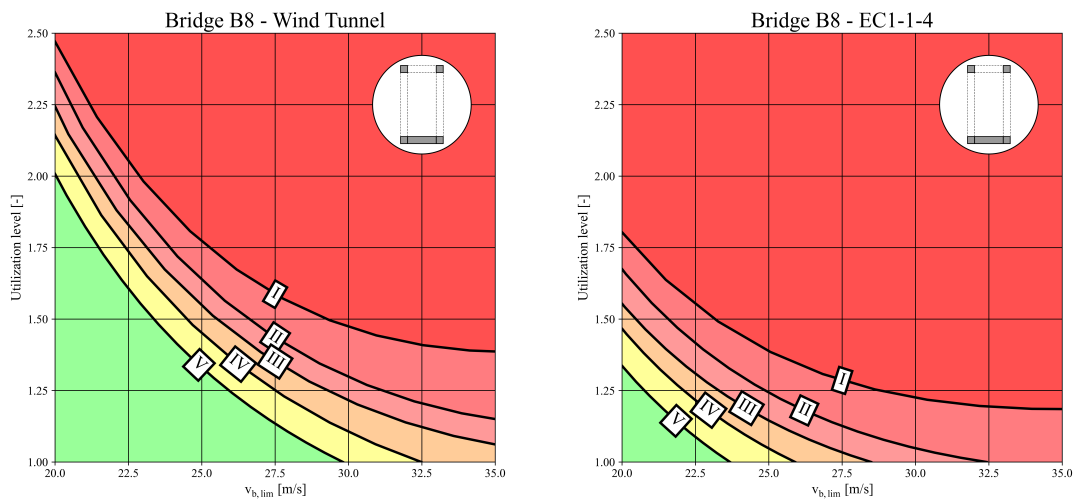


Figure 9.13: Bridge B8: $v_{b,lim}$ – Utilization Level, Wind tunnel (left), EN 1991-1-4 (right).

When considering reliability index $\beta_1 = 3.7$, for all bridge types the level of reliability is sufficient even though the bridge fails the EQU verification according to EN 1991-1-4. The trend is similar for majority of the bridges with exception of Bridge B4 and B6. Bridge B4, Plate girder bridge with lower bridge deck has no issues with in the EQU verification due to the relatively low structural height and favorable bearing spacing, it was observed during the verification that even when bridge should fail in EQU using the

unloaded train per EN 1991-2 the bridge still satisfies the code check when the real train is assumed. Bridge B6, Truss girder bridge with upper bridge deck and parabolic bottom chord satisfies the EQU verification due to the shape of the superstructure, where due to the parabolic bottom chord the overturning effect of the wind on the superstructure is insignificant when assumed with 4 m high unloaded train. However, once the EQU verification limit is exceeded, hidden safety vanishes due to the position of the bridge deck and higher profile of the trains.

Following is the demonstration of the method application on a steel plate girder bridge without bridge deck in km 4.256 of the railway line Hanušovice – Staré Město pod Sněžníkem. The bridge was built in 1905 and was reconstructed several times during the service life. The bridge has 3 simple spans and the superstructure consists of pair of riveted plate girders. The bridge has no bridge deck with the wooden sleepers directly fixed to the top flange of the main girders. See Figure 9.14 for a bridge photo and Figure 9.15 for schematic cross-section of the bridge. Table 9.4 shows the additional parameters of the bridge.



Figure 9.14: Bridge in km 4.256 Hanušovice – Staré Město pod Sněžníkem.

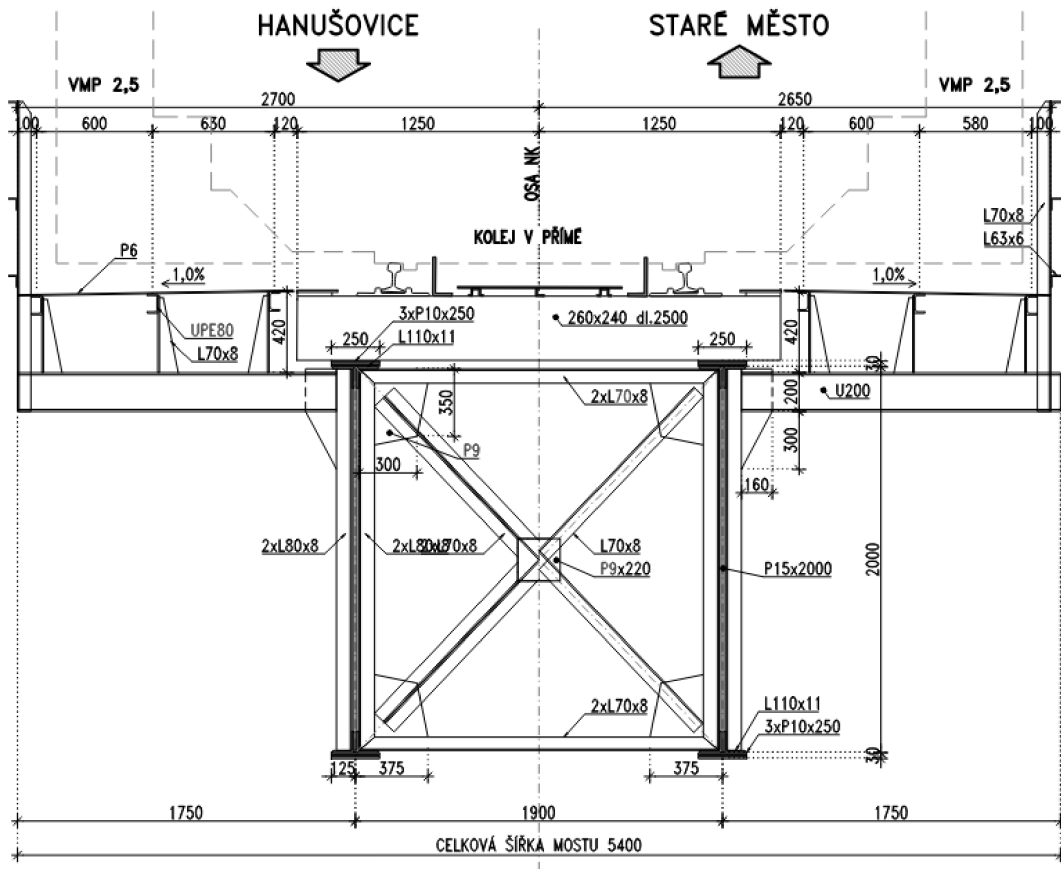


Figure 9.15: Bridge in km 4.256 Hanušovice – Staré Město pod Sněžníkem (cross-section).

Superstructure:	Steel riveted plate girder superstructure without bridge deck.
Static layout of the superstructure:	3 simple spans
Total length of bridge:	67.74 m
Span length:	21.34 + 21.50 + 21.34 m
Number of tracks:	1
Transverse arrangement of the bridge:	VMP 2.5
Structural depth:	2.35 m
Clear depth (decisive):	10.5 m
Structural width:	5.50 m
Wind load parameters	
Wind Zone:	III
Terrain category:	III
Reference height z_e :	13.68 m
Wind pressure $q_p(z_e)$:	906 Pa
Reference area A_{ref} :	6.35 m ² /m
Force coefficient $c_{f,x}$:	2.24
Wind load F_w :	12.9 kN/m
EQU verification per Eurocodes	
Bridge weight:	44.9 kN/m
Bearing spacing:	1.90 m
Center of wind reference area z_w :	3.18 m
Destabilizing moment M_w :	$12.9 \cdot 3.18 = 41.0$ kNm/m
Stabilizing moment M_G :	$(44.9 + 10) \cdot 1.90 / 2 = 52.2$ kNm/m
EQU verification:	$1.50 \cdot 41.0 / (0.95 \cdot 52.2) = 1.26$

Table 9.4: Bridge B1 – plate girder bridge with rail directly fixed to the top flange (additional parameters).

The bridge fails the EQU verification per Eurocode, the utilization level is $E_d/R_d = 1.26$. According to Figure 9.7 (Bridge type B2 – plate girder bridge without bridge deck) the wind speed limit $v_{b,lim} \geq 35$ m/s for bridge in wind zone III meets the annual minimum target reliability $\beta = 3.7$. Therefore, the trains can run without any additional restrictions from the railway operator.

Chapter 10

Conclusions

The main objective of this dissertation was to propose and develop procedures to investigate and refine the inputs for analysis and verification of existing steel railway bridges for combined effect of wind and traffic load. Eight representative types of steel railway bridges were selected and tested in the wind tunnel along with five representative types of light-weight railway vehicles. Analysis of the wind tunnel experiments and their critical comparison to the EN 1991-1-4 wind load model revealed that:

1. The obtained horizontal, vertical, and torsional forces at different horizontal bridge inclinations to the direction of wind demonstrated that the actual loads on railway bridges are often considerably different in comparison to the largely simplified Eurocode model.
2. For plate girder bridges, the drag coefficient measured in the wind tunnel, C_D , can be directly compared to the force coefficient $c_{f,x0}$ according to EN 1991-1-4. It appears that the Eurocode slightly underestimates the force coefficient for bridges without traffic, which is, however, rarely the governing design situation for railway bridges. When considering the wind-on-train effect, the Eurocode is conservative for all combinations of bridges and trains under consideration (Figure 6.1). This is why reduction coefficient is proposed to update the effect of wind load on plate girder bridges. Depending on the assumed type of the bridge and vehicle, the reduction coefficient ranges from 0.65 up to 0.93 (Table 6.1).
3. EN 1991-1-4 fails to provide unambiguous guidance on how to determine wind loads on truss girder bridges. Several alternatives provided in the Eurocode lead to distinctly different wind pressures. The approach when plane truss girders are

taken into account separately from the bridge deck (Method M2) seems to match reasonably with the force coefficients based on wind tunnel tests; see Figure 6.2. Correction coefficient ranging from 0.77 to 1.18 – is then proposed to modify the effect of wind load on truss girder bridges for a specific bridge-vehicle combination (Table 6.2). The reduction of the horizontal component of the wind load on truss girder bridges is rather insignificant as the preferred method M2 was selected based on the closest comparison to the wind tunnel experiments.

4. For all bridges under investigation, the lift coefficient measured in the wind tunnel C_L can be directly compared to the vertical component force coefficient c_z according to EN 1991-1-4. It is demonstrated that the Eurocode overestimates the vertical wind component on all bridge types (Figure 6.4). A coefficient is thus proposed to reduce the effect of vertical wind component on steel railway bridges by a factor of 0.30-0.91 depending on the type of a bridge (Table 6.3).
5. For the purpose of equilibrium limit state verification, all components of the wind load are taken into account to derive the modification factor for all types of bridges (Table 6.4). The average reduction of 70-80 % was achieved depending on bridge and vehicle types. Only for Bridge type B6 (truss girder bridge with upper bridge deck and parabolic bottom chord) and B8 (truss girder bridge with lower bridge deck), the comparison revealed that the Eurocode might underestimate the wind load on bridge with traffic.
6. The experimental verification of the turbulence effect on aerodynamic coefficients showed that the drag coefficient C_D is approximately 14 % lower for all bridges under investigation. For plate girder bridges, the intensity of turbulence has insignificant effect on the lift coefficient C_L and torsional moment coefficient C_M . In contrast, the turbulence plays a role depending on the position of the deck of truss girder bridges. For bridge with an upper deck, a decreasing effect on C_L and C_M can be observed when turbulent air flow is achieved. For bridge with lower bridge deck an increasing effect of the C_L and C_M can be observed.
7. The height of the bridge above the terrain has a considerable bearing on the aerodynamic coefficients, the drag coefficient is on average 10 % higher if the clear depth between the terrain and the bridge is 2.5 m. The experiment suggests that an increase in wind loads should be expected when designing bridges with a low height

above the terrain. However, it should be noted that in the case of such low heights, the roughness of the terrain already plays a significant role.

8. The horizontal wind force on leeward truss girder can be 40-70 % lower compared to the windward truss girder due to the shielding effect which is dependent on the girder spacing. The assumption of Eurocode of equal loading on all trusses is unrealistic. However, when the methodology for loading of truss girders (Method M2, recommended in EN 1991-1-4) is applied along with the proposed modification factors, the estimated load effect is close to that measured in the wind tunnel.
9. The applicability of the wind tunnel experiments and resulting modifications factors is based on bridge similarity. The results are applicable only to the 8 bridge types under consideration. The geometric similarity is expressed by the aspect ratio b/d_{tot} . Based on author's judgment and experience it is assumed that the aspect ratio should be within $\pm 20\%$ range.

Many existing historic steel railway bridges fail to comply with the criteria for equilibrium limit states according to Eurocodes while no failures have been experienced by railway operators over decades. In order to preserve these bridges, the method for updating wind load effects using wind tunnel tests is proposed in this doctoral thesis. The application to a range of representative existing steel railway bridges based on measurements in the wind tunnel, free-field wind speed records and traffic flow records prove that:

1. The assessment using the partial factor methods in Eurocodes seems to include several "hidden safeties." The unnecessary conservatism can be overcome by using the probabilistic approach and case-specific measurements. In comparison to the guidance provided in Eurocodes for design of new structures, about 20 % is gained when the updated force coefficients along with realistic minimum train weights are taken into account. Further hidden safeties where probabilistic assessment helps to avoid unnecessary conservatism in EQU verification include improved modeling of site-specific wind speeds, description of wind-on-light-weight train situations, and modeling of actual geometry and weight of a bridge.

It should be noted that the list of "hidden safeties" is still incomplete. Depending on project-specific conditions, measurements or mathematical models can be used to reduce uncertainties and update the effects of wind directionality, orography and terrain roughness. Dynamic analysis may then improve the estimate of the global interaction between bridge and railway traffic.

2. The wind load model based on wind speed records is proposed. Only the strong wind speed event where $v_b \geq 10m/s$ is assumed and the wind speed distribution parameters are shown in Table 7.2, the assumed uncertainties of all the wind load components are described in Table 9.2. It should be noted that the variation of aerodynamic coefficients determined in the wind tunnel is lower than that related to the Eurocode coefficients.
3. The light-weight traffic model can be proposed based on records of trains whose self-weight is less than 2.0 t/m. The probabilistic model based on traffic intensity records makes it possible to reflect distinct character of traffic flows on different railway lines (Table 8.1).
4. The target reliability index is the key component of the reliability assessment. It is argued that annual target reliability index of $\beta=3.7$ can be considered for EQU verification of existing railway bridges. The probabilistic model of combined effect of strong wind and light-weight railway traffic is presented in Section 9.3. By reasonably simplified limit state function according to Eq. 9.3, it allows to adequately describe all significant uncertainties affecting reliability of bridges in EQU verification. The probabilistic models of basic variables provided in Table 9.1 might be utilized in subsequent reliability studies after possible adjustment to bridge-specific conditions.
5. The limiting wind speed, $v_{b,lim}$ – the threshold above which railway traffic is interrupted – is governing reliability of the bridge in the EQU verification while the type of light-weight train is less important. The probabilistic assessment is demonstrated on the example of truss girder bridge with intermediate bridge deck (Bridge B7) in wind zone II assuming the traffic distribution of high intensity railway line S1. Reliability of the bridge under investigation can be considered sufficient for $v_{b,lim} \leq 26m/s$ when the probabilistic analysis is based on the wind tunnel results while bridge reliability is low for $v_{b,lim} \leq 23m/s$ when the force coefficient per EN 1991-1-4 model with relevant uncertainty is taken into account.
6. Sensitivity analysis using the Pearson's correlation coefficients reveals that the most important factors affecting the bridge reliability in EQU are bridge type, wind speed limit $v_{b,lim}$, and utilization level of the bridge in EQU. Section 9.7 presents in Figures 9.5 thru 9.12 the relationship between $v_{b,lim}$ and utilization level of the bridge

in EQU for all bridges and wind speed zones. The presented results were evaluated assuming the target reliability index of $\beta = 3.7$.

The wind tunnel experiments and probabilistic approach to reliability verification of existing bridges revealed many hidden safeties in the assessment of bridges for combined effect of wind and traffic loads. The conclusions of the thesis were used to update the methodology of verification of existing bridges and were applied in the engineering practice. The feedback from bridge engineers suggests that the updated methodology led to significantly favorable results in 30 % of re-assessed bridges which would otherwise fail the code requirements.

It should be noted that the list of hidden safeties is still incomplete and there is still potential for additional research activities such as:

1. Depending on project-specific conditions, site specific measurements or mathematical models can be used to reduce uncertainties and update the effects of wind directionality, orography and terrain roughness.
2. Experimental results can be used to validate numerical models. Additionally, computational fluid dynamics models can be validated by wind tunnel experiments and used in parametric studies to verify applicability range with respect to the aspect ratio and extend scope of the results obtained in the wind tunnel. In this way, the knowledge of wind load on steel railway bridges of complex shapes can be further extended.
3. Dynamic analysis may improve the estimate of the global effect of the wind on the complex system of a bridge with traveling vehicles. The traveling train speed effecting the wind breaking may lead to different values of wind pressure.
4. The probabilistic approach proposed in the thesis can be utilized to update characteristic values and partial factors and combination factors for EQU or STR. In particular, assessment value of total load effect may be significantly updated (decreased) by considering reduced uncertainties in wind pressure, wind-on-light-weight train effect, and permanent load effect. Reduced target reliability level for assessment can further substantiate reduction of assessment value of load effects.

Bibliography

- AASHTO LRFD (2020). *AASHTO LRFD Bridge Design Specifications (9th Edition)*, American Association of State Highway and Transportation Officials (AASHTO).
- Adasooriya, N. D. (2016). Fatigue reliability assessment of ageing railway truss bridges: Rationality of probabilistic stress-life approach, *Case studies in structural engineering* **6**: 1–10.
- AlSalih, H., Juno, M., Collins, W., Bennett, C. and Li, J. (2021). Application of a digital image correlation bridge inspection methodology on geometrically complex bifurcated distortion-induced fatigue cracking, *Fatigue and Fracture of Engineering Materials and Structures* **44**(11): 3186–3201.
- ARCHES (2009). Assessment and rehabilitation of central european highway structures, D08: Recommendations on the use of results of monitoring on bridge safety assessment and maintenance, Annex A: Recommendations on bridge traffic load monitoring, *Technical Report final report*.
- ASCE/SEI 7-16 (2017). *Minimum design loads and associated criteria for buildings and other structures*, American Society of Civil Engineers.
- Baravalle, M. and Kohler, J. (2018). On the probabilistic representation of the wind climate for calibration of structural design standards, *Structural Safety* **70**: 115–127.
- Baravalle, M., Mikoschek, M., Colling, F. and Kohler, J. (2017). Calibration of simplified safety formats for structural timber design, *Construction and Building Materials* **152**: 1051–1058.
- Bien, J., Elfgrén, L. and Olofsson, J. (2007). *Sustainable bridges: Assessment for future traffic demands and longer lives*, Dolnoslaskie Wydawnictwo Edukacyjne, Wrocław.
- Binder, K. (1979). *Monte Carlo methods in statistical physics*, Springer.

Bibliography

- BS 5400 (1978). *BS 5400: Steel, concrete and composite bridges - 2: Specifications for loads*.
- Burt, P. J. A. (2004). The great storm and the fall of the first tay rail bridge, *Weather* **59**(12): 347–350.
- Cardoso, F. S., Zhang, H., Rasmussen, K. J. R. and Yan, S. (2019). Reliability calibrations for the design of cold-formed steel portal frames by advanced analysis, *Engineering Structures* **182**: 164–171.
- CEN/TC250 (1996). Background document ec1: Part1: Basis of design, *Technical Report 2nd draft*.
- COMPOST (Accessed 2016). Centralni aplikace pro prijimani informaci o slozeni vlaku, (in Czech; Central application for receiving train composition information), CD - Informacni Systemy.
URL: <https://compost.spravazeleznice.cz/webcompost/>
- Cowdrey, C. (1971). Time-average aerodynamic forces on bridges, *Technical report*, NPL Aero Report 1327.
- Cowdrey, C. (1972). Time-average aerodynamic forces on bridges (second series), *Technical report*, NPL Mar. Sci. No 1-72.
- CSN 73 0038 (2014). *CSN 73 0038 - Navrhovani konstrukci - Doplnujici ustanoveni pro hodnoceni existujicich konstrukci (in Czech; Assessment and verification of existing structures - Supplementary guidance)*, UNMZ: Prague.
- Davenport, A. G. (1960). Rationale for determining design wind velocities, *ASCE Journal of the Structural Division* **86**(5): 39–68.
- DB Richtlinie 807.04 (2006). *Bautechnik, Leit-, Signal- und Telekommunikationstechnik. Ausgewählte Massnahmen und Anforderungen and das Gesamtsystem Fahrweg/Fahrzeug - Aerodynamik/Seitenwind (in German; Civil Engineering, Control-, Signalling- and Telecommunications Technology: Selected Measures and Requirements for System Track/ Vehicle - Aerodynamics / Transverse Loading from Wind Effects)*, DB Netz AG, Frankfurt a.M.

- Diana, G., Fiammenghi, G., Belloli, M. and Rocchi, D. (2013). Wind tunnel tests and numerical approach for long span bridges: The Messina Bridge, *Journal of Wind Engineering and Industrial Aerodynamics* **122**: 38–49.
- Ditlevsen, O. and Madsen, H. O. (1996). *Structural reliability methods*, John Wiley and Sons, Chichester.
- EN 1990 (2002). *Eurocode - Basis of structural design*, CEN, Brussels.
- EN 1991-1-4 (2005). *Eurocode 1: Actions on structures - Part 1-4: General actions - Wind actions*, CEN, Brussels.
- EN 1991-2 (2003). *Eurocode 1: Actions on structures - Part 2: Traffic loads on bridges*, CEN, Brussels.
- fib bulletin 80 (2016). *Partial factor methods for existing structures (fib bulletin 80, recommendation)*, fib.
- fib Model Code 2020 (2022). *fib Model Code 2020 (draft submitted for review)*, fib, Lausanne.
- Fisher, O., Kolousek, V. and Pirner, M. (1977). *Aeroelasticita stavebnich konstrukci (in Czech; Aeroelasticity of building structures)*, Academia: Prague.
- Fisher, O. and Pirner, M. (2003). *Zatizeni staveb vetrem (in Czech; Wind loading of structures)*, CKAIT: Prague.
- Formichi, P., Danciu, L., Akkar, S., Kale, O., Malakatas, N., Croce, P., Nikolov, D., Gocheva, A., Luchinger, P., Fardis, M., Yakut, A., Apostolska, R., Sousa, M. L., Dimova, S. and Pinto, A. (2016). Elaboration of maps for climatic and seismic actions for structural design with the Eurocodes (JRC Science and Policy Report), *Technical Report JRC103917*.
- Fujii, T., Maeda, T., Ishida, H. and Imai, T., Tanemoto, K. and Suzuki, M. (1999). Wind-induced accidents of train/vehicles and their measures in Japan, *Quarterly Report of Rtri* **40**: 50–55.
- Goss, W. F. M. (1898). Atmosphere resistance to the motion of railway trains, *The Engineer*.

- Gulvanessian, H., Calgaro, J. A. and Holicky, M. (2012). *Designers guide to Eurocode: Basis of structural design: EN 1990, Second edition*, Thomas Telford, London.
- Hansen, S. O., Pedersen, M. L. and Sorensen, J. D. (2015). Probability based calibration of pressure coefficients, *Proc. ICWE14*.
- Hay, J. (1992). *Response of bridges to wind*, HMSO: London.
- He, X., Qin, H., Liu, W., Chen, Y., Zhai, J. and Yu, L. (2016). Design, analysis and construction of a steel truss cable-stayed bridge for high-speed railway in China, *Structural Engineering International* **26**: 381–388.
- He, X. and Zou, S. (2021). Advances in wind tunnel experimental investigations of train-bridge systems, *Tunnelling and Underground Space Technology* **118**: 104157.
- Holicky, M. (2009). *Reliability analysis for structural design*, SUN MeDIA, Stellenbosch.
- Holicky, M. (2015). *Aplikace teorie pravdepodobnosti a matematicke statistiky (in Czech; Applications of probability theory and mathematical statistics)*, 1. edn, CTU Publishing, Prague.
- Holicky, M., Diamantidis, D. and Sykora, M. (2018). Reliability levels related to different reference periods and consequence classes, *Beton- und Stahlbetonbau* **113**: 22–26.
- Holicky, M., Retief, J. V. and Viljoen, C. (2016). Partial factors for wind actions considering hidden safety due to time invariant components, *Proc. SEMC 2016*, pp. 687–692.
- Holicky, M. and Sykora, M. (2009). Reliability analysis of static equilibrium, *Proceedings of the 7th International Probabilistic Workshop*, pp. 111–118.
- Holicky, M. and Sykora, M. (2016). Probabilistic models for wind actions, *Proceedings - 2nd International Symposium on Stochastic Models in Reliability Engineering, Life Science, and Operations Management, SMRLO 2016*, pp. 172–175.
- Holmes, J. D. (1998). Wind loading of structures: application of probabilistic methods, *Progress in Structural Engineering and Materials* **1**(2): 193–199.
- Holmes, J. D. and Bekele, S. (2020). *Wind loading of structures*, CRC Press, Milton.
- Huan, I., He, X., Hu, L. and Xu, G. (2021). Quantification of aerodynamic forces for truss bridge-girders based on wind tunnel test and kriging surrogate model, *Advances in Structural Engineering* **24**.

-
- Humphreys, W. (1964). *Physics of the air*, New York: Dover.
- ISOR (Accessed 2016). Informacni system operativniho rizeni (in Czech; Central Dispatchinf System), Oltis Group.
URL: <https://isor.spravazeleznic.cz/>
- James, G. (2003). *Analysis of traffic load effects on railway bridges (Ph.D. thesis)*, Structural Engineering Division, Royal Institute of Technology, Stockholm.
- JCSS PMC (2021). *JCSS Probabilistic Model Code (periodically updated, online publication)*, Joint Committee on Structural Safety.
- Jirsak, M. (2009). *Studie budov a konstrukci ve vetrnych tunelech (in Czech; Studies of buildings and structures in wind tunnels)*, CKAIT: Prague.
- JRC (2022). JRC Technical Report - Reliability background to Eurocodes, *Technical report*, Luxembourg: Publications Office of the European Union.
- JRC (2023). Reliability Background of the Eurocodes (in press), CEN/ TC250/ SC10/ Ad-Hoc Group Reliability (chair ACWM Vrouwenvelder), JRC Technical Report, *Technical report*.
- Jung, H., Kim, G., Oh, J. and Park, J. (2019). Design criteria for impact factors based on dynamic on-site data in railway bridges, *Structure and Infrastructure Engineering* **15**(4): 484–491.
- Karman, T. (2005). Collapse of the Tacoma Narrows Bridge, *Resonance* **10**(8): 97–102.
- Kasperski, M. (2003). Specification of the design wind load based on wind tunnel experiments, *Journal of Wind Engineering and Industrial Aerodynamics* **91**: 527–541.
- Kasperski, M. (2009). Specification of the design wind load - a critical review of code concepts, *Journal of Wind Engineering and Industrial Aerodynamics* **97**(7): 335–357.
- Kat, R. and Oudheusden, B. W. (2012). Instantaneous planar pressure determination from PIV in turbulent flow, *Exp Fluids* **52**: 1089–1106.
- Katembo, A. L., Kandu, V. V. and Shitikova, M. V. (2020). Numerical analysis of forced vibrations of the Golden Gate suspension bridge in the case of the 1:1 internal resonance, *IOP conference series. Materials Science and Engineering* **747**(1): 12052.

- Kral, J. (2010). *Navrhovani konstrukci na zatizeni vetrem (in Czech; Designing structures for wind loading)*, CKAIT: Prague.
- Kruger, A. C., Retief, J. V. and Goliger, A. M. (2013). Strong winds in South Africa: Part 1: Application of estimation methods, *Journal of the South African Institution of Civil Engineering* **55**(2): 29–45.
- Kuznetsov, S., Pospisil, S. and Kral, R. (2015). Climatic wind tunnel for wind engineering tasks, *Czasopismo Techniczne* **2-B**.
- Li, H., Frangopol, D., Soliman, M. and Xia, H. (2015). Fatigue reliability assessment of railway bridges based on probabilistic dynamic analysis of a coupled train-bridge system, *Journal of Structural Engineering* **142**: 04015158.
- Lukacevic, I., Dujmovic, D. and Androic, B. (2014). Fatigue reliability assessment of steel railway bridges based on field monitoring, *Proc. EUROSTEEL 2014*.
- Macho, M., Ryjacek, P. and Matos, J. (2019a). Fatigue life analysis of steel riveted rail bridges affected by corrosion, *Structural Engineering International* **29**(4): 551–562.
- Macho, M., Ryjacek, P. and Matos, J. C. (2019b). Static and fatigue test on real steel bridge components deteriorated by corrosion, *International Journal of Steel Structures* **19**(1): 110–130.
- Melchers, R. E. (2001). *Structural reliability analysis and prediction*, 2nd edn, Wiley, Chichester.
- Miyata, T. (2003). Historical view of long-span bridge aerodynamics, *Journal of wind engineering and industrial aerodynamics* **91**(12): 1393–1410.
- Moreira, V. N., Fernandes, J., Matos, J. C. and Oliveira, D. V. (2016). Reliability-based assessment of existing masonry arch railway bridges, *Construction and Building Materials* **115**: 544–554.
- Nadolski, V., Rozsas, A. and Sykora, M. (2019). Calibrating partial factors - methodology, input data and case study of steel structures, *Periodica Polytechnica-Civil Engineering* **63**(1): 222–242.
- Nakayama, A., Okamoto, D. and Takeda, H. (2010). Large-eddy simulation of flows past complex truss structures, *Journal of Wind Engineering and Industrial Aerodynamics* **98**(3): 133–144.

- Niemann, H. J. and Diburg, S. (2013). Statistics of extreme climatic actions based on the Gumbel probability distributions with an upper limit, *Computes and Structures* **126**: 193–198.
- NPL (1954). Bridge Wind Tunnel Test, Photographed in 1954, in the Aerodynamics Division of the National Physical Laboratory, Teddington, UK.
- O'Brien, E. J., Schmidt, F., Hajjalizadeh, D., Zhou, X. Y., Enright, B., Caprani, C. C., Wilson, S. and Sheils, E. (2015). A review of probabilistic methods of assessment of load effects in bridges, *Structural Safety* **53**: 44–56.
- O'Connor, A., Pedersen, C., Gustavsson, L. and Enevoldsen, I. (2009). Probability-based assessment and optimised maintenance management of a large riveted truss railway bridge, *Structural Engineering International* **19**(4): 375–382.
- Orcesi, A., Diamantidis, D., O'Connor, A., Palmisano, F., Sykora, M., Boros, V., Caspeepe, R., Chateauneuf, A., Ivankovic, A. M., Kohler, J., Lenner, R., Maric, M. K., Kuster, M., Nadolski, V., Nielsen, S. T., Roldsgaard, J. H., Schmidt, F., Skokandic, D. and Spuy, P. (2022). Investigating the use of the partial factor format for the assessment of existing bridges, (*complete draft, to be submitted to Structural Engineering International - Journal of IABSE*).
- Pirner, M. and Fischer, O. (2003). *Zatizeni staveb vetrem (in Czech; Wind loading of structures)*, 1 edn, CKAIT, Praha.
- Plachy, T., Polak, M. and Ryjacek, P. (2017). Assessment of an old steel railway bridge using dynamic tests, *Procedia Engineering*, Vol. 199, pp. 3053–3058.
- Prebble, J. (1979). *The high girders*, Penguin Books: Harmondsworth.
- Proppe, C. and Wetzel, C. (2007). Overturning probability of railway vehicles under wind gust loads, *Solid Mechanics and its Applications* **2**.
- Reid, S. G. (2007). A probabilistic traffic load model for reliability assessments of bridges, *Progress in Mechanics of Structures and Materials - Proceedings of the 19th Australasian Conference on the Mechanics of Structures and Materials, ACMSSM19*, pp. 223–227.
- REVOZ (Accessed 2016). Registr vozidel (in Czech; Register of vehicles), Oltis group.
URL: <https://provoz.spravazeleznic.cz/REVOZ>

- Roach, P. E. (1987). The generation of nearly isotropic turbulence by means of grids, *International Journal of Heat and Fluid Flow* **8**(2): 82–92.
- Rozsas, A., Kovacs, N., Vigh, L. G. and Sykora, M. (2016). Climate change effects on structural reliability in the carpathian region, *Idojaras* **120**(1): 103–125.
- Ryjacek, P. (2019). The diagnostic techniques for the assessment of the historical steel bridges, *IABSE Symposium, Guimaraes 2019: Towards a Resilient Built Environment Risk and Asset Management - Report*, pp. 1651–1657.
- Ryjacek, P., Macho, M., Stancik, V. and Polak, M. (2016). Deterioration and assessment of steel bridges, *Proc. IABMAS 2016*, pp. 1188–1195.
- Ryjacek, P., Zitny, J., Markova, J., Sykora, M., Kuznetsov, S. and Pospisil, S. (2017). Pokrocile metody posuzovani existujících ocelových mostu na ucinky zatizeni vetrem, brzdných a rozjezdových sil - zaverečna zprava pro szdc za roky 2016-2017 (in Czech; advanced methods for the assessment of existing steel bridges for the effects of wind loading, braking and acceleration forces - final report for szdc 2016-2017), *Technical report*.
- Saltelli, A. (2002). Sensitivity analysis for importance assessment, *Risk Analysis* **22**(3): 579–590.
- Saltelli, A. (2008). *Global sensitivity analysis*, John Wiley: Chichester, England.
- Scanlan, R. H. and Sabzevari, A. (1969). Experimental aerodynamic coefficients in the analytical study of suspension bridge flutter, *Journal of Mechanical Engineering Science* **11**(3): 234–242.
- Scanlan, R. H. and Tomko, J. J. (1971). Airfoil and bridge deck flutter derivatives, *Journal of the Engineering Mechanics Division* **97**(6): 1717–1737.
- Scruton, C. (1952). An experimental investigation of the aerodynamic stability of suspension bridges with special reference to the proposed Severn Bridge, *Proceedings of the Institution of Civil Engineers* **1**(2): 189–222.
- Seo, J., Kim, H., Park, J., Kim, K. and Kim, G. (2013). Interference effect on vortex-induced vibration in a parallel twin cable-stayed bridge, *Journal of wind engineering and industrial aerodynamics* **116**: 7–20.

- Shellard, H. (1963). The estimation of design wind speeds, *Proceedings of a Symposium on Wind Effects on Buildings and Structures* .
- Sifre, S. P. and Lenner, R. (2021). Partial factors and reliability verification for the site load factor approach for the assessment of existing bridges, *Structures* **33**: 307–317.
- Sobol, I. (1967). On the distribution of points in a cube and the approximate evaluation of integrals, *USSR Computational Mathematics and Mathematical Physics* **7**(4): 86–112.
- Soerensen, J. D. and Hansen, S. O. (2016). Background for partial safety factors in Danish NA to EN 1990 (CEN/TC 250/SC 10, number of document N 10), *Technical report*.
- Steenbergen, R. D. J. M., Maljaars, J., Napoles, M. O. and Abspoel, L. (2012). Probabilistic assessment of an aged highway bridge under traffic load, *Proceedings of the 10th international probabilistic safety assessment and management conference, ESREL 2011*, pp. 1906–1910.
- Steinman, D. B. (1956). The design of the mackinac bridge for aerodynamic stability, *Journal of the Franklin Institute* **262**(6): 453–468.
- Sykora, M., Holicky, M., Jung, K. and Diamantidis, D. (2016). Target reliability for existing structures considering economic and societal aspects, *Structure and Infrastructure Engineering* **13**(1): 181–194.
- Sykora, M., Holicky, M., Markova, J. and Senberger, T. (2016). *Probabilistic reliability assessment of existing structures (focused on industrial heritage buildings)*, 1st edn, Czech Technical University in Prague, CTU Publishing House, Prague.
- Truesdell, C. and Rajagopal, K. R. (2000). *An introduction to the mechanics of fluids*, Birkhauser, Boston.
- Wisniewski, D. F., Casas, J. R. and Ghosn, M. (2009). Simplified probabilistic non-linear assessment of existing railway bridges, *Structure and Infrastructure Engineering* **5**(6): 439–453.
- Wisniewski, D. F., Casas, J. R. and Ghosn, M. (2012). Codes for safety assessment of existing bridges - current state and further development, *Structural Engineering International* **22**(4): 552–561.
- Xia, H., Guo, W. W., Zhang, N. and Sun, G. J. (2008). Dynamic analysis of a train-bridge system under wind action, *Computers and Structures* **86**(19): 1845–1855.

- Xu, Z., Dai, G., Chen, Y. F., Rao, H. and Huang, Z. (2023). Extreme response analysis of train-track-bridge-wind interaction system based on in-situ monitoring wind data, *Structural Safety* **100**: 102288.
- Zhang, G., Liu, Y., Liu, J., Lan, S. and Yang, J. (2022). Causes and statistical characteristics of bridge failures: A review, *Journal of Traffic and Transportation Engineering (English Edition)* **9**(3): 388–406.
- Zhang, J., Zhang, M., Huang, B., Li, Y., Yu, J. and Jiang, F. (2021). Wind tunnel test on local wind field around the bridge tower of a truss girder, *Advances in Civil Engineering* **2021**: 8867668.
- Zhang, P., Peterson, S. D. and Porfiri, M. (2019). Combined particle image velocimetry/digital image correlation for load estimation, *Experimental Thermal and Fluid Science* **100**: 207–221.
- Zhang, T., Xia, H. and Guo, W. (2013). Analysis on running safety of train on bridge with wind barriers subjected to cross wind, *Wind and Structures* **17**.
- Zitny, J. and Ryjacek, P. (2017). Reserves in load capacity assessment of existing bridges, *IOP Conference Series: Materials Science and Engineering* **236**(1): 12–61.
- Zitny, J., Ryjacek, P., Markova, J. and Sykora, M. (2019). Hidden safety in equilibrium verification of a steel bridge based on wind tunnel testing, *Proc. the Sixth International Symposium on Life-Cycle Civil Engineering (IALCCE2018)*, pp. 307–313.
- Zitny, J., Ryjacke, P., Sykora, M., Pospisil, S. and Hracov, S. (2023). Probabilistic assessment of equilibrium of steel railway bridge based on wind tunnel and traffic records, *Structural Engineering International (accepted for publication)* .

Author's Publications

Peer Reviewed Journals:

Zitny, J., Ryjacke, P., Sykora, M., Pospisil, S. and Hracov, S. (2023). Probabilistic assessment of equilibrium of steel railway bridge based on wind tunnel and traffic records, *Structural Engineering International (accepted for publication)*.

International Conference Proceedings:

Zitny, J., Ryjacke, P., Sykora, M. (2022). Assessment of steel railway bridges for wind and traffic load effects, *Proc. IABSE Symposium Prague, 2022: Challenges for Existing and Oncoming Structures - Report*, pp. 897–902.

Zitny, J., Ryjacek, P., Markova, J. and Sykora, M. (2019). Hidden safety in equilibrium verification of a steel bridge based on wind tunnel testing, *Proc. the Sixth International Symposium on Life-Cycle Civil Engineering (IALCCE2018)*, pp. 307–313.

Zitny, J. and Ryjacek, P. (2017). Reserves in load capacity assessment of existing bridges, *Proc. IOP Conference Series: Materials Science and Engineering* **236**(1): 12–61.

Zitny, J. and Ryjacek, P., Leps, M. (2017). The complex approach to optimization of composite bridges, *Proc. Life-Cycle of Engineering Systems: Emphasis on Sustainable Civil Infrastructure - 5th International Symposium on Life-Cycle Engineering (IALCCE 2016)*, pp. 1881–1890.

National Conference Proceedings:

Zitny, J., Ryjacke, P. (2020). Metodika posuzovani životního cyklu mostů (in Czech; Methodology for life cycle assessment of bridges), *Proc. 25. mezinárodní sympóziium Mosty - Bridges 2020*, pp. 166–170.

Zitny, J., Ryjacek, P., Pospisil, S., Kuznetsov, S. (2018). Zatížení ocelových železničních mostů větrem (in Czech; Wind loading of steel railway bridges), *Proc. 23. mezinárodní sympóziium Mosty - Bridges 2018*, pp. 148–153.

Zitny, J., Ryjacek, Sykora, M., P., Pospisil, S., Kuznetsov, S. (2018). Zatížení ocelových železničních mostů větrem (in Czech; Wind loading of steel railway bridges), *Proc. 23. ročník konference Železniční mosty a tunely 2018*, pp. 139–146.

Ryjacek, P., Zitny, J., Pospisil, S., Kuznetsov, S. (2017). Zatížení ocelových mostů větrem (in Czech; Wind load on steel bridges). *Proc. 22. mezinárodní sympóziium Mosty - Bridges 2017*, pp. 147-151.

Applied Certified Methodology and Software:

Zitny, J. and Ryjacek, P. (2021). HAT – Holistic Assessment Tool, *Software*.

Ryjacek, P. and Zitny, J. (2019). Metodika posuzování mostů s ohledem na hodnocení životního cyklu (in Czech; Methodology for the assessment of bridges with regard to life cycle assessment), *Applied Certified Methodology*.

Zitny, J. and Ryjacek, P. (2017). Nástroj pro optimalizaci spřažených ocelobetonových mostů (in Czech; Tool for optimization of composite steel-concrete bridges). *Software*.

Others:

Zitny, J. (2019). Zatížení ocelových železničních mostů větrem – pravděpodobnostní hodnocení (in Czech; Wind loading of steel railway bridges - probabilistic assessment), *Proc. Sborník semináře doktorandů katedry ocelových a dřevěných konstrukcí 2019*, pp. 47-53.

Zitny, J., Ryjacek, P., Sykora, M., Kuznetsov, S., Pospisil, S. (2018). Posuzování ocelových železničních mostů na účinky větru a dopravy (in Czech; Assessment of steel railway bridges for wind and traffic effects), *Časopis Stavebnictví*, pp. 58-64.

Zitny, J. (2018). Zatížení ocelových železničních mostů větrem – výsledky měření ve větrném tunelu (in Czech; Wind loading of steel railway bridges - results of wind tunnel measurements), *Proc. Sborník semináře doktorandů katedry ocelových a dřevěných konstrukcí*.

Zitny, J. and Ryjacek, P. (2017). Nástroj pro optimalizaci spřažených ocelobetonových silničních mostů (in Czech; Tool for optimization of composite steel-concrete road bridges), *Technical report*.

Zitny, J. and Ryjacek, P. (2017). Hodnocení mostů pro VRT z hlediska LCC a LCA (in Czech; Assessment of HSR bridges based on LCC and LCA criteria), *Technical report*.

Ryjacek, P., Zitny, J., Markova, J., Sykora, M., Kuznetsov, S., Pospisil, S. (2017). Pokročilé metody posuzování existujících ocelových mostů (in Czech; Advanced assessment methods for existing steel bridges), *Technical report*.

Zitny, J. (2017). Pokročilé metody posuzování existujících ocelových mostů na účinky zatížení větrem, brzdných a rozjezdových sil (in Czech; Advanced methods for assessing existing steel bridges for the effects of wind loading, braking and acceleration forces), *Proc. Sborník semináře doktorandů katedry ocelových a dřevěných konstrukcí*, pp. 25-26.